UCLouvain

École polytechnique de Louvain

Experimental and numerical analysis of the collapse of a granular column in water at rest

Author: **Flora Nennen**
Supervisors: **Miltiadis Papalexandris, Sandra Soares-Frazão**
Readers: **Anouk Riffard, Benoît Spinewine**
Academic year 2020–2021
Master [120] in Mechanical Engineering

Abstract

Collapsing of a granular column is a case study often used to observe granular media. The goal of this master thesis is to contribute to granular media modelling research by designing a granular column collapse experiment. The purpose of this experiment is to obtain usable video recordings of collapsing sand columns in water at rest. Based on the recordings, an analysis and a comparison with the model of Monsorno *et al.* is performed.

This paper is set out to explore the design of the experiment, including its limits and boundaries. First, a review of the existing literature is realized : this allows to place the relevance of this document in its context. An other chapter of this document elaborates on a summary of the main parameters which may have an influence on the collapse of a granular column. Regarding the experiment, a parametric analysis of the initial aspect ratio, grain size and volume fraction is provided. Finally, results are compared with simulations based on the model of Monsorno *et al.*.

Experiments and videos are realised in the laboratory in the LEMSC at UCLouvain with a high-speed camera. Two sort of sand, four different aspect ratios and two sort of initial volume fractions are used.

The water-free surface and sand deposit are analysed by the means of a `Matlab` procedure.The velocities of the granular flows at various timings are analysed through Particle Image Velocimetry (PIV) via the software `DaVis 8` (LaVision).

This work allows to highlight the differences between a theoretical model and experimental results. It provides a panel of videos allowing researchers to compare their results with laboratory experiments. Finally, this work treats on the possibility of using PIV analysis to observe granular media.

Acknowledgments

Un mémoire ne se fait pas seul; loin de là. Je souhaite remercier toutes les personnes m'ayant apporté leur aide, de près ou de loin.

Tout d'abord, je remercie ma promotrice, Madame Sandra Soares-Frazão, pour son aide précieuse, sa disponibilité, ses relectures attentives et ses encouragements. Je remercie également mon promoteur, Monsieur Militiadis Papalexandris, pour ses conseils et sa réactivité.

Ensuite, j'ai eu la chance de travailler toute l'année avec Anouk Riffard qui m'a accompagnée au laboratoire sans hésiter à mettre la main à la pâte. Je la remercie pour son aide aussi bien théorique que pratique et pour ses nombreuses relectures. Sans elle, je n'aurais tout simplement pas pu réaliser mes expériences.

Une autre personne sans qui les expériences auraient été impossible à réaliser est Pierre Mertens de Wilmars qui s'est rendu disponible autant qu'il le pouvait pour réparer le canal autant de fois que nécessaire. Je l'en remercie.

Je remercie également Robin Meurice pour son accompagnement de l'ombre. Il m'a donné plusieurs idées, a consacré du temps pour moi et s'est occupé des détails administratifs pour nous procurer le matériel. Je le remercie pour sa gentillesse.

De plus, je remercie Alain Godefroid et Célia Nennen pour la relecture linguistique de mon mémoire. Le rédiger en anglais était pour moi un challenge.

Pour finir, je remercie du fond du coeur ma famille qui est toujours là pour me rassurer mais aussi pour me booster si nécessaire. Je pense particulièrement à mon grand-père qui m'aide à avancer dans la vie par son soutien, son enthousiasme et sa confiance qu'il m'accorde depuis toujours.

Contents

1 State of the Art **5**

2 Theoretical model **11**

3 Parameters of interest **17**
3.1 Shape and size of the grain 17
3.2 Initial volume fraction 18
3.3 Aspect ratio 19
3.4 Liquid phase and flow regimes 22

4 Experimental setup **25**
4.1 General information 25
4.2 Image processing 27
4.2.1 Davis 27
4.2.2 Matlab 29
4.3 Experimental procedure 29
4.3.1 Luminosity and contrast 30
4.3.2 Calibration 32
4.3.3 Repeatability 34
4.4 Limits of experiments 36
4.4.1 Wall effect 36
4.4.2 Free surface 36
4.4.3 Gate opening 39

5 Experimental results **43**
5.1 Parametric study with respect to the aspect ratio and its impact on the collapse of columns 43
5.1.1 Collapse behavior 43
5.1.2 Interfaces analysis through the `Matlab` procedure 46
5.1.3 Velocities analysis through `Davis 8` 50
5.2 Comparison between our sand and a finer one 55

5.3 Comparison of the behaviour of a loose column and a dense column . . 57

6 Comparison with simulations **59**
6.1 Computation of the initial volume fraction 59
6.2 Comparison between simulations and experimental data in terms of shape of deposit 63
6.3 Collapsing process and velocities simulations: comparisons with the experimental results 66
6.4 Influence of the grain-size parameter 69

A Laboratory manual **82**
A.1 First experience of a trial day 82
A.2 Following experiments 84
A.3 Calibration 84
A.4 End of the experiment session 84
A.5 Installation of the removable door 85

B Time Line of granular media **86**

C Additional illustrations **88**

Introduction

Granular Materials

Cereals, sand, asteroids belt, and so many other materials in the universe are granular materials; a very surprising category of materials which is not yet completely understood. These materials are all composed of grains large enough not to be powder and their behavior is influenced by contact, collisions and frictions (See Figure 1).
Granular media are found in a multitude of domains in nature and industry. Few examples are fabrication of concrete, corn agriculture, drugs preparations but also landslides, submarines avalanches, dunes and mudflows.
Usually, the world is divided in three states: solid, liquid and gaseous. In fact, the behaviour of granular materials at the macroscopic scale can be so different from what is common for liquids and solids, that it has been proposed to consider the granular state as a new state of matter [1]. Some simple experiments can give this intuition. For instance, naturally flowing sand from an hourglass will act as a liquid, whereas a quickly overthrown bucket of compacted sand will cause a relatively solid block of sand to fall. Other examples are shown by Olivier Pouliquen during his conference in Rennes in 2016 [2] such as the Janssen's experiment highlighting the counter-intuitive pressure distribution and illustrated on Figure 2. In this experiment, a hollow cylinder is filled with grains. At first the weight measured by the scale increases, then the weight measured by the balance becomes saturated and the addition of the grains does not change it anymore. In the end, the total weight measured by the balance is much lower than the weight actually poured by the experimenter.
Olivier Pouliquen also illustrated the Reynold's dilatancy. The dilatancy of Reynold is the fact that, unlike most other solid materials, a compacted granular material tends to expand when it is sheared. One other particularity of a granular media is that shear stress and the past treatment given to the material can have an influence on its future.

Granular materials are the second most used material in the industry in terms of quantities [2]. Nowadays, Humans want to be safe, optimize their resources and uses, and understand how their surroundings work. Unfortunately, granular media still have many well-kept secrets.
Being able to predict the flow of a granular material would significantly increase the

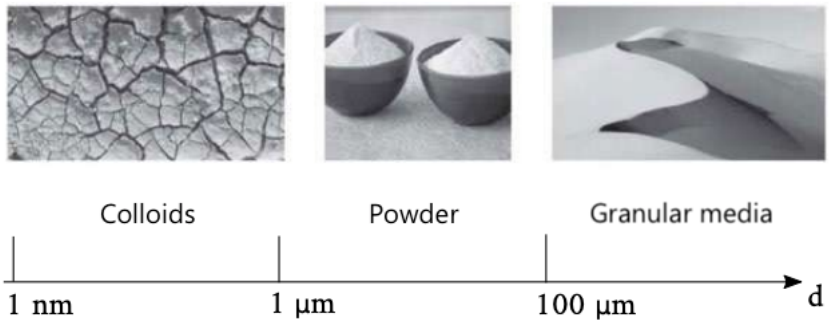

Figure 1: Scale of divided media [3]

efficiency of plants producing and using granular materials and save time and energy. From a safety point of view, understanding the behavior of granular media would improve precautions and solutions against natural disasters such as land avalanches and underwater avalanches. Anticipating the distance traveled by a landslide, the generation of a tsunami, the contamination of protected areas by certain pollutants carried by an underwater avalanche, so many applications justify the increasing amount of researches being carried out in the field of granular environments.

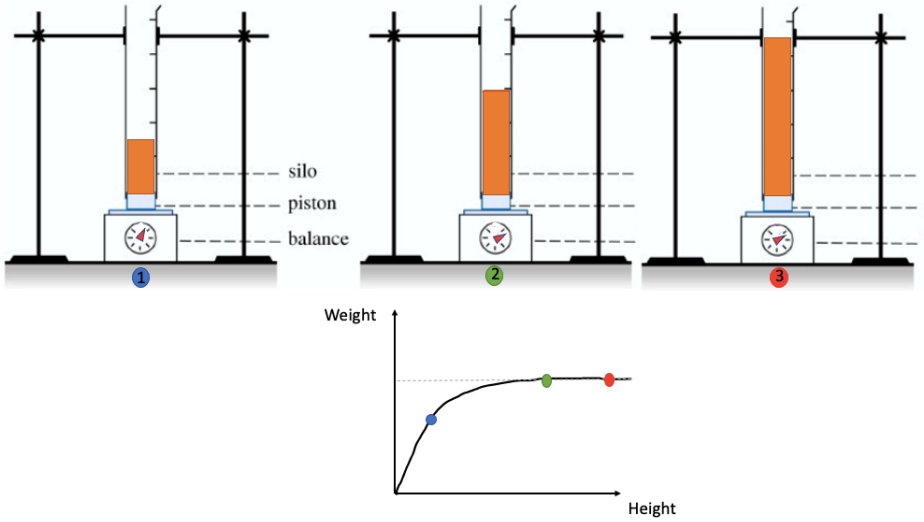

Figure 2: Janssen's experiment: Global shape of the pressure distribution as a function of the height in a granular column

Which sort of materials in which configuration

In this dynamic of contribution to granular media modelling research, it is necessary to create laboratory experiments to validate the developed models. Sand being the most exploited resource on Earth after water and air and being a granular medium, it is interesting to use it in experiments. According to Arte France [4], "more than 15 billion tons of sand are extracted in the world every year, a tonnage equivalent to the natural production of these sediments by rivers".

At the end of the 2000s, attention was focused on the collapse of granular columns because of its aesthetic simplicity, on the richness of the observed dynamics and the obvious geophysical and astrophysical applications. This experiment consists of causing the collapse of a rectangular or cylindrical column of sand and observing its behaviour; how the sand collapses, over what distance, with what envelope shape and how much time is required for it to find a stable position [5]. The collapse of a granular column, which mimics the collapse of a cliff, has been extensively studied in the case of dry granular material, when the interstitial fluid plays no role [6].

Experimental data on the collapse of dry granular columns exist in the literature. However, the presence of a fluid in the medium increases the mobility of the granular phase. In natural sediment flows involving particle transport, the suspensions are therefore usually in water.[1].

This thesis focuses on the collapse of a column of sand in the water. In nature, this experimental case would represent the observation of an underwater avalanche.

Submarine avalanches are different from terrestrial avalanches because of the fluid in which they take place. Under the sea, an avalanche will set a large quantity of sediment in motion. The slopes of the terrain may be much lower, but underwater avalanches can be several hundred kilometers long. Their initiation and propagation remain partly unpredictable. This is why it is necessary to carry out experiments and models on this subject.

A model and its experimental validation regarding granular environments and, more precisely, sand in water would make it possible to avoid human and/or economic losses.

There are many disasters caused by underwater avalanches. Among these, one can consider the case of Nice airport located on the seafront. It was built partly by gaining ground on the sea (See Figure 3). On 16 October 1979, a major submarine landslide took place and caused part of the airport to disappear into the sea. At the same time, after a relative drop in the sea level, a tidal wave of several meters submerged the coastline on a front of about 100 km.

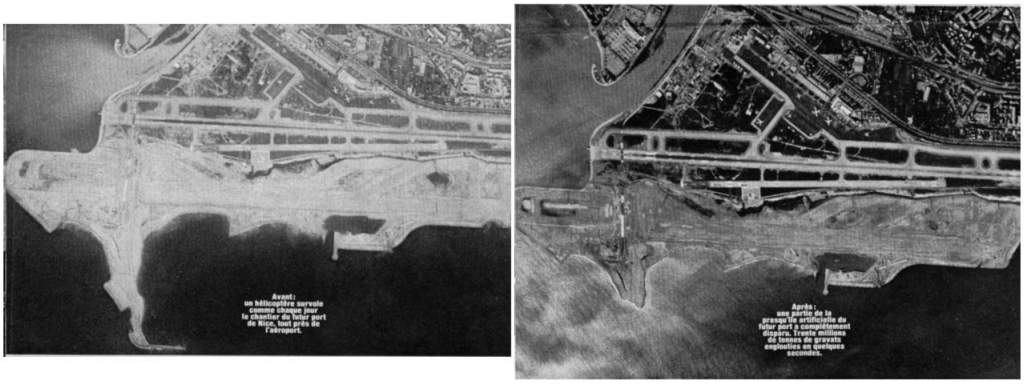

Figure 3: before/after picture of the collapse [7]

Nowadays, nations and cities such as Nice, Venice, Singapore, Hong-Kong and Japan continue to build on polders (artificial expanses of land reclaimed from the water). Therefore, understanding of underwater avalanches and their after-effects could save a lot of time and energy. [8].

Chapter 1

State of the Art

Although granular media have only really attracted a lot of research work and experiments in the last 50 years, it is a vast field with many different approaches and techniques. We will describe non-exhaustively advances in this research area in this chapter, in chronological and logical order. A time line is available in the Appendix B.
The challenge in understanding granular media is the fact that these are not like other materials usually sorted in three main categories: solid, liquid, gaseous. Reynolds, in 1885, already highlighted that granular media are a particular media. While grains like sand and seeds are solid, their behaviour is not really as a solid behaviour. Reynolds showed that, unlike most other solid materials, a compacted granular material tends to expand when it is sheared. The phenomena is called "The Reynolds dilatancy". That would create a new field of research: the study of granular media.

Then, between 1900 and 1911, Einstein studied the increase of viscosity when adding a few particles to a viscous Newtonian fluid. He calculated this first linear correction of the viscosity by considering the volume fraction of the mixture and the perturbation induced by a single particle immersed in a shear flow [9].
Brown and Hawksley (1947) have photographed the variation of packing of equal spheres contained in an open box when the parallel side walls are inclined to produce shear [10]. They have shown the fact that a loosely-packed granular media will not act like a dense packing. A challenge is to determine which volume ratio can be named *loose* or *dense*. Nowadays, the evaluation and measurement of the packing is still a difficulty in modeling and predicting the behaviour of granular media. Indeed, it is not enough to be able to say whether the column is dense or loose; it is also necessary to be able to quantify its volume fraction. Unfortunately, as far as we know, few experimental methods have focused on the exact measurement of the volume fraction, whereas it is essential in numerical models.

After that, limited by technologies available at the time, it was not easy to understand by simple observations the mechanisms taking place during the motion of granular me-

dia. This is why most available works about granular media between 1950 and 1975 are experiments and observations on a small number of particles. Over time, more and more data have shown that granular media has its own laws of behaviour. Among them, Bagnold [11] in 1954 highlighted the influence of the presence of the interstitial fluid and established a law to link stresses with the square of the shear stress. To do so, he realized experiments with wax spheres in a glycerin-water-alcohol mixture. Fowler and Glastonbury [12] studied the flow through an orifice depending on the shape, the size and the density of the granular medium used. Meanwhile, Carrigy [13], thanks to a rotating drum, focused on the critical angle of inclination to trigger avalanche and the angle at rest after the collapse for different kind of granular media. This angle at rest depends on the drag studied by Wieghardt [10]. Numerous experimental data have been collected on these angles, such as those of Dury and Rishow in 1998.

Subsequently, some models were developed with the aim of finding a model as efficient as the existing models in the fields of fluid mechanics and soil mechanics. Experimental works and theoretical models evolved in parallel. Both are linked and enable researchers to improve again and again prediction and understanding about granular media. Events like rockfalls, landslides and snow avalanches motivated the work of Savage and Hutter [14], Campbell [15] and Moreau [16]. The aim became to describe and model granular materials with quite a lot of particles. Moreau introduced in 1990 his numerical method to take into account a lot of particles and collision between them. Kruyt and Rothenburg focused on the strain tensor [17].

Until then, granular media were studied on the basis of continuum mechanics. However, with this approach, it was not possible to study each individual grain and its interaction with the others and the fluid [18]. In the 2000's, thanks to the available experiments developed in the past years and thanks to discrete modelling, researchers have increasingly understood the behaviour of a granular medium at the microscopic scale.

The question was still whether a collection of macroscopic particles could be described as a continuum, and whether its constitutive relations could be properly accounted for in a global continuum theory. In fact, attempts to develop continuum theories for granular suspensions until now were not unequivocally accepted [19]. Nowadays, this question remains open and both approaches are still used: considering the problem in a continuous or discrete way. Both approaches have their strengths and weaknesses and no one is currently able to convince the entire scientific community that one approach is more representative of reality than the other. "In fact, available continuum theories typically ignore the normal viscosity of the granular phase, employ them in an ad-hoc fashion or obtain scalings that do not match experimental data" [1]. While Discrete Elements Method could be computationally demanding, the number of particles is limited and solutions found to spare make assumptions and loose precision for example using

averaged equations for the presence of solid phase.
A mixture made of a granular media suspended in a fluid can be treated with different approaches. One can find a lot of "Two-phases" models which can in fact characterize three approaches. The first two-phases approach is an Eulerian-Lagrangian model where water phase is considered as a continuum and grains tracked individually. The discrete approach for two-phases model exists too. There are the Lagrangian-Lagrangian models which depict both phases as particles. The third two-phases approach is the Eulerian-Eulerian model considering both as continuous media. We will therefore divide researches into three main categories always working in parallel with each other: the experimental, the discrete and the continuous approach. Discrete modelling contains Eulerian-Lagrangian and Lagrangian-Lagrangian models.

Discrete modelling
In the context of a "dry" granular medium, i.e. in the presence of a negligible fluid such as air, the Discrete Elements Method or DEM can be used to obtain the Lagrangian trajectory of particles and it seems very satisfactory. This method has been introduced in 1979 Cundall and Strack [18]. When particles are mixed with a fluid, that can be seen as a single-phase with its effective rheological properties, its effective viscosity and non-newtonian phenomena [9] but it can also be seen as a two-phase system wherein the fluid and particles can experience relative motion.

The fluid and the grains can then be analyzed at different scales and considered as two phases that have different velocities. In 2008, Zhu *et al.* [20] developed a model. Then, a lot of researchers such as Mutabarak [21] and Butler and Snook [22] did it too. Recently, Lacaze *et al.* [23] presented a paper to show the different regimes that can be encountered in the case of the collapse of a granular column depending on several dimensionless parameters, namely, the column Bond number Bo (Equation 1.1) [24], the grain diameter to capillary length ratio d/l_c, the initial aspect ratio a, the Stokes number St (Equation 1.2) , and the initial volume fraction ρ. They have made varying the properties of the interstitial fluid and of the grains, the geometry, and the compaction of the initial granular column [23].

$$Bo = \frac{\Delta\rho g L^2}{\sigma} \tag{1.1}$$

$$St = \frac{1}{18}\frac{\rho_p {d_p}^2 v}{\mu L_c} \tag{1.2}$$

For both equations 1.1 and 1.2, the index p is for "particle", ρ is the density, L or L_c are the characteristic length, d is the diameter, μ is the viscosity of the fluid, v is the velocity of the fluid and σ is the surface stress.

Continuum modelling

Regarding models based on continuum mechanics, Jiang and Liu [25] developed a model for the dry case. Then two-phases models have been studied by Pouliquen and Pailha in 2009 [26] taking into account the volume ratio. Few years later, Gidaspow proposed a book in which he demonstrated how multiphase flow equations can be used to provide applied, practical, predictive solutions to industrial fluidization problems [**?**].

Currently, at the UCLouvain, within the framework of the research carried out at the Institute of Mechanics, Materials and Civil Engineering, attention is paid to both the discrete approach via the work of the Migflow team [27] and the continuous approach via the work of Professor Papalexandris and his research team [1].

Experimental observations

About experimental research, after having listed and compared a few experiments already existing, the French research group "Groupement De Recherche Milieux Divisés"[1] in 2004 [28] concluded their work with an important idea that, with their knowledge of granular flows and the amount of data available, they could no longer consider a single geometry as a test for the constitutive laws but must consider the different geometries. The collapse of a granular column initially at rest is one of the exploited configurations. This is the case that is considered and studied in this thesis. A single configuration is not sufficient to analyze granular media but, in addition, it is necessary to take into account the physical properties of granular media such as their shape, roughness, size, the presence or absence of an interstitial fluid, the nature and viscosity of this fluid. In the literature, one can find experiments with air as the interstitial fluid and grains made of polypropylene [5] or rice [29], sand, ... Glass beads are also often used because of their perfect sphericity and constant size. They are used immersed in water [30] but also in other fluid like Ucon oil mixed with water[6]. The four main laboratory experiments are illustrated below, in Table 1.1.

Finally, the experiment which appears to be the closest to what we want to study in the present thesis is the experiment of Thompson and Huppert made in 2007 [31] in which a water-sand mixture is analyzed."They show that the liquid dramatically changes the way the column collapses compared to the dry case" [6]. The main problems with this experiment are the quality of recording and the disturbance of the initial conditions due to the initiation of the collapse via a door being pulled upwards. The aim of this thesis is to produce the same kind of experiment to provide experimental data for the purpose of studying in detail a larger number of plural cases (different aspect ratio, different compaction, better initial conditions).

[1] The Groupement De Recherche Milieux Divisées (GDR MiDi) : A French research network supported by the CNRS. The goal of this network is to exchange and discuss scientific results among the members of the French laboratories involved in granular media.[28]

Illustration	Summary
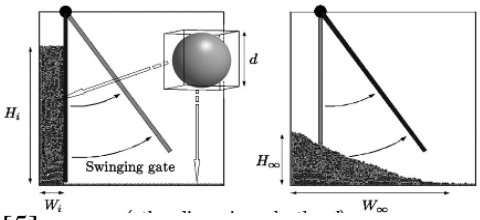 [5]	• Dry case • Grains: polypropylene particles. Diameter: 2.5 mm • New sort of experimental set-up which can be modeled by using DEM simulations. The aim was to observe the collapse process, the internal motion, jamming and crystallization. The persistent problem is to manage the friction coefficient of the wall in the simulation. In addition, this experimental process does not allow the observation of a column immersed in water.
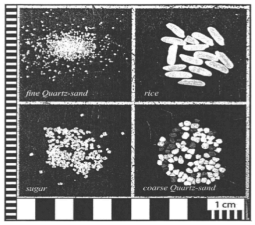 [29]	• Dry case • The experiments investigate two-dimensional granular flows created by rapidly releasing columns of grains, initially contained in a rectangular box, into a wide channel [29].
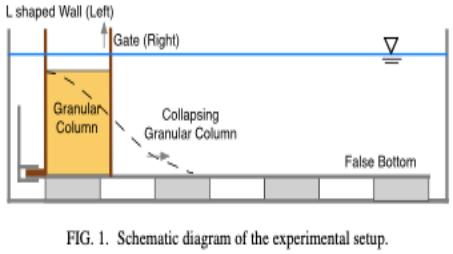 FIG. 1. Schematic diagram of the experimental setup. [30]	• Fluid: Water • Grains: glass beads. Diameter: 0.12 - 0.56 mm • They analysed the spreading velocity and the runout distance for loose and dense columns to find the critical volume ratio to switch from loose to dense. They also observed column collapse for different aspect ratios. Finally, they observed the presence of vortices.
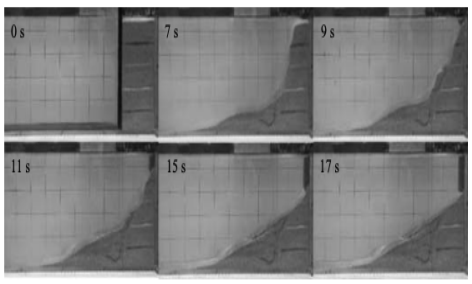 [31]	• Fluid: Water • Grains: sand. Diameter: 0.5mm • They did dry experiments to compare the collapse of a cylindrical column and a rectangular column. After that, they added water. They wanted to observe which was the initial position of the grain that landed further after collapse came. Unfortunately, they did not conclude on this.
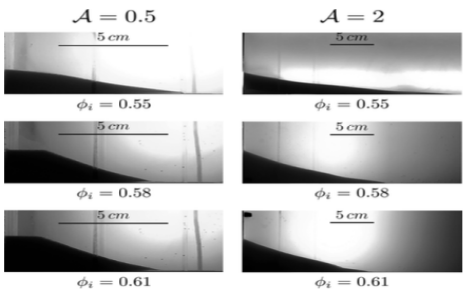 [6]	• Fluid: A mixture of water and Ucon oil • Grains: glass beads • They observed the shape of the deposit and the influence of the volume fraction on it. They also compared dense and loose packing and determined what is the critical volume fraction that marks the transition between dense and loose.

Table 1.1: Main laboratory experiments

Chapter 2

Theoretical model

Model
In the following equations and table 2.1, subscripts f and s refer to the fluid and the solid phase respectively. The subscript i is either f or s.

V	Volume of the mixture
V_i	Control volume for the phase i
g	Constant of gravitational acceleration
u_i	Velocity field of the phase i
p_i	Pressure field of the phase i
ϕ_i	Volume fraction of the phase i
μ_i	Shear viscosity of the phase i
μ_n	Normal viscosity of the solid phase
ζ_i	Bulk viscosity of the phase i
μ_c	Compaction viscosity proposed in [32]
μ_n	Normal viscosity [33]
β_s	Configuration pressure
γ_s	Related to the micro-structure
δ	Interphasial drag coefficient proposed in [34] (HKL-type correlation)
χ_i	Constants of the model
f	Interphasial momentum exchange
$\mathbf{s}_s$	Entropy of the solid phase
$\mathbf{D}_s$	Strain rate tensor of the solid phase
$\mathbf{D}_s^d$	Deviatoric part of $\mathbf{D}_s$

Table 2.1: List of symbols

The model for the numerical simulations used in this thesis is developed at the Insti-

tute of Mechanics, Materials and Civil Engineering and detailed in [35]. As this thesis is a contribution to the testing of the model and not to its improvement or implementation, it will be described in a relatively concise way. Indeed, the validation of this model has already been done [1] but this thesis aims to provide another test configuration for the model as well as to contribute to the validation of the algorithm solving the equations of this model. In order to assess the reliability and accuracy of the solving algorithm, it would be necessary to compare the simulations produced with a panel of experimental data which, at our present knowledge, is not sufficiently large.

The starting point of our model is that the space studied is shared in two phases with i={f,s}.

$$V = V_f + V_s \tag{2.1}$$

$$\phi_i = \frac{dV_i}{dV} \tag{2.2}$$

Assumptions are made that these two systems are immiscible, not in equilibrium and the solid phase is isotropic at microscopic scale.

Governing equations are established for both phases. For the solid phase and for the liquid phase, in a control volume $V_i \subset V$, the conservation of mass and momentum equations are used. If the volume fraction ϕ_f was unity and we had only water instead of a grain-water mixture, these equations would be the incompressible Navier-Stokes equations.

For the fluid phase, the viscous stresses expressed at equation 2.8 are Newtonian (i.e. whose deformation rate law is linear) whereas the viscous stresses of the solid phase (equation 2.13) are non-Newtonian but isotropic by assumption.

$$\frac{\partial \phi_f}{\partial t} + \nabla \cdot (\phi_f u_f) = 0 \tag{2.3}$$

$$\frac{\partial \phi_s}{\partial t} + \nabla \cdot (\phi_s u_s) = 0 \tag{2.4}$$

$$\rho_f \frac{\partial (\phi_f u_f)}{\partial t} + \rho_f \nabla \cdot (\phi_f u_f \otimes u_f) = \nabla \cdot \sigma_f - f + \rho_f \phi_f \mathbf{g} \tag{2.5}$$

$$\rho_s \frac{\partial (\phi_s u_s)}{\partial t} + \rho_s \nabla \cdot (\phi_s u_s \otimes u_s) = \nabla \cdot \sigma_s + f + \rho_s \phi_s \mathbf{g} \tag{2.6}$$

$$f = \delta(u_f - u_s) + p_f \nabla \phi_s \tag{2.7}$$

$$\sigma_{\mathbf{f}} = -\phi_f p_f \mathbf{I} + \phi_f \zeta_f (\nabla \cdot u_f)\mathbf{I} + 2\phi_f \mu_f \mathbf{D}_f^d \tag{2.8}$$

$$\mathbf{D}_i = 2(\nabla u_i + \nabla(u_i)^\top) \tag{2.9}$$

$$\mathbf{D}_i^d = \mathbf{D}_i - \frac{2}{3}(\nabla \cdot u_i)\mathbf{I} \tag{2.10}$$

In the two established momentum conservation equations 2.5 and 2.6, the interphasial momentum exchange f ($f \triangleq f_s$ and $f_s = -f_f$) and the tensor stresses σ_i are used. Term ζ_s is equivalent to the bulk viscosity in simple fluids [1] and $\zeta_f = 2.7 \cdot 10^{-3}[Pa]$ for water.
Constitutive expressions for f, σ_s and σ_f as well as an evolution equation for ϕ_s are provided by exploiting the constraints imposed by the second thermodynamic axiom, and according to the thermodynamic formalism for mixtures of immiscible continua of Papalexandris [36] and Monsorno *et al.* [1].

The solid phase is a collection of discrete particles but in this model, it is a continuous medium where we account for the microstructure. Because of this micro-structure, the phase is more ordered than the fluid phase, the thermodynamics is more complex and there is additional work due to this order inducing two additional degrees of freedom imposed by the configuration of the grains in space.For the solid phase, an additional viscosity is expressed in the model in equation 2.13 via additional coefficients terms $\zeta_{s'}$, $\mu_{s'}$, χ_1 and χ_2 given in [1]. These four coefficients are all functions of the strain rate tensor and the normal viscosity μ_n [33]. The equation 2.11 is obtained in [33] where $\mu_f = 8.9 \cdot 10^{-4}[Pa]$ and μ_s of the equation 2.12 are developped in [37].

$$\mu_n = 0.75\mu_f \frac{\phi_s}{(\phi_{max} - \phi_s)^2} \tag{2.11}$$

$$\mu_s = \mu_f \Big((2.5 - \frac{2}{\phi_{max}})\phi_s + (5.2 - \frac{3}{\phi_{max}^2})\phi_s^2 + (1 - \frac{\phi_s}{\phi_{max}})^{-2} - 1 \Big) \tag{2.12}$$

$$\begin{aligned}\sigma_{\mathbf{s}} = -\phi_s p_s \mathbf{I} + \gamma_s \nabla\phi_s \otimes \nabla\phi_s + ((\zeta_s + \zeta_{s'})\nabla \cdot u_s + \chi_1)\phi_s \mathbf{I} \\ + 2(\mu_s + \mu_{s'})\phi_s \mathbf{D}_s^d + \chi_2 \phi_s \mathbf{D}_s \cdot \mathbf{D}_s\end{aligned} \tag{2.13}$$

$$\gamma_s = 2\rho_s \phi_s \frac{\partial \mathbf{s}_s}{\partial |\nabla\phi_s|^2} \tag{2.14}$$

$$\chi_1 = -\sqrt{2}\mu_n \Big(2\sqrt{\mathbf{D}_s^d : \mathbf{D}_s^d} - \frac{3}{2} \frac{\mathbf{D}_s^d : \mathbf{D}_s^d}{\sqrt{\mathbf{D}_s : \mathbf{D}_s}} \Big) \tag{2.15}$$

$$\chi_2 = -\frac{\sqrt{2}\mu_n}{\sqrt{\mathbf{D}_s : \mathbf{D}_s}} \tag{2.16}$$

To establish the model, we had to consider μ_s and μ_n empirically on the basis of experiments and the problem is that it is hard to measure experimentally viscosities of our solid phase.

$$\mu_{s'} = \frac{\mu_n}{\sqrt{2}} \frac{det\mathbf{D}_s}{(\mathbf{D}_s : \mathbf{D}_s)^{3/2}} \tag{2.17}$$

$$\zeta_{s'} = \frac{\mu_n \sqrt{2}}{3} \frac{det\mathbf{D}_s}{(\mathbf{D}_s : \mathbf{D}_s)^{3/2}} \tag{2.18}$$

$$\beta_s \triangleq \rho_s \phi_s \frac{\partial \mathbf{s}_s}{\partial \phi_s} \tag{2.19}$$

To then study the temporal evolution of the volume fraction ϕ of each phase, we use the compaction equation 2.20. In this equation, β_s represents the intergranular stress which expresses the resistance of the solid phase to compaction. The terms u are velocities, p are pressures, μ_c is the compaction viscosity and γ_s is the derivative of the Helmholtz free energy of the granular phase with respect to $\nabla\phi_s$ [1]. The compaction viscosity μ_c is considered equal to μ_f by [1].

$$\frac{\partial \phi_s}{\partial t} + u_s \cdot \nabla \phi_s = Re \frac{\phi_s \phi_f}{\mu_c} (p_s - p_f - \beta_s + \nabla \cdot (\gamma_s \nabla \phi_s)) \tag{2.20}$$

Algorithm

A numerical method often used to solve Navier-Stokes equations is the Projection method first introduced by Chorin. This algorithm is based on the Helmholtz's decomposition in which any vector field is split into two parts: one solenoidal and one irrotational. Our algorithm is a time-accurate projection-based algorithm, inspired by the projection method for the Navier-Stokes equations.

In order to test the model with an other configuration that what have already been done and its algorithm, it would be useful to be able to compare their results with experimental data. By example, the length and height of the column before and after collapse as well as the angle of repose, the shape of the collapse envelope at different times. A difficulty will be to link the time in real life with the non-dimensional time of simulations. Since the code allows the analysis of differences between the collapse of dense and loose columns, it would be interesting to do the same experimentally. Here, the difficulty would be to have a repeatable procedure to always get the same volume fraction for the dense case.

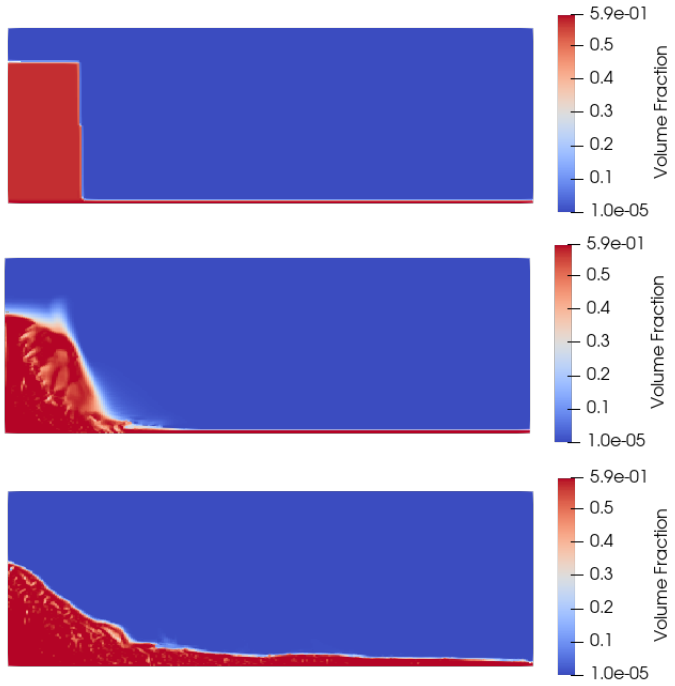

Figure 2.1: Example of simulation obtained thanks to the model and algorithm. Quantities are dimensionless

Chapter 3

Parameters of interest

This chapter describes the parameters that can be chosen before carrying out the experiment and that will have a potential influence on the behaviour of the column collapse, its run-out distance (which is the distance measured from the origin by tracking the farthest particle that is still in contact with the main granular mass) and its final deposit. The values of these parameters in our experiments are given in the following chapter 4 except for the grain shape which will be neglected and for the volume fraction which is discussed in chapter 6.

3.1 Shape and size of the grain

It has been demonstrated that the shape of particles has a great importance in the behaviour of granular column collapse. Cabrera and Estrada [38] observed that the measurement mostly affected by grain-size effects are the column mobility and the collapse duration. To avoid significant grain-size effects, the system-size to grain-size ratio L_i/d must be larger than 75 for short columns and larger than 50 for tall columns (where d is the mean diameter of particles and L_i the initial length of the column). Lee *et al.* [30] showed that the collapse duration and the run-out distance are longer for very fine particles than for coarse particles. It is also viewable in the work of Bougouin *et al.* at Figure 3.1.

Besides, granular media such as sand can be polydisperse. It influences the maximum concentration of a column and it has to be taken into account if necessary. The other possibility is to consider the mean diameter.
Finally, the shape of the grains is important too. With the words of Jian Chen [39], "the strength of a granular assembly is basically a result of the competition between rolling and sliding of the particles in a granular matrix: For round particles, even large coefficients of friction will not be able to stabilize a granular structure against disintegrating

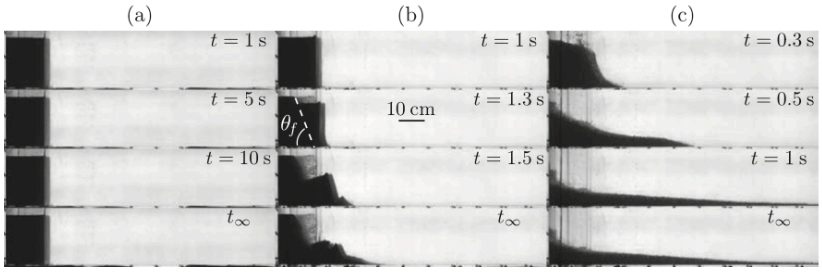

Figure 3.1: Snapshots of some water-saturated granular collapses for various grain diameters: (a) d = 120 m, (b) d = 500 m, and (c) d = 5 mm. In Fig. 2(b), the failure angle f with respect to the horizontal plane is indicated. In all cases, the initial aspect ratio is a 1.3 and the initial volume fraction is 0.64 (i.e., initially densely packed) [24]

by relative rolling at inter-particle contacts". In the literature, if grains are not spherical but regular, it is most of the time fibres or platelets where the challenge is that the rheology depends on the orientation of the particle during the flow [9].
Few experimental data are available for a column of sand in water due to the difficulty in characterising the rheology of the mixture. Usually, glass beads are used because their rheology is easier to characterize. However, comparing sand with glass beads is often not meaningful. Indeed, glass beads can be perfectly spherical as opposed to sand. In addition, glass beads can be transparent and more resistant to abrasion.

3.2 Initial volume fraction

The volume fraction is defined as the volume of grains divided by the total volume of the immersed column (Equation 2.2). Rondon *et al.* [6] have proven that the concentration of a granular column (i.e the volumetric fraction or volume fraction) had an influence on the behaviour of the collapse. For a loose and a dense column containing the same amount of sand, they obtained the Figure 3.2. The aspect ratio of columns is different since they contain the same quantity of sand but the dense one is compacted.

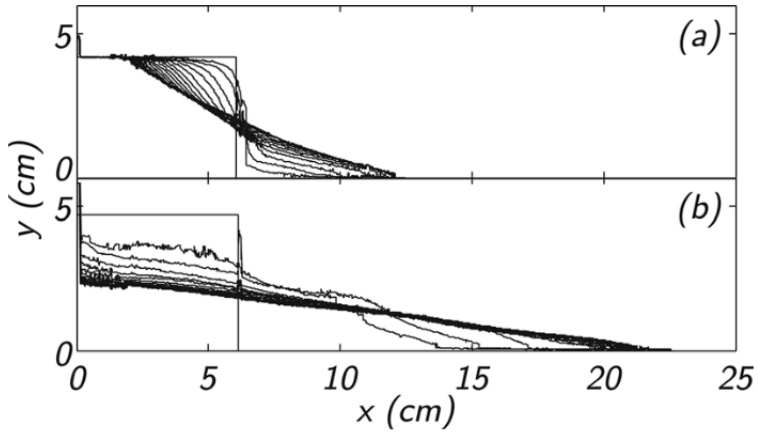

Figure 3.2: Collapse of a dense and a loose column containing the same amount of sand for an aspect ratio A = 0.67. (a) $\phi_i = 0.6$, $L_i = 6$ cm, $H_i = 4.2$ cm, 3 s between profiles; (b) $\phi_i = 0.55, L_i = 6$ cm, $H_i = 4.8$ cm, 0.66 s between profiles.[6]

Indeed, the morphology of the deposit after collapsing depends on the initial volume fraction. The collapsing process also depends on the initial volume fraction. By example, for a dense granular flow (high concentration), the flow takes place at the top surface of the pile while it happens in the bulk for a loose packing column (low concentration). For loose column, according to Lee *et al.* [30], the collapsing duration is shorter than for a dense column and the run out distance is longer for loose than for dense columns.
The critical value for the concentration to switch from loose to dense packing is 0.58 according to Rondon *et al.* [6] but Shi *et al.* consider 0.57 to be dense for their work[40]. It is important to notice that the concentration of a column is not perfectly vertically uniform because of the weight of grains. In the literature, the concentration is assumed to be uniform or a concentration considered as average in some articles is used.

Initial volumetric fraction is most of the time given for experimental data published but it is not obvious to understand how it can be obtained. Overall, two methods are used. Either the volume fraction of the experimental tests is determined by trial and error by comparison with simulations, or an experimental procedure is followed in order to calculate the volume fraction and always reproduce the same one over the tests. Sometimes, concentration is just given as "dense" or "loose" without quantifying this concentration.

3.3 Aspect ratio

The aspect ratio A is defined as the ratio between the initial height and the initial length of the column.

$$A = \frac{H_i}{L_i} \tag{3.1}$$

The aspect ratio has an influence on some different data of the collapsing of a granular column such as the run-out length, the shape of the final deposit and the collapsing duration. For low values of A, only the front corners of the initial column are in motion whereas for large A the entire free surface flows from the beginning [29].
According to Rondon et al., for an aspect ratio $A \leq 0.7$ in dense packing, the shape of the deposit is the same in water as the one in air [6]. As the duration of the collapse t_∞ is concerned, for $A \leq 4$, Lacaze *et al.* [5] observed that the non-dimensional time T defined in Equation 3.2 was decreasing with increasing aspect ratio until it reached an asymptotic value of $T = 2.8$ [5].

$$T = \frac{t_\infty}{\sqrt{g/H_i}} \tag{3.2}$$

where t_∞ is the time needed to observe no more particle movement.
Bougouin and Lacaze [41] obtained a critical value of $A = 2$ for the run-out length. For $A \lesssim 2$, the run-out distance increases linearly with A; when for $A \gtrsim 2$, it increases as a power-law with dependence on A.
About the shape of the deposit, several values are critical to switch from one shape to another one considering the work of Lee *et al.*[30], Bougouin *et al.* [41], Lacaze *et al.* [5] and Rondon *et al.*[6]. First, for an aspect ratio bigger than 3, the initial failure surface is deeply buried in the column, then the entire upper part of the column descends in the initial stage of the collapse process and the granular material in the lower part of the column slides forward and downward along a smaller failure surface (Figure 3.3(a)). In this case study, two more cases can be considered. Either $A \gtrsim 8$, so the failure surface is so small that there is not enough shear force from the failure surface to resist the motion of the granular material. As a result, the entire column descends like a free-fall and when the top layer of the granular mass hits the bottom, it pushes out the granular material at the base of the column creating a final deposit morphology like a Mexican hat (Figure 3.3(a)). Or, for $A \lesssim 8$, the shear force from the failure surface can provide some resistance to the descending of the granular material so that the descending velocity of the column is smaller than that for $A \gtrsim 8$ and the final deposit morphology has a triangular shape (Figure 3.3(b)).

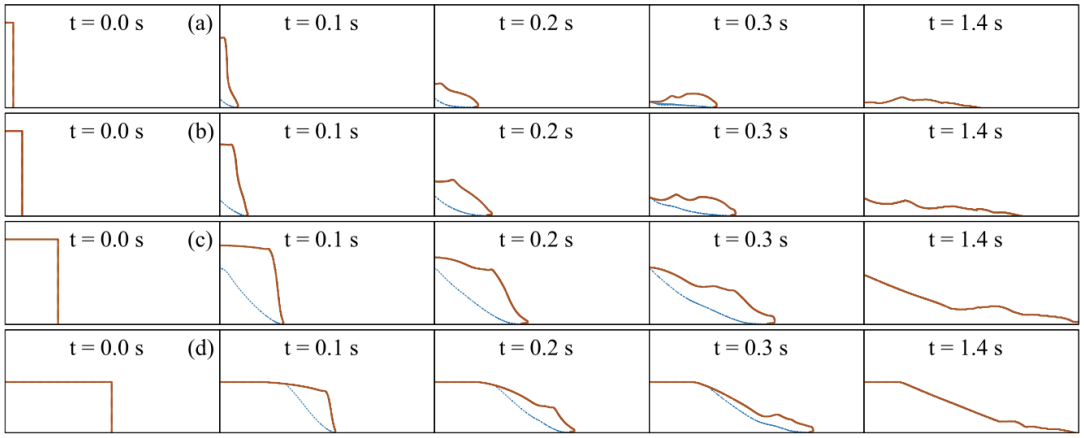

Figure 3.3: Collapses of submerged granular columns for the coarse particles with (a) A = 10 (L_i = 1 cm and H_i = 10 cm), (b) A = 5 (L_i = 2 cm and H_i =10cm), (c) A=1.67 (L_i =6cm and H_i =10cm), and (d) A=0.5 (L_i =12cm and H_i =6cm). The red solid lines are the contour lines of concentration of 0.5. The blue dashed lines are the failure surface defined by $|u_1|$ = 5 cm/s. The final deposit morphology is a Mexican hat for (a), a triangle [(b) and (c)], or a trapezoid (d) [30].

Then, for an aspect ratio lower than 3, the failure surface is not buried deep enough in the column, then a significant portion of the top layer slides forward down at the initial stage of the collapse process (Figure 3.3(c) and (d)).

According to Lacaze *et al.* [5], above $A = 1.2$, the entire column always participates in the collapse as opposed to under $A = 1.2$ where the dynamics at the back of the column does not influence the flowing front. In moderate aspect ratio, a trapezoidal or a triangular final deposit can be observed. Indeed, a portion of the top layer can never be affected by the collapse process and the final deposit morphology has a trapezoidal shape (Figure 3.3 (d)). Otherwise, the deposit has a triangular shape (Figure 3.3 (c)). For Rondon et al., the critical value to go from a trapezoidal shape to a triangular one is $A_H = 0.8$ (Figure 3.4) but the fluid is a mixture of water and Ucon oil. In the work of Lee *et al.* [30], this value A_H depends on the sort of particles. For coarse particles, they agree with Bougouin *et al.* [41] to take 0.75 as the critical value. For fine particles, the critical value becomes 0.6.

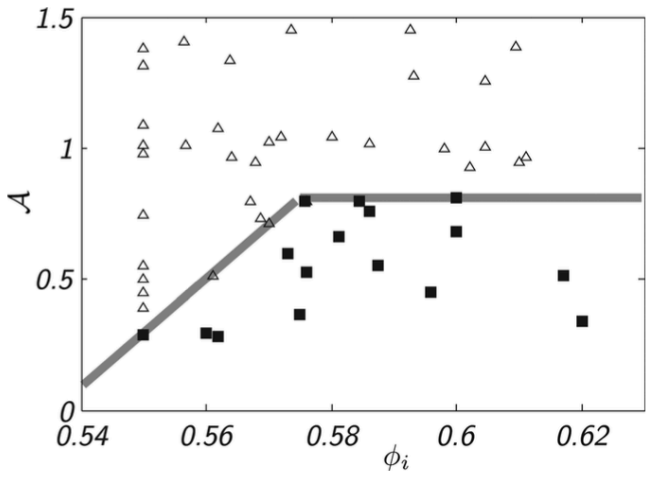

Figure 3.4: The two deposits morphologies observed (triangle △, trapezium ■) in the (A, ϕ_i) plane [6]. Experiment performed for this master thesis are added to this graph at the Figure 5.14 even if the fluid used to obtain this graph is a mixture of water and Ucon oil.

3.4 Liquid phase and flow regimes

Since the column is submerged, the surrounding fluid can affect the dynamics. According to Bougouin [41], the role of the surrounding fluid in the granular collapse remains uncertain and still deserves experimental investigation. Investigations have been carried by Courrech du Pont *et al.* [42] for the case of a rotating-drum configuration. With a rotating drum setup, results indicate the existence of three regimes (Figure 3.5): (i) a free-fall regime for which there is no fluid influence and that corresponds to the classical dry regime, and two regimes where the interstitial fluid governs the avalanche dynamics, namely (ii) a viscous regime and (iii) an inertial regime. These regimes were shown to depend on two dimensionless numbers, the Stokes number St (Equation 3.3) and the grain-fluid density ratio which will be called r (Equation 3.4).

$$St = \frac{1}{18\sqrt{2}} \frac{\sqrt{\rho_s \Delta\rho g d^3}}{\mu_f} \tag{3.3}$$

$$r = \left(\frac{\rho_s}{\rho_f}\right)^{\frac{1}{2}} \tag{3.4}$$

where symbols are the same as used in the chapter 2.

Bougouin [41] carried out experiments on dense column collapsing and managed to find these same three regimes (Figure 3.6).

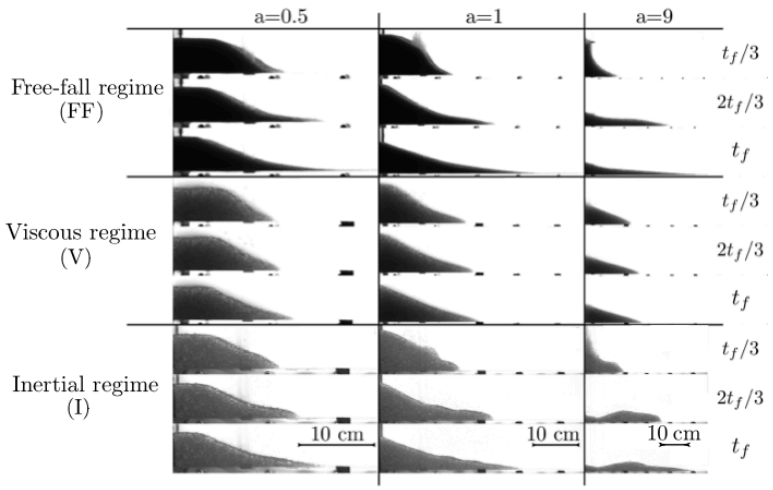

Figure 3.5: Snapshots of the granular collapse for regime FF, regime V, and regime I for three different aspect ratios and at three different times [41]

Situations such as rockfalls, pyroclastic flows can be related to the free-fall regime where the fluid can be neglected ($St \in [10^2; 10^8]$ an $r \in [40 : 50]$). In the case of submarine avalanches, the density ratio is characterized by $r \approx 1.5$ while the Stokes number can be found in the large range of $St \in [10^{-1}, 10^6]$. In these situations, the dynamics of the flow can belong to the inertial regime or the viscous regime, depending strongly on the grain size, and the influence of the fluid should therefore not be disregarded. Other atmospheric situations, such as snow avalanches or dust storms, can also lead to the situation of the inertial regime for which r remains moderate and $St \gg 1$. In our experiments, as written in the following section, $St = 17.73$ and $r = 1.64$. So it is expected to obtain data corresponding with the inertial regime.
Mutabaruka [21] has shown that it is necessary to analyse separately the collapse phase, where the particles acquire their kinetic energies, and the spreading phase where the energy acquired in the first phase controls the distance and stopping time. The effect of the fluid in the first phase is to dissipate some of the energy, while in the second phase it partially lubricates the contacts, thus reducing the dissipative effect of the drag forces.

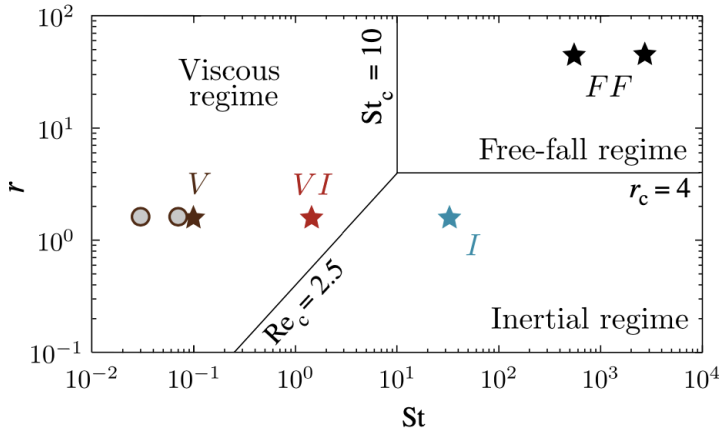

Figure 3.6: Granular-fluid flow regimes in the (St, r) plane. Stars and circles correspond to the experimental series performed in [41]

Chapter 4

Experimental setup

4.1 General information

The present thesis has been realised thanks to a channel (Figure 4.1) in the Laboratoire Essais Mécaniques Strutures et génie Civil (LEMSC) of the UCLouvain. B. Spinewine [44] and I. Fent [45] also have worked with this channel to obtain experimental data about dam breaks.
The channel has a length of 6 meters but only 1 meter would have been enough for our experimental case. The cross section is a rectangle of 0.25×0.5 meters. The walls are vertical, perfectly perpendicular to the bottom of the channel. They are made of transparent glass while the bottom of the channel is made of lined wood planes.

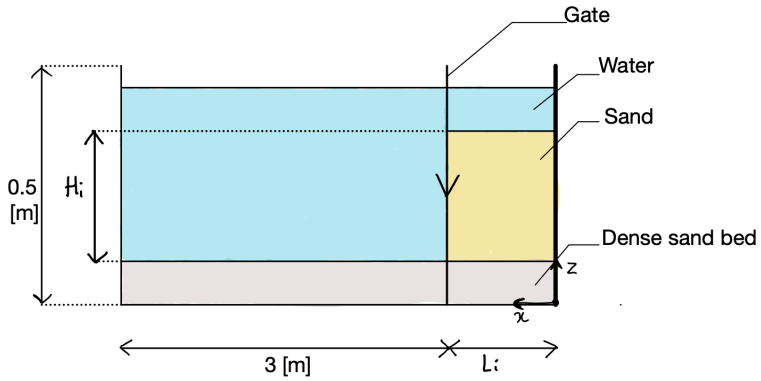

Figure 4.2: Experimental set-up

The width of the channel is neglected and the experiment is considered in the (x,z) plan as indicated in Figure 4.2. The gate separates the two sides of the channel. On one side is the sand column and an additional removable door that allows the length of the

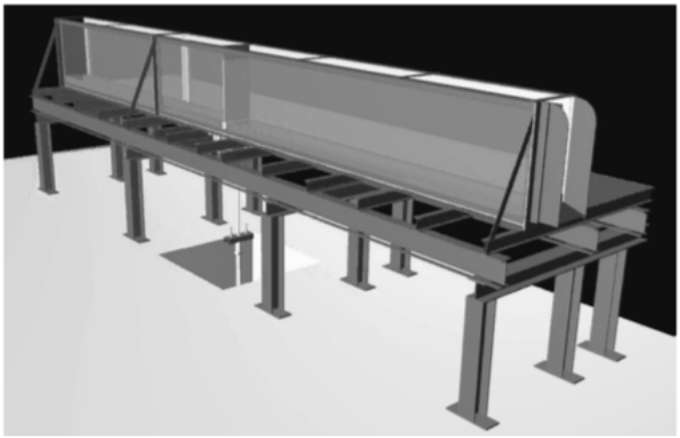

Figure 4.1: Overall view from Spinewine 2005 [43]

column to be chosen in x. On the other side, the channel is simply a tank filled with water. At the bottom of the channel, along its entire length, there is the compacted sand bed.
In the middle of the channel, there is a downward moving gate used to simulate the instantaneous collapse of the granular column. It is separated from the wall with two hollow and thin PVC pipes that ensure water tightness between the gate and the glass wall. The gate goes down very quickly thanks to a pneumatic system. This system contains a compressor, a compressed air receiver, a pressure gauge and a valve.
The pressure in the pneumatic system is equal to 8 bars. It is important to keep 8 bars to have a good repeatability from one experiment to another. The entire circuit to link the channel to the camera is controlled by a Programmable Logic Controller (PLC) associated with the software PFV (Photron Fastcam Viewer) version 3620. The buttons of the controller allow the door to be lowered or raised and this is linked to the camera trigger so that the recording starts when the door is lowered. The camera used to record experiments is a high speed camera and, more precisely, the Fastcam SA3 Photron. The fast camera offers high resolution images 1024 x 1024 pixel at frame rates up to 1000 fps. For our experiments, 500 fps is sufficient. The used lens is the Zeiss Distagon 2/25 mm ZF.2 lens.

We define parameters H_i and L_i as shown in Figure 4.2. These two parameters have to be chosen by the channel user depending on what is to be observed. In this master thesis, $H_i \in [20; 30][cm]$ and $L_i \in [15; 40][cm]$. In reality, it is the ratio H_i/L_i that matters as explained previously in the chapter 3. The time t_0, which represents the starting point of the collapse, is considered to be the moment when the top of the gate reaches the sand bed at the bottom of the channel as illustrated at Figure 4.21.
The extraction of data from the images is done either via `Matlab` or via *LaVision* depending on what is required.

Both sides of the channel are filled with water. The granular media is sand whose characteristics can be found in Table 4.1.

Figure 4.3: Picture of sand used in experiments

Characteristic of the sand	Value
Density	2682 kg/m^3
Median diameter	1.72 mm
Dry volumetric weight	14.54 kN/m^3
Porosity	0.42
Friction angle	38°

Table 4.1: Characteristics of sand used in experiments

Since fluid and solid of our experiments are known, the flow regime in which the experiment takes place can be determined thanks to both equation 3.3 and 3.4 given by Bougouin *et al.*[41]. For a Stokes number $St = 17.73$ and the grain-fluid density ratio $r = 1.64$, we expect to be in the inertial regime.

4.2 Image processing

4.2.1 Davis

`DaVis 8 (LaVision)` is the software used to compute velocities by the non-intrusive method PIV (Particle Image Velocimetry) from the images of the laboratory experiments. This method gives velocity vectors from two or more images of the observed flow. Our videos are composed of 1361 images recorded by the high-speed camera. Usually, the detection of velocity by PIV requires a tracer of particle and the illumination of the studied longitudinal section (parallel to the walls) thanks to a laser sheet. Nevertheless, in our case, the sand suspended in the water in the vortices interferes with the ability of the laser to illuminate the entire study area. It is why the luminosity of the experiment required several attempts to detect particles via `Davis 8` as discussed in subsection 4.3.1. Analysis of water velocities could be considered. However, in this Master's thesis, attention is paid to the movement of sand.

Once the snapshot of the calibration plate is uploaded, the calibration of all images recorded during the experiment is automatically completed by the software (See section 4.3.2). Preprocessing is performed on the images after they have been calibrated. Thus, an intensity particle normalization is done and geometric masks can be applied to take into account only the desired areas of the image (See Appendix C.1 and C.2).

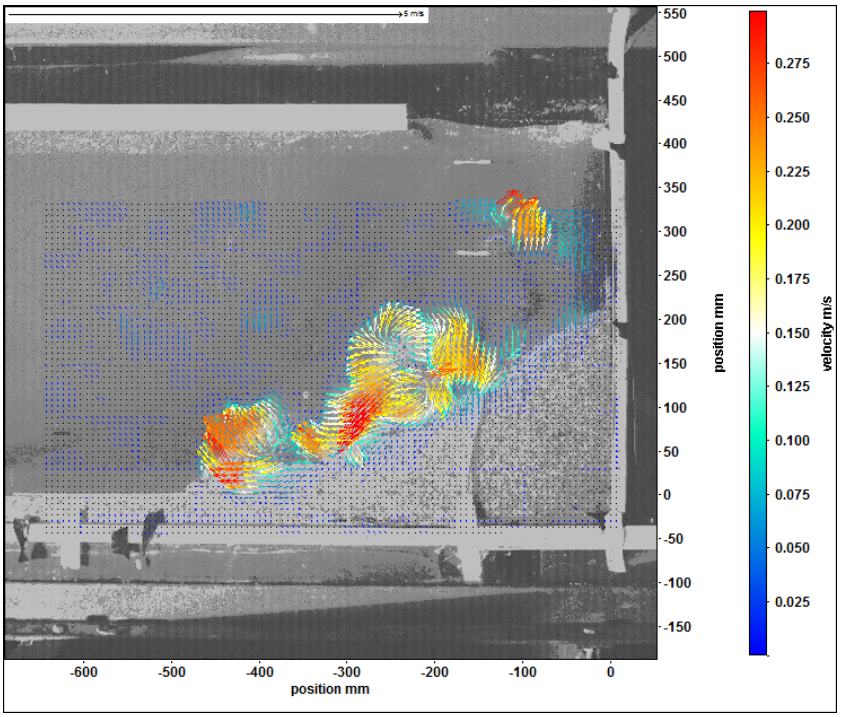

Figure 4.4: Example of figure obtained via `Davis 8`

Thereafter, as indicated in [46] on the website of `LaVision`, to apply the detection of velocity, images are divided into small interrogation windows. During the time interval dt between two images, the particles of each interrogation window move by a displacement ds. The velocity is then given by the ratio ds/dt.

Finally, a multi-pass post-processing is performed to remove outliers and vectors detected with too little correlation between the different time steps. Indeed, some particles are detected going from a time t to a time t+1 with a too low probability of existing; the correlation between the two interrogation windows is low. In this case, it is better to delete them.

Since Davis 8 is not used with a laser, the detection is not ideal and the challenge is to find this out which time interval between two images is best to obtain the desired vectors and which geometric mask gives the best result. In our case, for 500 fps recordings, the PIV analysis is done with an increment between 10 and 25 dt between 2 images. Geometric masks are chosen to target the movement to be observed.

An example of the figures we obtain is shown on Figure 4.4. The *Display* tool of `LaVision` allows you to change the quantity of vectors displayed, the size of these vectors and their color palette (See Appendix C.3).

4.2.2 Matlab

When aiming at studying the shape of deposit and the water level variation of the free surface during the collapse of the column, `Matlab` is relatively efficient. The image processing consists of choosing the moments of the collapse that are going to be analysed, displaying them via `Matlab` and the `imread()` and `imshow()` functions. Then, via `ginput()`, the origin of the reference frame is manually placed and the points delimiting the desired interfaces are selected. It should be possible to implement a `Matlab` routine that automatically detects these interfaces but this would be time consuming and not much better. In order to be as accurate as possible, it is useful to select a large number of points. Once the interfaces are plotted, it is necessary to convert from pixels to centimetres thanks to the tape measures placed horizontally and vertically on the channel walls. Finally, to compare more easily graphs and simulation results a simple orthogonal translation is done. This procedure is considered acceptable in view of the low or non-existent distortion due to the lens presented later in the subsection 4.3.2.

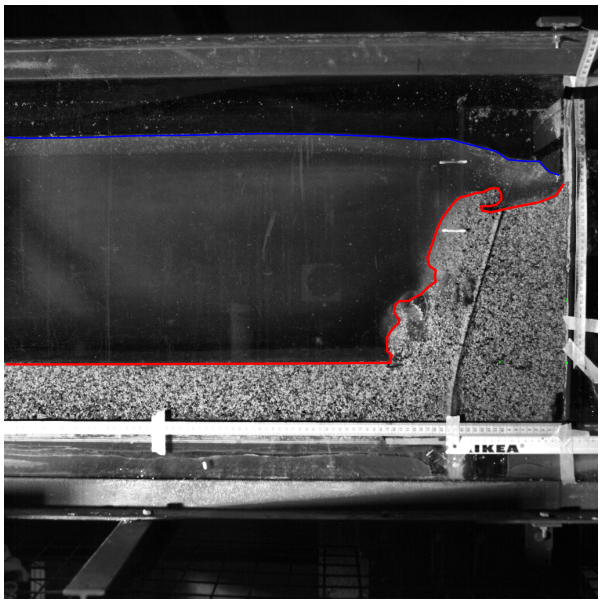

Figure 4.5: Example of image obtained with the `Matlab` procedure. The graph obtained with these interfaces is available in the appendices at Figure C.4.

4.3 Experimental procedure

The assumption is made that the observed flow is two dimensional, the width of the flume is neglected since walls are smooth and closely spaced. The involved forces are in

the 2-D plane (x,z). The flume and the gate are assumed to be perfectly watertight even if in reality water permanently flows out at the bottom of the channel along the gate. The gate opening is considered instantaneous.
First, the bed surface is made flat. Then, the flume is filled with water. Only after having half-filled the right side of the channel, the sand is poured to form the column. This prevents bubbles from escaping out. It minimises the presence of air between the grains. This procedure also leads to the loosest possible column. After that, the water level on both sides of the gate is adjusted to be the same. Finally, the gate is opened and this triggers both the collapse of the column and the recording.

4.3.1 Luminosity and contrast

The PIV made thanks to `Davis 8` uses the contrast of grey images to detect particles. Usually, to do that, experiments are performed in the dark with a laser sheet to light on the experiment area. In our case, since a laser would not pass through the sand, it was necessary to bring a source of light. Several trials have been done and the best found solution is to use a spotlight illuminating the front channel and positioned diagonally to avoid light reflections. It enables to observe the behaviour inside the column and to better detect particles thanks to PIV than in the darkness.
In addition to the luminosity, to increase the contrast and delete some visual disturbances, a plain background has been put. A white one was less efficient than a black one to ignore reflections. The recorded images are similar to the one shown in Figure 4.8.

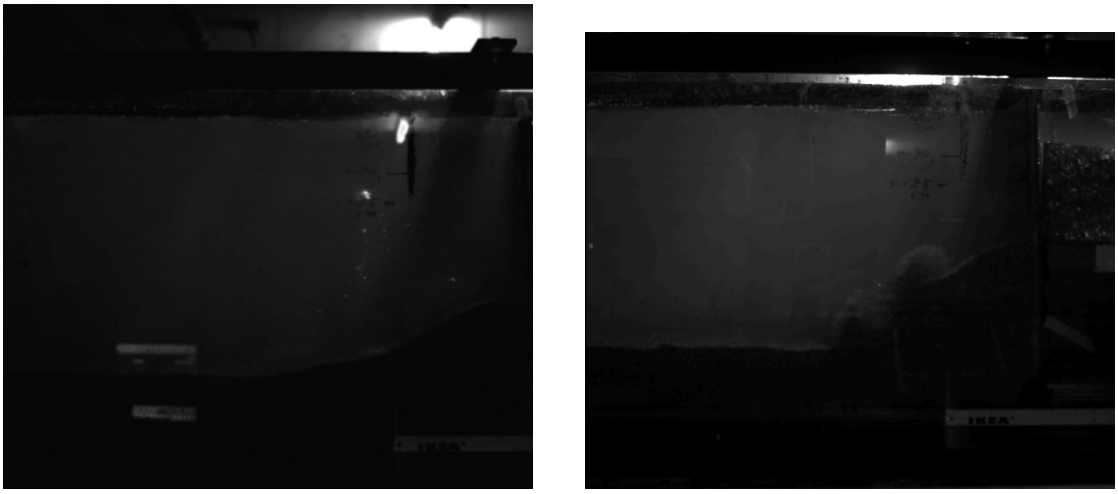

(a) Without plain background (b) With white plain background

Figure 4.6: Visibility with the light on

(a) Spotlight placed parallel to the plane of the channel

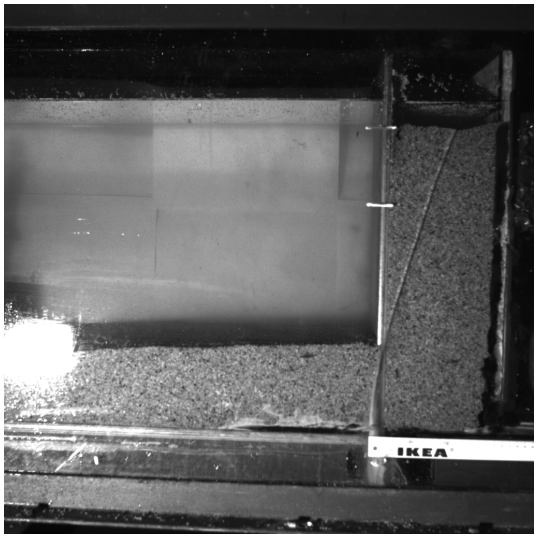

(b) Spotlight placed in front of the channel

Figure 4.7: Visibility light off with white background and a spotlight

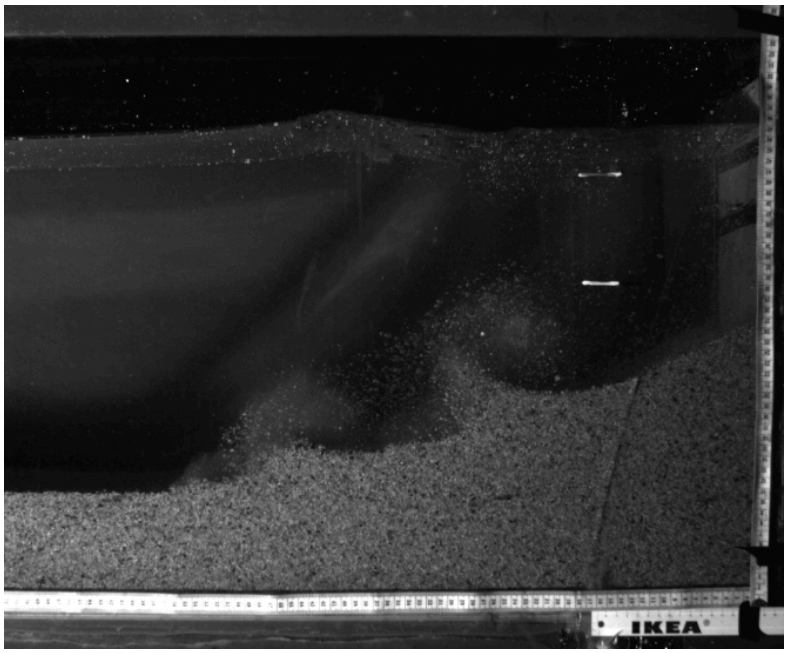

Figure 4.8: Final luminosity and contrast with light off, black background and spotlight oriented from the front

4.3.2 Calibration

Pictures can suffer from distortion depending on the lens used (Figure 4.9) or due to water (Figure 4.10). Since it was planned to use the DaVis Software to analyse the recordings of our experiments, it was recommended to carry out a calibration.

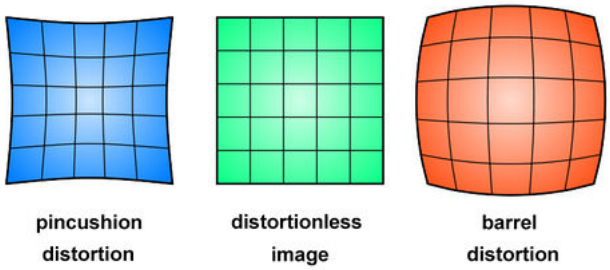

Figure 4.9: Types of distortion due to the lens of the camera [47]

(a) Without water (b) Half filled with water

Figure 4.10: Distorsion due to water [48]

For this purpose, before starting the experiment, the camera is placed in front of the channel filled with water. The balancing of the camera is tested and an image of the calibration plate is taken. This picture will be numerically corrected to delete effects of distortion. The calibration plate used is the one on the left of Figure 4.11 and in Figure 4.12. It is placed vertically inside the water. The perpendicularity of the calibration plate is verified by the `DaVis` spirit level command. The calibration of all the other images recorded during the experiment is automatically completed by the software DaVis (LaVision), once the calibration plate is uploaded.

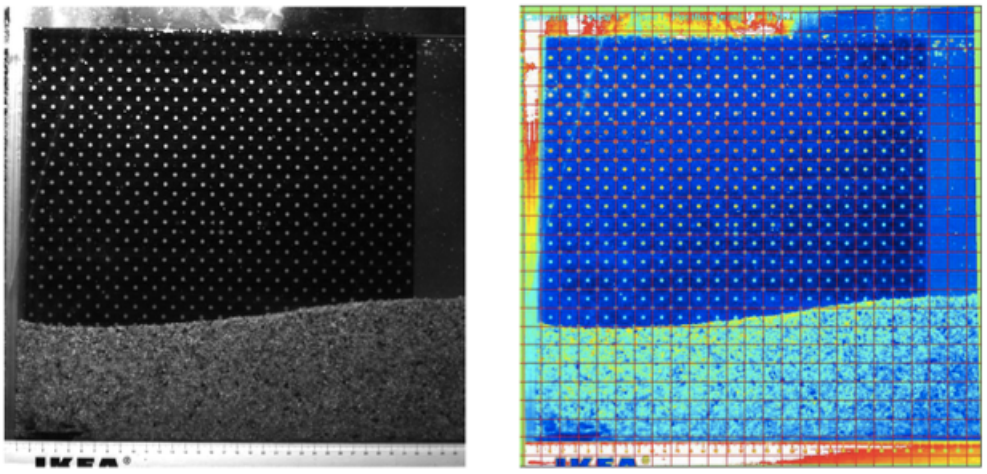

Figure 4.11: Before/after illustration of calibration via the software LaVision. From Master thesis of Donifan Camacho and Pauline Radelet

However, it is quite complicated to do an automatic calibration of all the images recorded via Matlab. This is why it is useful to ask whether a calibration is, in our case, necessary. The real dimensions of the calibration plate are known. Between two consecutive dots, there is 15 millimeters. Images in `Matlab` are in pixels. If there is no distortion, the distance between two points should be the same number of pixels regardless of the location of the points on the image. This would indicate that in the pixel image, the distance between two points does not depend on where they are located and is always equal to 15 millimeters like in reality. To test this possible distortion, the photo taken for calibration is loaded into `Matlab`. Then, via the function `imread()` and `imshow()`, the position of certain points in pixels is recorded. It is then easy to see that the pixel distance between two points on the calibration sheet is the same for the green points and for the light blue points but also quite the same for the red points and for the dark blue points.
We can conclude that the measurements taken via `imread()` and `imshow()` on images as well as those taken via the camera placed 1m10 from the channel are valid without any calibration and that the distortion is negligible or non-existent for this type of treatment. Based on the Figure 4.12, for experimental trials recorded when the camera is placed 1m10 from the channel wall, 1 centimeter in the reality is approximately represented by 12.48 pixels in the recordings.

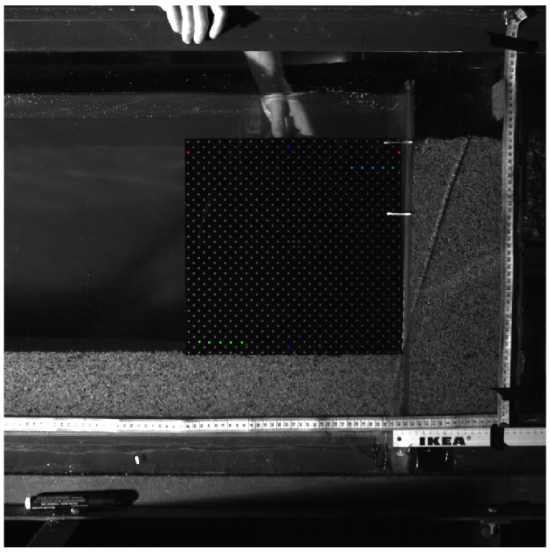

Figure 4.12: Research of possible distortion of image

4.3.3 Repeatability

It is important to be sure that the experimental data collected are not random and are repeatable. We consider the gate opening instantaneous and to improve the repeatability of the tests, we always follow the same procedure for each test. From the videos, `Matlab` is used to manually detect interfaces via `imread()` and `ginput()`. Then, the conversion between pixel data and centimeters is done and interfaces curves are plotted. For three runs with the same initial conditions, we observe the final deposits in Figure 4.13. The deposit is considered final when there are no more grains that are in movement. It is not expected that the dust and the last grains in suspension in the water will completely fall out because it would take much longer than what is recorded in the videos. Some example of final deposit are shown in section 5.1. The average time needed to observe the final deposit with no more particle in movement is respectively equal to 2.542 , 2.306 and 2.352 seconds. It is assumed that the good similarity between the final deposits and between the duration of the collapse indicates that the collapsing features are also similar.

This assumption is quite verified thanks to the Figure 4.14 which is the graph of the interface after 0.816 seconds for three runs without considering vortices as illustrated by the image of Figure 4.15. The experiment is therefore repeatable. The difference between the three deposits is quite small. The mean curve and the standard deviation are calculated at 18 different locations for the three trials along the final deposit. On these 18 positions, the average standard deviation is 0.3736 [cm].

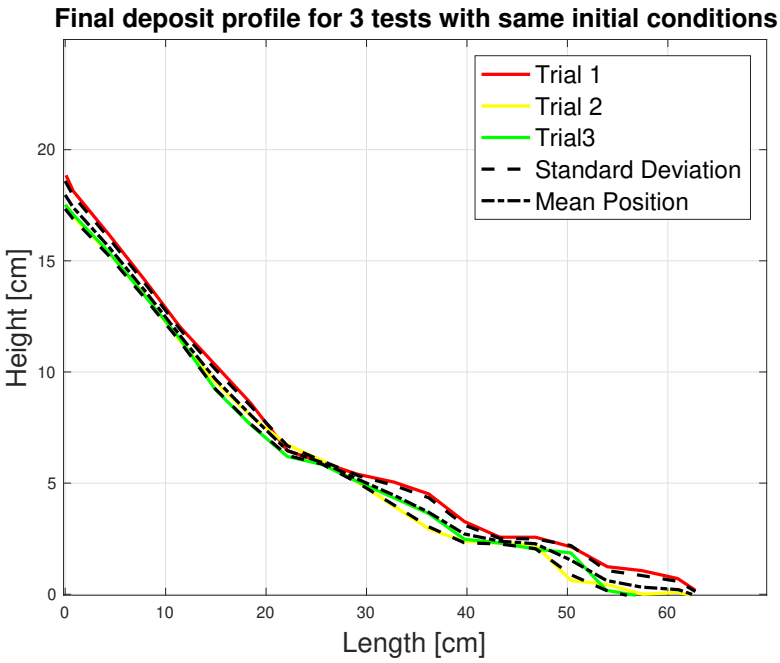

Figure 4.13: Illustration of the repeatability of the experiment (initial conditions of loose column and aspect ratio of 2)

Figure 4.14: Profile of interfaces after 0.816 [s] without taking into account the vortices of sand in suspension in the water

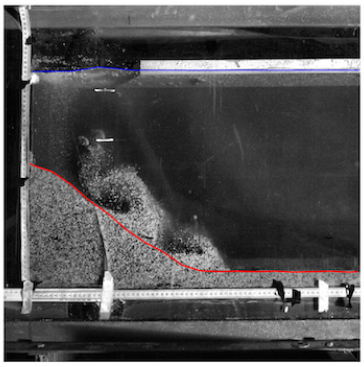

Figure 4.15: Envelope of the intermediate sand deposit without taking into account the vortices in movement

4.4 Limits of experiments

4.4.1 Wall effect

The walls would have an effect on the flow, but to carry out our experiments it is essential to have a volume bounded by transparent walls. These sidewalls exert shear stresses which are here assumed to be negligible. In the present thesis, the flow is assumed to be two-dimensional and effects of sidewall friction are neglected. No noticeable transverse variation is observed during the flow, indicating that wall effects are negligible and that the flow is essentially two-dimensional. Furthermore, the walls are made of glass with a very low roughness.

4.4.2 Free surface

In a small reservoir, one could think the free surface movement has an influence on the velocities, movements and position of particles. Even if the gate opening is considered to be instantaneous as discussed in subsection 4.4.3, it induces waves visible to the naked eye. A proposed solution is to put a floating polystyrene panel on the water surface downstream of the gate to avoid large waves.

In order to check the efficiency of this polystyrene panel, two experiments are considered; both with a column of aspect ratio $A = 1$. One experiment is with the panel and the other one is without the panel. Seven moments of each experiment are selected. The interval time between two images is equal to 0.4 seconds. The mean initial position of the water and the position of the gate are drawn. Then, with the procedure `Matlab` of the subsection 4.2.2, the water surface position is stored for forty x-axis positions for each seven free-surface configuration (which correspond to the seven selected moments). At each of these forty positions, the mean and the standard deviation over the seven steps are computed. The black lines represent the curves of the mean and of the mean plus and minus the standard deviation.

At Figure 4.16, one can see the mean level of water is below the mean initial level of water. It indicates that before recording, the level of water was already oscillating. When the recording began, the water level was therefore high, but the rest of the test is done during a downward oscillation. By the way the mean position at the step 7 would be lower than the mean position at step 1. The highest level of water is found to be during the step 4 near the gate. It is possible that the step 4 corresponds to the moment where the wave induced by the gate opening reaches the gate after bouncing against the end of the channel.

At Figure 4.17, the highest wave is the wave at the step 7 at the x-axis 0. The mean level of water is really close to the mean initial level of water. The surface of water seems to be really horizontal and regular along the polystyrene panel and the waves are located where there is no panel. Thanks to the Figure 4.18, one can observe that the

polystyrene panel does not reduce the variation of level above the initial column and that the variation of the water level along the channel does not decrease significantly in the presence of the polystyrene panel. It is probably due to the fact that the panel is shorter than the length of the canal. It is very difficult to reproduce exactly the same free surface movement twice because of the simple fact that the water level on the side of the column falls much faster than the water level on the other side. Therefore, observations could be due to initial conditions which were not ideal. In other words, the trials are realised with a free surface initially already in motion. Besides, a difference in water level on both sides of the gate before it opens impact a lot the free surface movement and it is not so easy to ensure a constant water level due to the rapid flow of water below the gate.

What is ultimately important for the free surface is whether its movement significantly influences the collapse of the column. To find out this, Figure 4.19 has been produced. It compares the collapse of the column at three different times. The dotted lines are the shapes for the test performed without the polystyrene panel and the solid lines are with the panel. The panel and the water surface movement do not seem to influence much the behaviour of a loose column with an initial aspect ratio of 1.

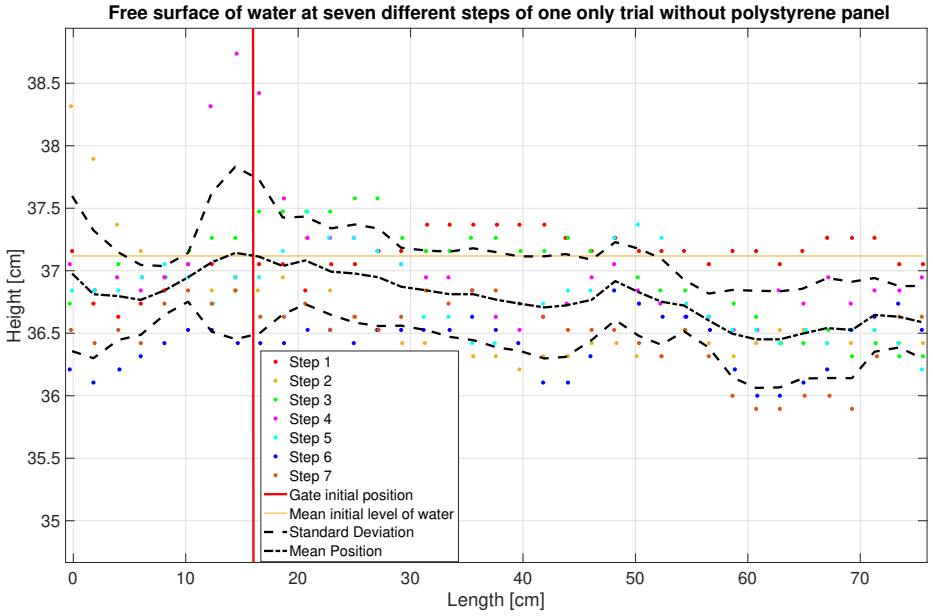

Figure 4.16: Evolution of the water free surface for a trial without polystyrene panel

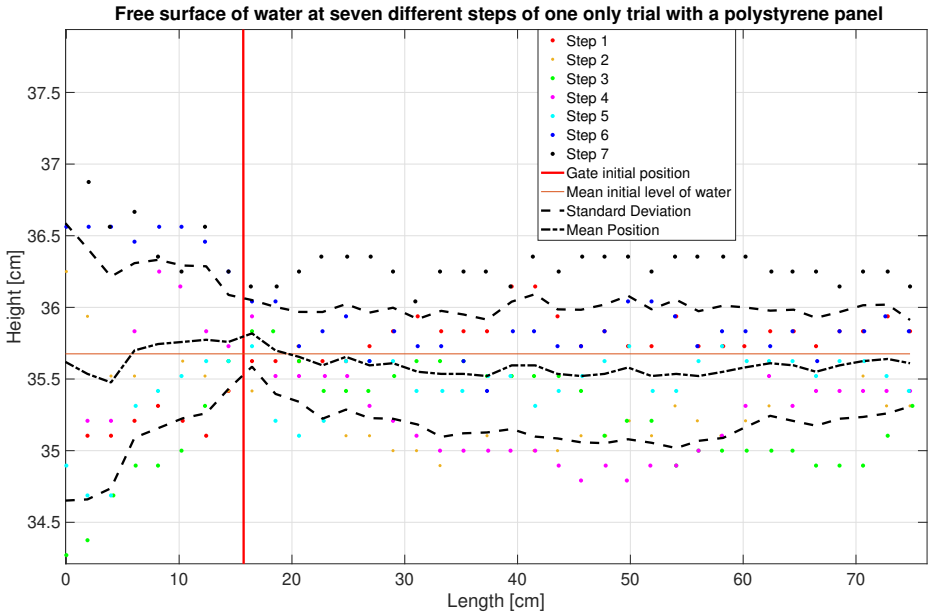

Figure 4.17: Evolution of the water free surface for a trial with a polystyrene panel

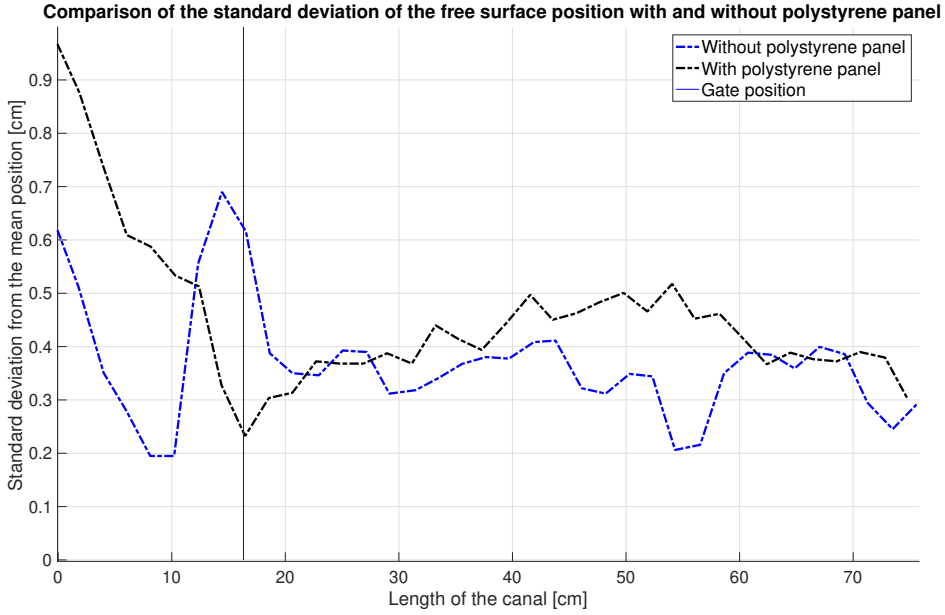

Figure 4.18: Standard deviations of water surface position with and without polystyrene panel

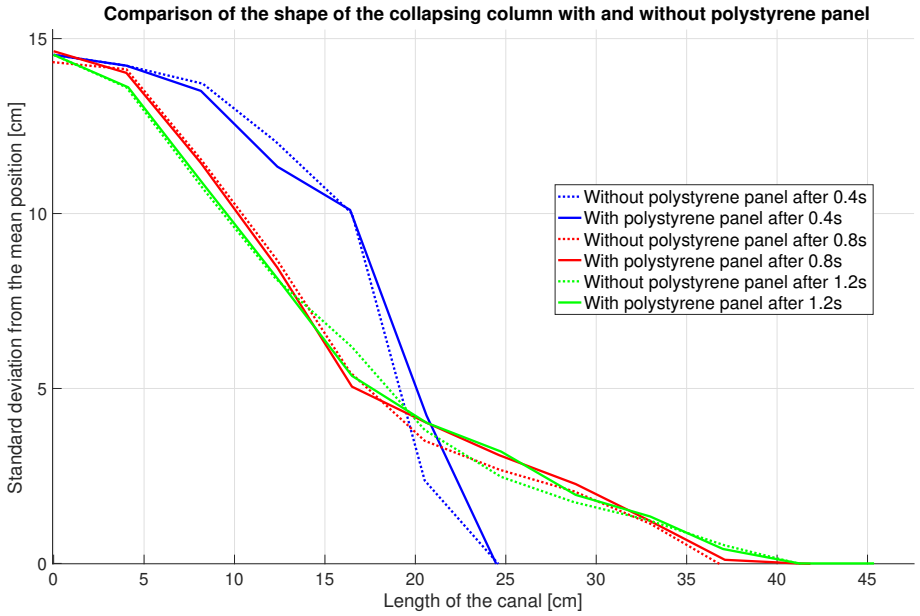

Figure 4.19: Comparison of the final deposit for trial between with and without polystyrene panel experiment

4.4.3 Gate opening

Granular column experiments in literature such as those presented in the state of the art are usually performed with a rising gate. However, in order to have initial conditions as close as possible to instantaneous collapsing, the gate of the flume used to obtain our experimental data is a lowering gate. A lowering gate has been considered to avoid disadvantages of a rising gate (Figure 4.20) as explain and illustrated in the work of Spinewine [43].

First, with a rising gate, the effect of the removal is felt first in the bed region where the pressure is maximal and the flow of granular particles can begin before the gate reaches the top of the column. Secondly, by friction, the gate tends to drag grains of sand with it and can disturb the water free surface. Thirdly, the strong depression created by the void left under the rising gate, induces an effect of suction that further eases the mobilisation of substantial lumps of sediments swept vertically.

A lowering gate makes it more complicated to obtain the water tightness of the flume and requires to put the flume high enough to have sufficient space to store the gate itself.

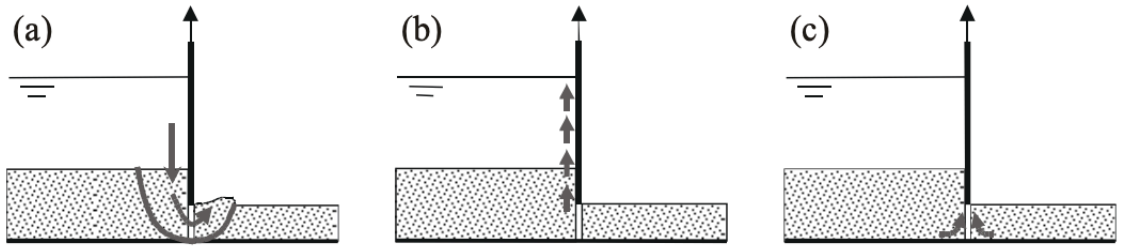

Figure 4.20: Drawbacks of a rising gate system, inducing movements during gradual lifting as a result of (a) mass failure; (b) friction; (c) depression and suction. [43]

The averaged time period needed to completely open the gate when the aspect ratio is the largest (A=2) with a a 3cm thick bed is equal to 0.138 seconds with a standard deviation of 0.0075 [s]. This time of opening is 6.39% of the collapse duration of our reference experiment under these initial conditions. To compute these data, the time t_0 is the instant when the gate reaches the free surface.

The faster the gate opens, the more we will tend towards the initial conditions of instantaneousness. In the frame of research about dam break, Lauber and Hager [49] proposed a criterion to determine if the removal time t_r of the gate is instantaneous depending on the initial water depth h_0 and the gravity acceleration g. Even if it is a criterion (Inequality 4.1) designed for a dam break experiment with only water flowing, it can give an indication regarding the speed at which the door opens.

$$t_r < \sqrt{\frac{2h_0}{g}} \tag{4.1}$$

In our case, for a 30 cm high column and h_0 equal to 41[cm], we have $t_r = 0.138[s]$ which is lower than the computed criterion of 0.289 [s]. So, our gate opening can be considered as instantaneous.
Furthermore, the opening of the gate is considered as not significant since the column remains rectangular after the gate has reached the sediment bed such as illustrated at Figure 4.21.

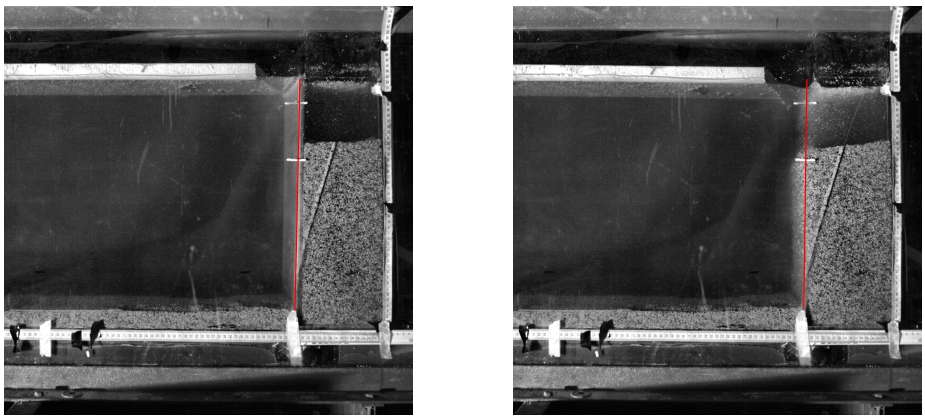

(a) Flume and column with closed gate

(b) Initial conditions after the gate opening; Instant when the gate reaches the sand bed which is the instant t_0

Figure 4.21: Disturbances on the initial conditions due to the opening of the door. The red line is the position of the gate before it has started to move.

Chapter 5

Experimental results

5.1 Parametric study with respect to the aspect ratio and its impact on the collapse of columns

First, the behaviour of each different aspect ratio is described on the basis of original recordings. The `Matlab` procedure is then applied. With the obtained graphs, different aspect ratios are compared with each other in terms of collapsing duration, mobility, repose angle and shape of deposit. Velocities are finally observed from original recordings through `Davis 8`.

5.1.1 Collapse behavior

Aspect ratio A=0.5
As soon as the gate opens, the top corner on the gate side collapses. Quickly after the gate opening, two vortices are generated; one at the top corner and one at the bottom corner. They move forward until they disappear at the same time. The final shape is trapezoidal with a small bump at the end of the run out distance.

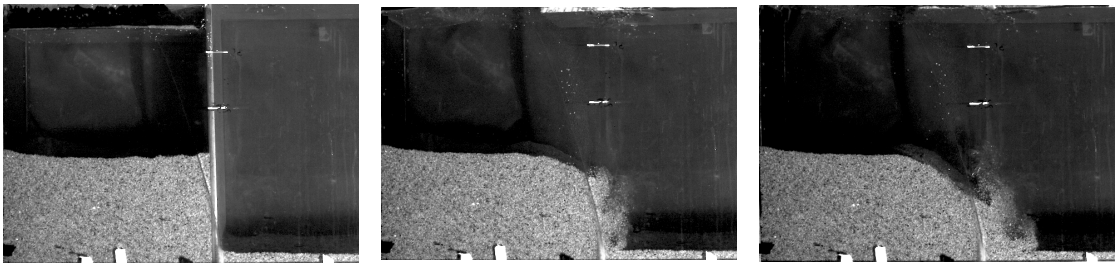

Figure 5.1: Successive stages of a collapsing column of aspect ratio $A = 0.5$

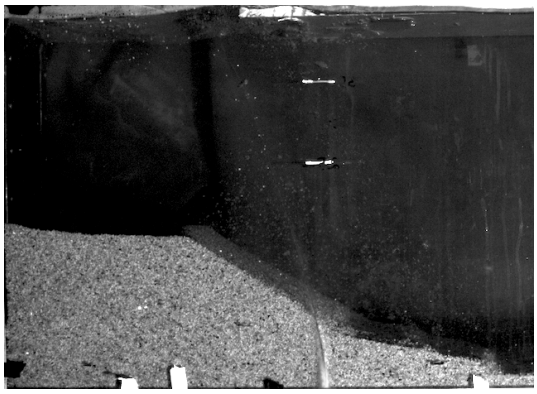

Figure 5.2: Final deposit of a collapsing column of aspect ratio $A = 0.5$

Aspect ratio A=1

Once the gate is opened, the top corner collapses and one vortex is created. It only becomes a vortex with evident recirculation when it reaches the bottom of the canal. While the vortex advances, the rest of the top of the initial column collapses too as confirmed via `Davis 8` on Figure 5.20. A triangular deposit is finally observed.

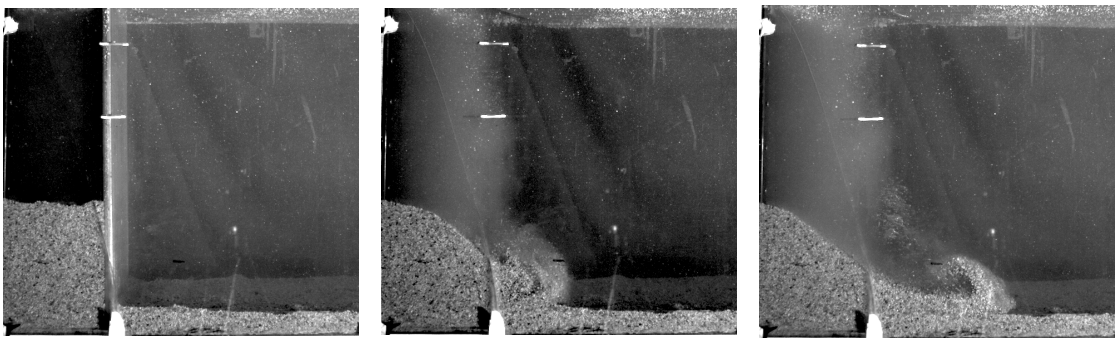

Figure 5.3: Successive stages of collapse of a column of aspect ratio $A = 1$

Aspect ratio A=1.5

Concerning the column with an aspect ratio $A = 1.5$, the vortex seems to be smaller and weaker. It is not directly created after the gate opening. It is generated at the front of the collapse and it disappears quickly. The final deposit is once more a triangle.

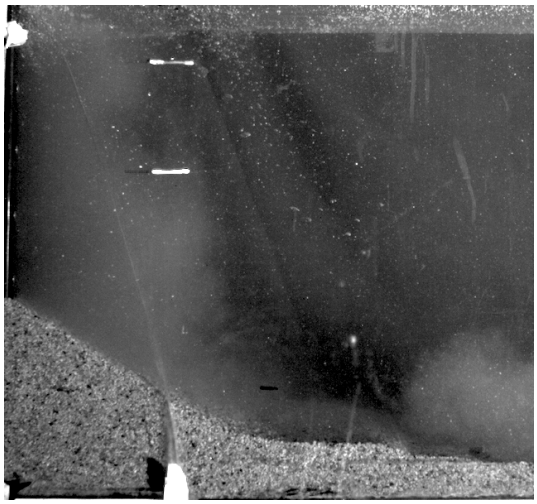

Figure 5.4: Final deposit of a initial column of aspect ratio $A = 1$

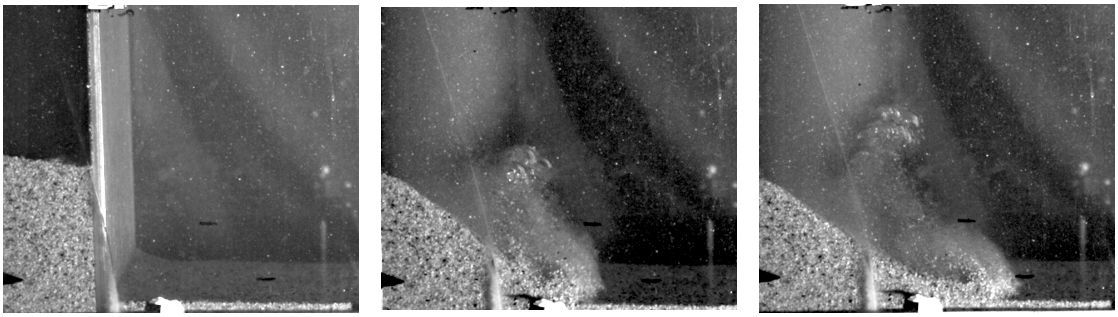

Figure 5.5: Successive stages of a column's collapse of aspect ratio $A = 1.5$

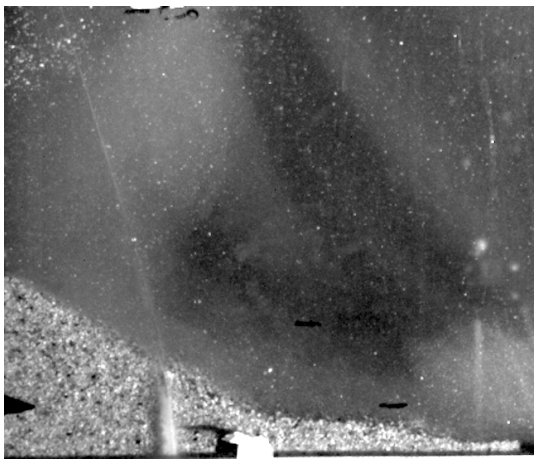

Figure 5.6: Final deposit of an initial column of aspect ratio $A = 1.5$

Aspect ratio A=2

The column of $A = 2$ starts by collapsing on itself while the top corner collapses to the downstream. One vortex is created at the bottom of the column while another bigger one is generated where the top corner is collapsing. Both vortices move forward during the collapse of the column. When the vortices have disappeared, the deposit no longer moves and a triangular final deposit is observed.

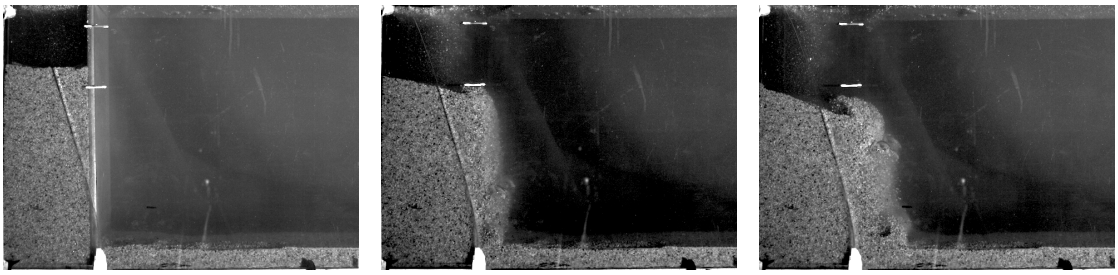

Figure 5.7: Successive stages of a column's collapse of aspect ratio equal to 2

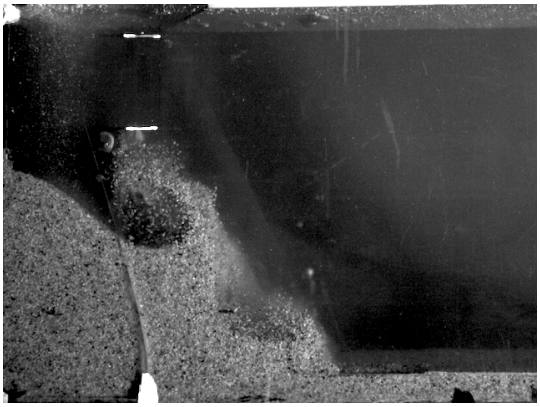

Figure 5.8: Vortex advancement of a collapsing column of aspect ratio of 2

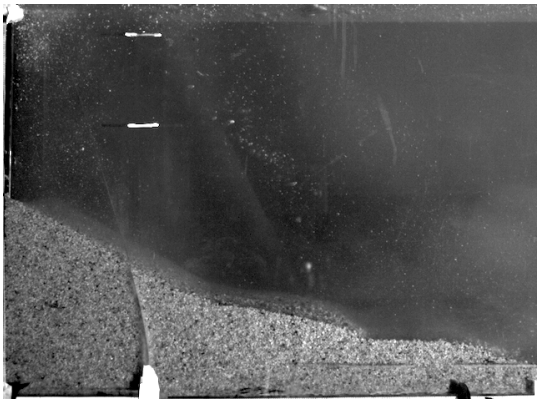

Figure 5.9: Final deposit of the collapsing of column of aspect ratio equal to 2

5.1.2 Interfaces analysis through the `Matlab` procedure

The Figures 5.10, 5.11, 5.12 and 5.13 are graphs obtained following the `Matlab` procedure developed in section 4.2.2 for four different aspect ratios. The main data to be interpreted via these graphs are the H_f/H_i ratio, the spreading distance and the shape of the deposit. The height H_f is the height of the final deposit at the origin while H_i is the initial height of the column. They can be equal or different.

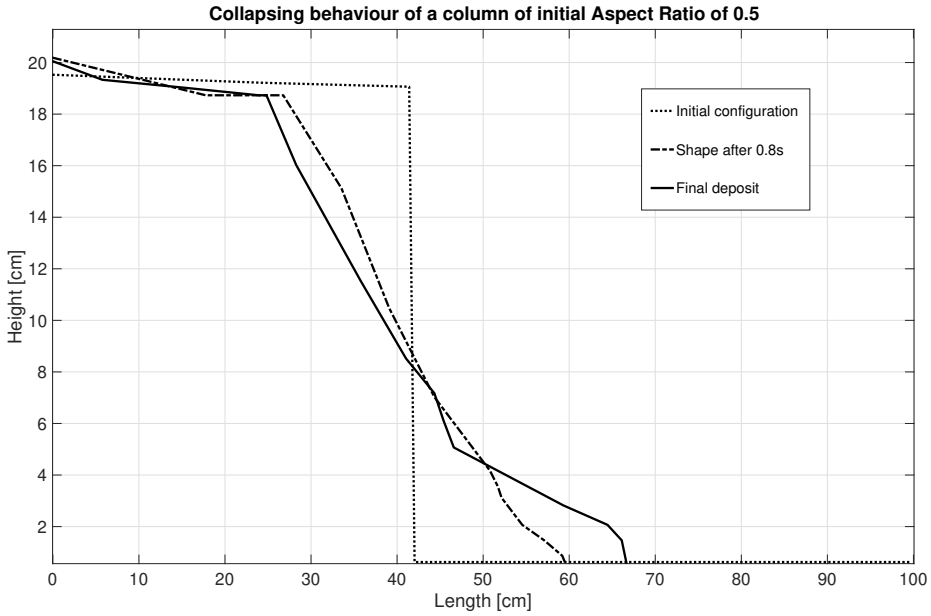

Figure 5.10: Experimental shape observed in a column collapsing. Initial aspect ratio $A = 0.5$

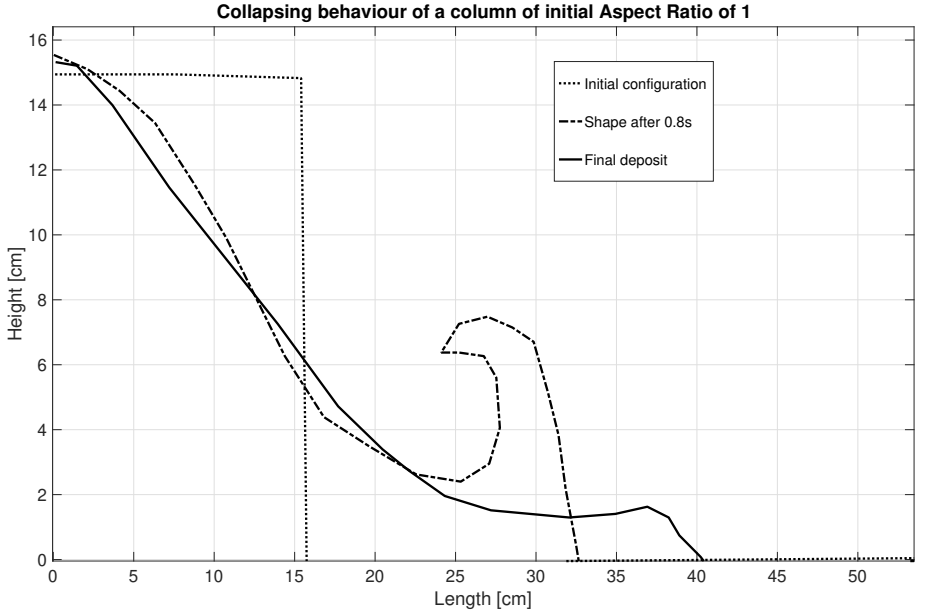

Figure 5.11: Experimental shape observed in a column collapsing. Initial aspect ratio $A = 1$

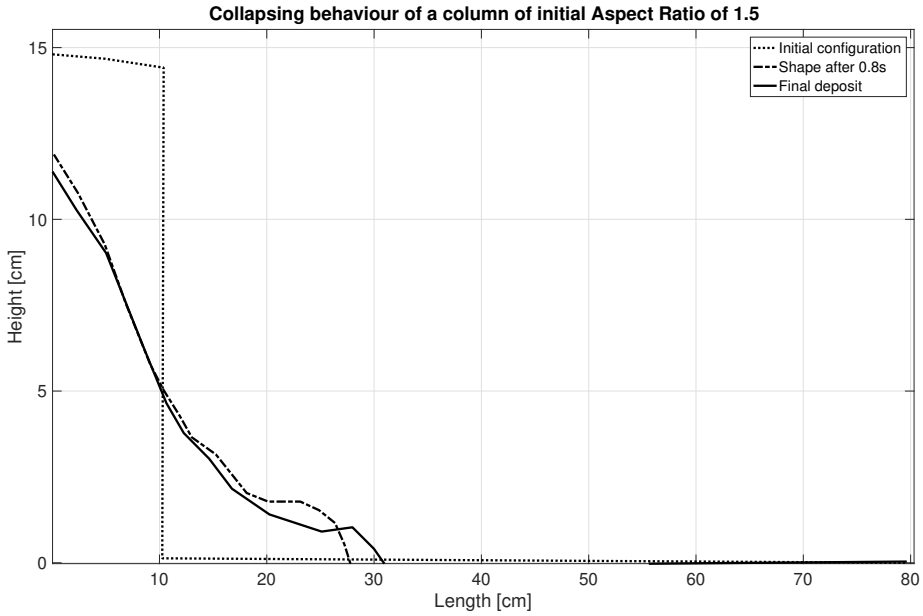

Figure 5.12: Experimental shape observed in a column collapsing. Initial aspect ratio $A = 1.5$

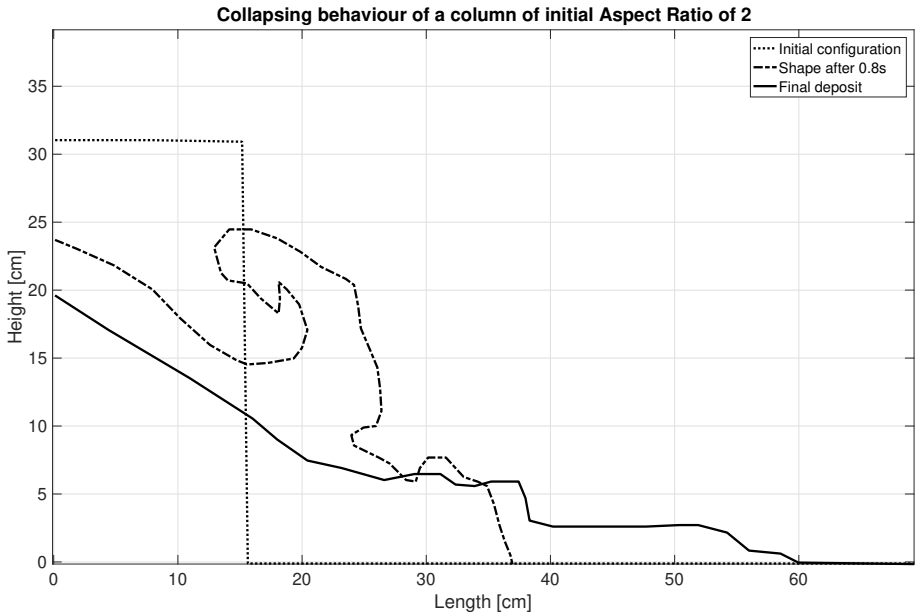

Figure 5.13: Experimental shape observed in a column collapsing. Initial aspect ratio $A = 2$

First, it can be observed that for lower aspect ratios (A equal to 0.5 and 1), the top left corner does not seem to move during the collapse while for aspect ratios of 1.5 and 2, the final height H_f is clearly lower than the initial height H_i. The ratio H_f/H_i is equal to 0.77 for $A = 1.5$ and it is equal to 0.67 for $A = 2$. It is from the beginning of the collapse that the height of the column decreases and goes from H_i to H_f. For the aspect ratios of 1.5 and 2, it can clearly be seen in the videos of the experiments that the column collapses on itself before collapsing to the side. This will be illustrated on Figure 5.19.

As far as the shape of the final deposit is concerned, only the column with an aspect ratio $A = 0.5$ is a trapezium. The three others are triangular. This is consistent with the critical value of $A_H = 0.8$ observed by Rondon *et al.* [6]. This critical value A_H have however been computed for dense column. As it can be observed at Figure 5.14, the column with an aspect ratio of 0.5 could have a triangular or a trapezoidal final deposit if the fluid was the same as the one Rondon *et al.* [6] used in their experiments (Ucon oil-water). For a volume fraction assumed to be $\phi = 0.55$ it should be a triangle whereas experimental results in water show a trapezoidal final deposit.

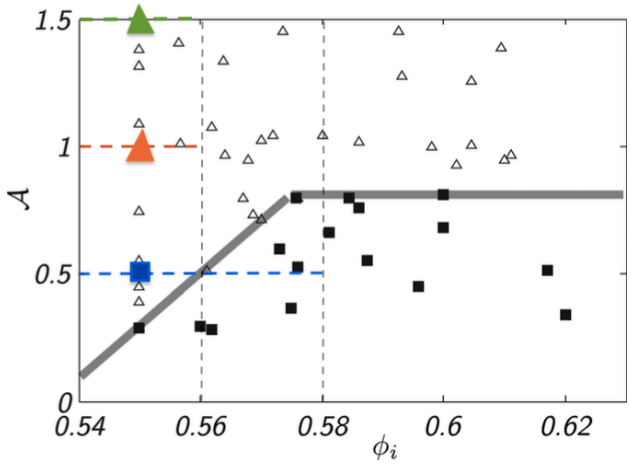

Figure 5.14: Adapted from the graph of Rondon *et al.*[6] where the fluid was a mixture of Ucon oil and water and the granular media is composed of glass beads. The experiments of this master thesis are added to the graph. Squares illustrate trapezoidal final deposit and triangles illustrate triangular final deposit. The colored symbols represent the experimental data of this master thesis in water.

The spreading distance can be considered as the run out distance L_f or as the difference between the final and the initial length L.

	A=0.5	A=1	A=1.5	A=2
L[cm]	15	25	20	45
α [degrees]	35.13	30.96	28.81	29.05
T[/]	0.1773	0.1293	0.0957	0.2355

Figure 5.15: Data on the final deposit of the collapse

The slope angle of the left part of the final deposit at rest illustrated in Figure 5.16 is called the repose angle of deposit α and is given in the table 5.15 above. Values might be inaccurate since the deposit is not a perfect triangle.

Equation 3.2 gives the expression of the dimensionless time T. For each aspect ratio, this time T can be computed and values are available in the table 5.15. These values don't reflect what it was expected. Indeed, with particles of diameter of 2.5 [mm] and aspect ratios 1.2, 1.5 and 1.9, Lacaze *et al.* [5] claimed to have a dimensionless time T decreasing with an increasing aspect ratio. It is the case in our experiments except for $A = 2$. In that case, the time T is the longest.

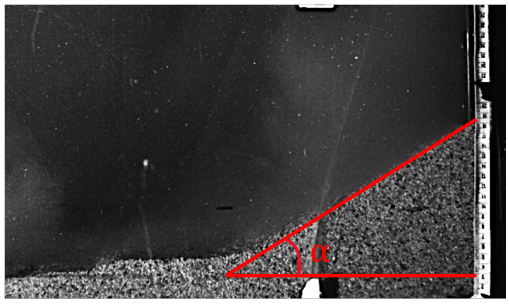

Figure 5.16: Definition of the repose angle of deposit α

5.1.3 Velocities analysis through `Davis 8`

The PIV analysis of the recordings should enable us to observe the velocities of the grains during the collapse. The result for some experiments is however not always what we expected. Indeed, the vortices observed for the columns of aspect ratio $A = 1.5$ and $A = 0.5$ are not detected by `Davis 8`.

Some of the vectors obtained give an approximate idea of the involved velocities. Nevertheless, these data should be considered with precaution. Indeed, `Davis 8` is not initially created for an use without laser. It would also be necessary to compare these vectors with other experiments and certain models. Directions of vectors however fit with what is observable with the naked eye. The background of the vectors is the image used to detect these vectors. This is how we can verify that the vectors coincide with the real movement of the sand even if some vectors are not correct.

As an example, the waves on the free surface are detected by `Davis 8` whereas no tracer is added to water and no laser is used. It is so possible with `Davis 8` to detect unwanted vectors. The movements of the water with the polystyrene panel can be observed (See Appendix C.7 and C.8). Velocities detected when we use a panel are lower than without a panel. In both case, the observed wave goes upstream of the granular collapse, bounces against the wall on the right of the picture and comes back downstream.

Considering that the detected vectors coincide with what is seen on the videos taken in the laboratory, it is feasible to observe the obtained velocities via `Davis 8`.

First of all, as expected for flows in the inertial regime (See Figure 3.5 and Figure 3.6), there are two collapsing phases highlighted by Mutabaruka [21]. The first is when the grains acquire kinetic energy (See Figure 5.17) and the second is when they lose it. This loss of energy determines the run out distance and the collapsing time (See Figure 5.18). These two phases are also observed in the simulations of the next Chapter. During phase 1, as observed on Figure 5.17, the column first collapses on itself and the velocity vectors are all oriented downwards. The velocity of the upper corner of the column then increases and all the vectors change orientation from downward to downward and downstream (as it can also be observed on Figure 5.19.a and Appendix C.15). At the end, the velocity increases again as the vectors are oriented in the direction of flow. During the phase 2 illustrated by Figure 5.18, the norm of the velocity is shown. As time progresses, the vortices progress more slowly and become less circular and the recirculation is weaker.

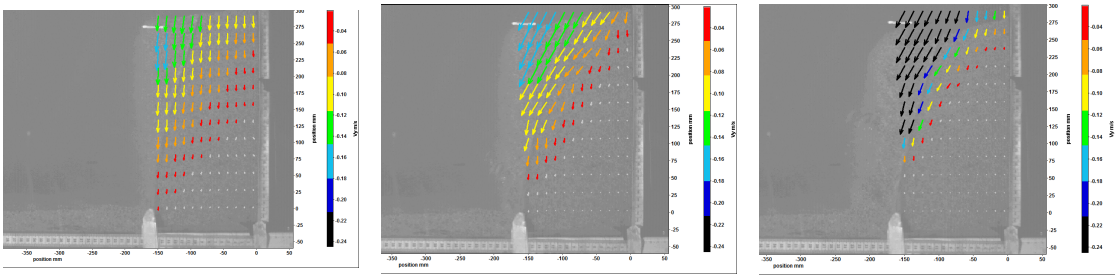

$t = 0.05[s]$ $t = 0.144[s]$ $t = 0.28[s]$

Figure 5.17: Evolution of the vertical component of velocity during the beginning of the collapsing process of a column of aspect ratio $A = 2$. For the sake of readability, a zoom of the color code of these 3 graphs is available in Appendix C.10 and the same figures in large format are at Appendix C.11,C.12 and C.13.

Depending on the aspect ratio of the column, the portion of sand set in motion is not the same. We observe on Figure 5.19 that from the beginning of the collapse, the fracture line for $A = 0.5$ and $A = 1$ does not reach the right wall of the channel while it does when $A = 1.5$ and $A = 2$. This could explain why the final deposit is trapezoidal

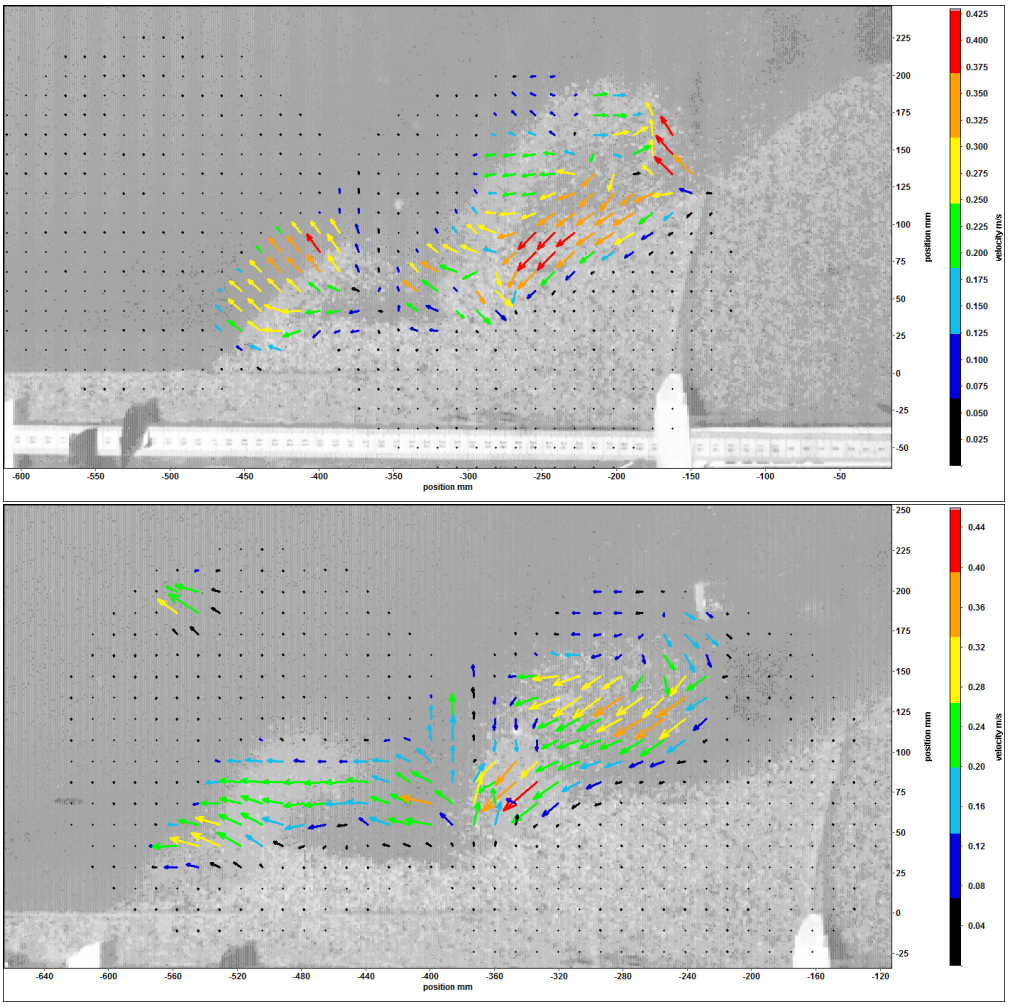

Figure 5.18: Evolution of velocity of vortices in 0.366 seconds (Top: $t = 0.764[s]$ and Bottom: $t = 1.13[s]$. For the sake of readability, a zoom of the color code of both graphs is available in Appendix C.14.

in these two cases. When $A = 1$, the deposit is however triangular at the end of the collapse.

Using `Davis 8`, it is possible to observe the velocities of the vortices during their creation and their move. It confirms what was seen with the naked eye. When the column of aspect ratio equals to 1 on Figure 5.20, the vortex is created. At the same time, the rest of the column is still collapsing from its initial position. When $A = 2$, two vortices are observed while when $A = 1$ there is only one vortex. We observe a recirculation of the sand grains in the vortices of the Figure 5.18 while with the column of $A = 1$ in Figures 5.20 and 5.21, we do not detect any obvious recirculation. It seems that the vortex is formed and then it moves in suspension in the water without creating recirculation.

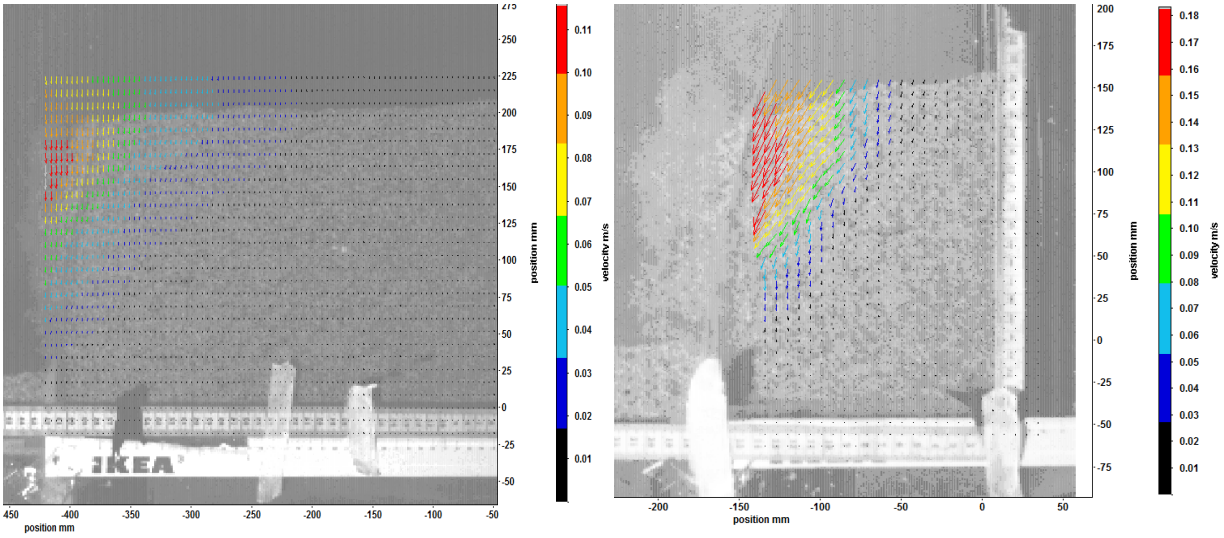

(a) Aspect ratio $A = 0.5$, $t = 0.312[s]$

(b) Aspect ratio $A = 1$, $t = 0.074[s]$

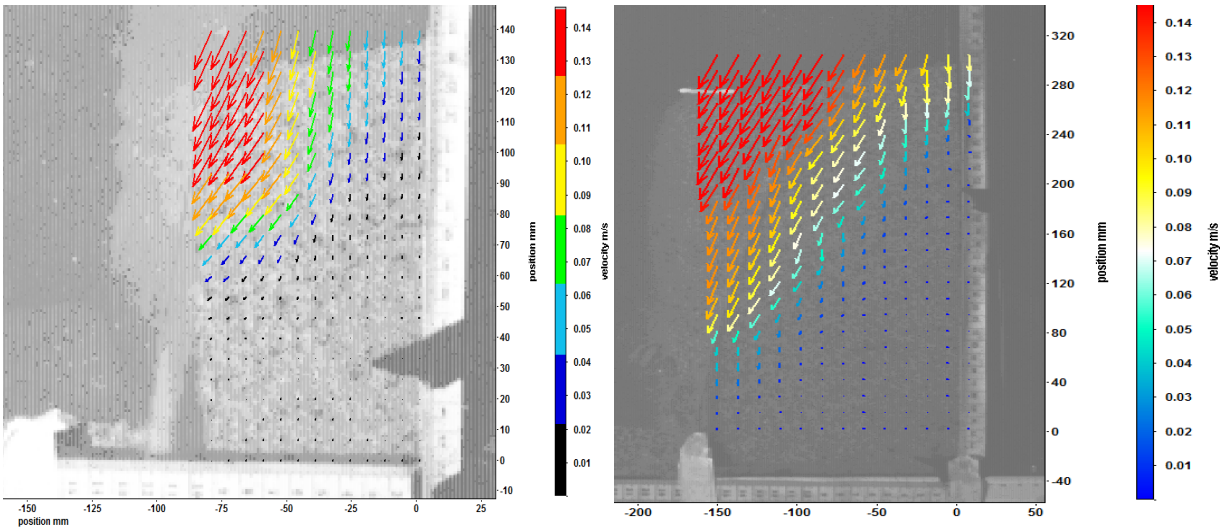

(c) Aspect ratio $A = 1.5$, $t = 0.002[s]$

(d) Aspect ratio $A = 2$, $t = 0.1[s]$

Figure 5.19: Comparison of velocities during the beginning of the collapsing for four aspect ratios

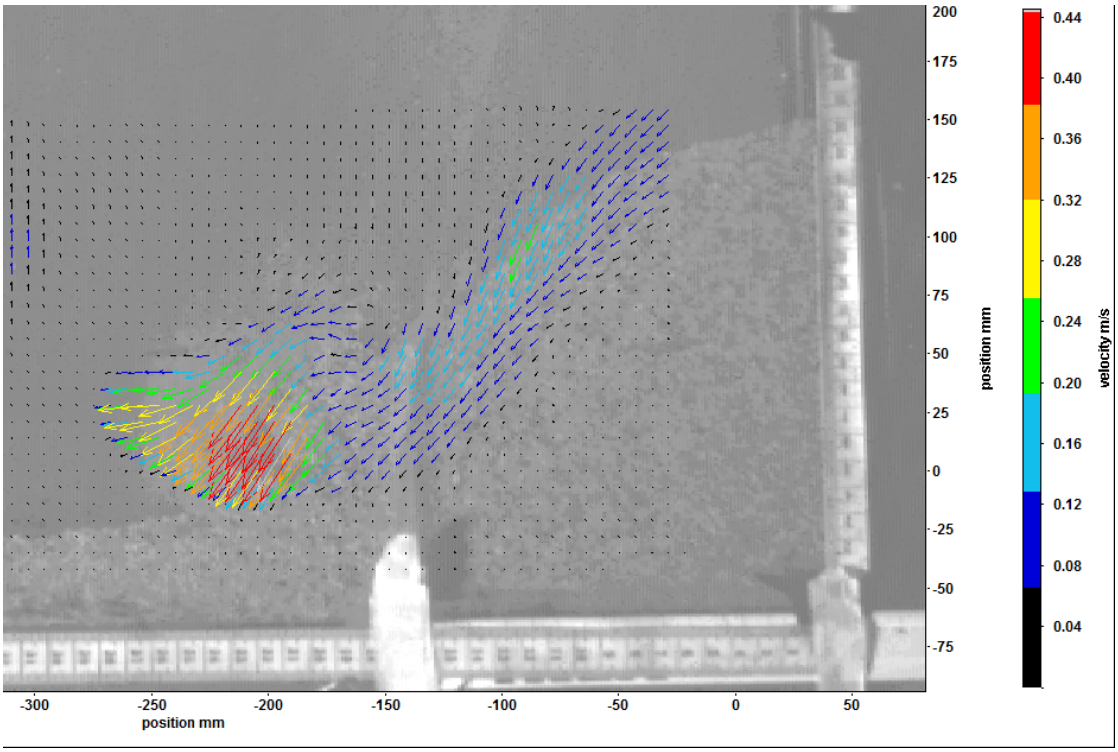

Figure 5.20: Illustration of the formation of vortex during the collapsing process of the column of $A = 1$. $t = 0.34[s]$

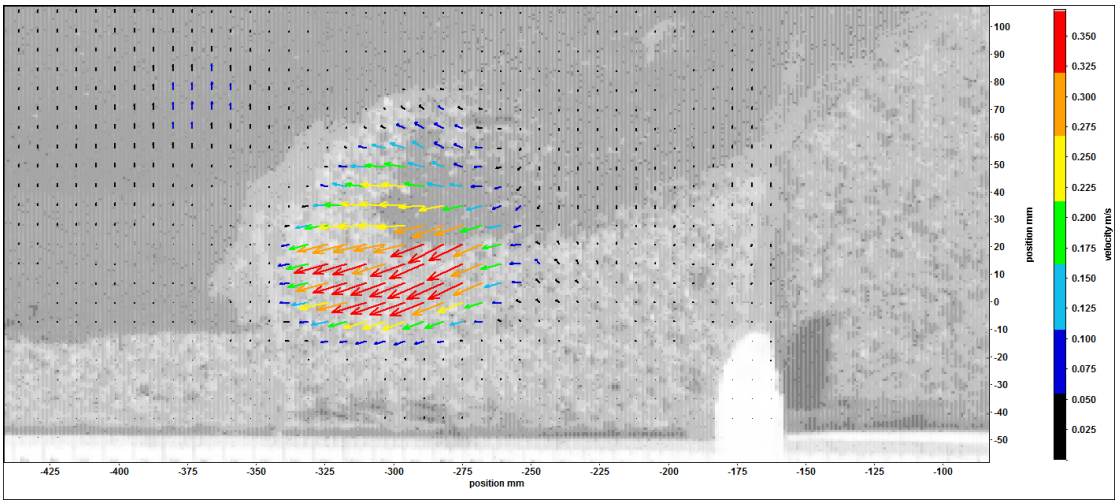

Figure 5.21: The only vortex observed during the collapse of a column of $A = 1$. $t = 0.568[s]$

5.2 Comparison between our sand and a finer one

As indicated in Chapter 3, there could be some grain-size effects in the collapse of a column. Theoretically, these effects influence the mobility of the column and the collapse duration. To observe that, an experiment with a finer sand has been realised. Results are compared with the experiment with the usual sand and the aspect ratio $A = 1$. Comparison between both experiments is shown in Table 5.23 and the final deposit is visible on Figure 5.24. As announced by Lee *et al.*[30] and by Bougouin *et al.*[24], the collapsing duration is longer with finer particles. With regards to the mobility of the column, with finer grains, two vortices are generated during the collapse while with larger grains the two vortices become quickly one vortex only which moves forward (See Figure 5.22).

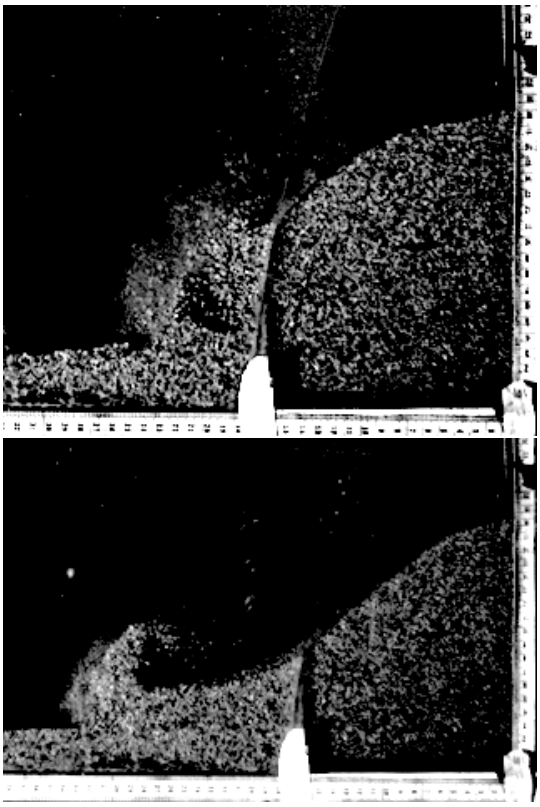

(a) Two vortices at t=0.316[s] which become one only vortex at t=0.572[s]with sand A

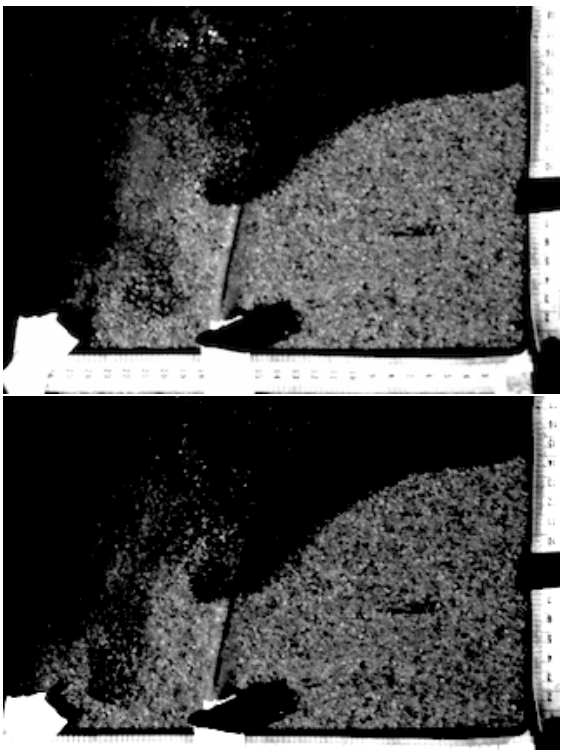

(b) Two vortices observed at t=0.394[s] and t=0.452[s] with sand B

Figure 5.22: Vortices of two identical experiments for two different mean diameter of grains

	Sand A	Sand B (the new one)
Mean diameter [mm]	1.72	1.35
Aspect ratio	1	1
Density $[kg/m^3]$	2682	2682
L_i [cm]	15	15
L_i/d	87.2	111.1
Collapsing duration t_∞ [s]	1.282	1.352

Figure 5.23: Comparison of two experiments to analyse the grain-size effects

In contrast, as visible on Figure 5.24, the run out distance does not seem to be influenced a lot by the grain-size. Cabrera and Estrada [38] indicated that grain-size effects were avoided if the ratio L_i/d was higher than 75. Since it is the case here, that could be normal that the run out distance is not influenced even if we observe a collapsing duration difference and different configuration of vortices.

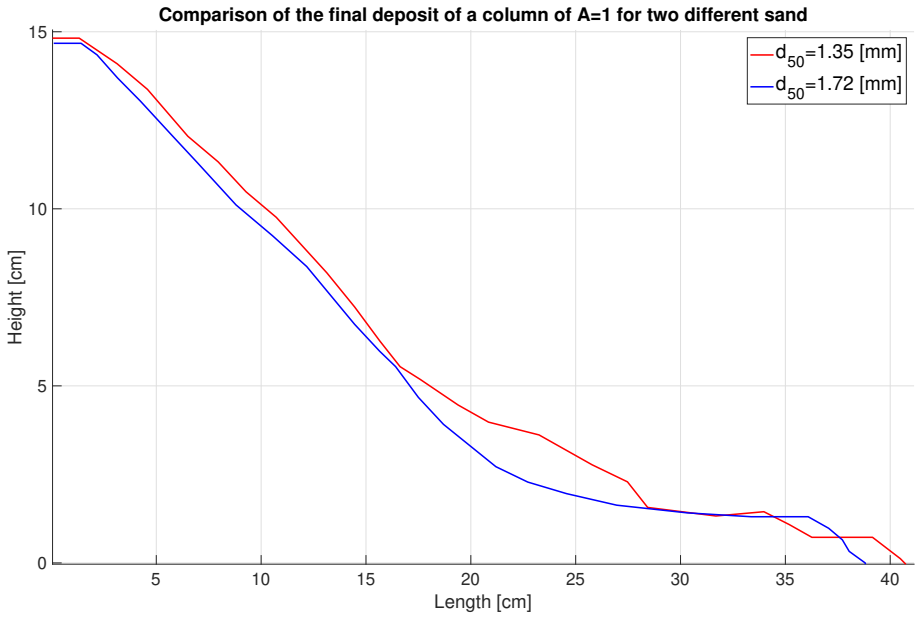

Figure 5.24: Comparison of final deposit for two different size of grains

5.3 Comparison of the behaviour of a loose column and a dense column

Since it is not so easy to compute experimentally the initial volume fraction of a column, the column built following the procedure described in the section 4.3 is considered to be the loose one. To obtain a dense column, the sand is placed before the water. Several layers are stacked and after a layer of sand has been poured in, it is compacted by hand by pressing a wooden brick against the sand. The column is thus built up to the desired height. Both experiments have been performed with the sand B of the Table 5.23.

The first thing to observe which is illustrated at Figure 5.25 is that the run out distance, in our case, does not seem to be influenced by the performed packing. The shape of the final deposit is however trapezoidal in the dense case. With regards to the behaviour of the collapse, as expected following the article of Lee *et al.* [30], the collapsing duration of the loose column is shorter than the dense one's. For the loose column, the collapsing duration is equal to $1.216[s]$ whereas it is equal to $1.509[s]$ with the dense column. Moreover, the grains flowing out of the dense column are a little portion of the top of the initial column while the flow section of the loose column is a little bit larger as illustrated at Figure 5.26.

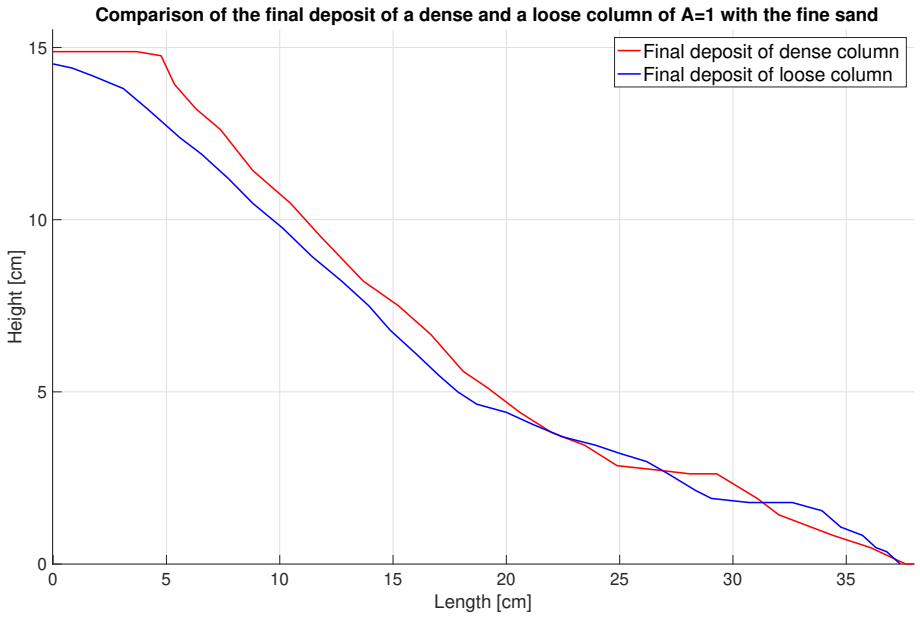

Figure 5.25: Final deposit of a dense and a loose column with similar initial conditions

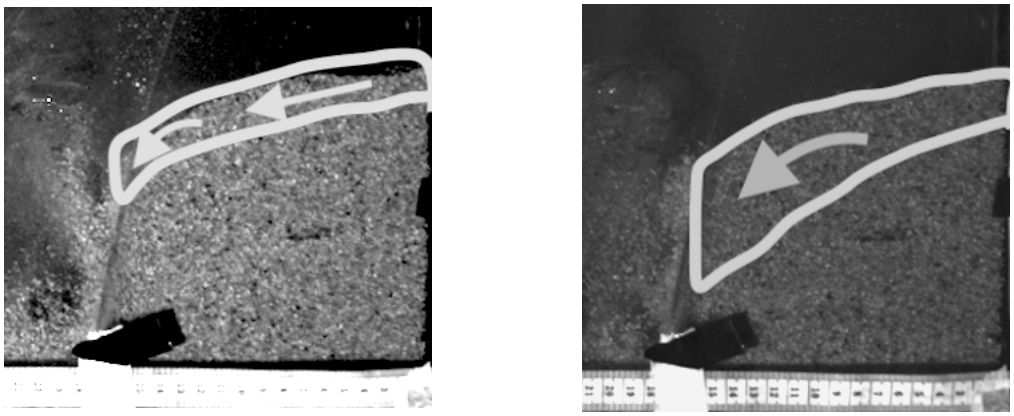

(a) Dense column

(b) Loose column

Figure 5.26: Region of the grains flowing during the collapsing of a loose and a dense column

Chapter 6

Comparison with simulations

6.1 Computation of the initial volume fraction

As explained in the section 3.2, the initial volume fraction ϕ_i is a parameter of interest. Two approaches are possible to compute the volume fraction of the columns built in our experiments. Either it is achieved through a trial and error research thanks to theoretical simulations or it is measured experimentally.
To do that, we use an experimental trial as reference (See Figure 6.1). This result is obtained from a column with an aspect ratio $A = 2$ and the usual procedure to experimentally get the loosest column possible.

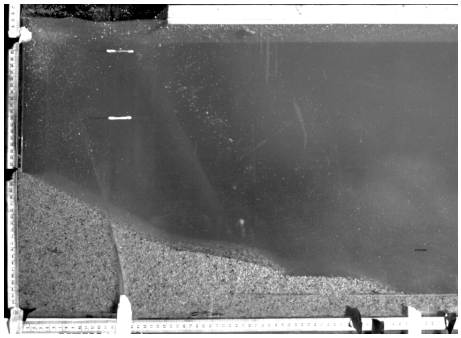

Figure 6.1: Reference final deposit for the purpose of determining the effective volume fraction

Experimental computation
In the article of Lee *et al.* [30], to compute the initial volume fraction, they used the equation 6.1. They partially filled in the water reservoir. Then they introduced a mass of dry spherical grains m, mixed and waited for the system to be at rest. The bulk volume V_{bulk} is known measuring the location of the interface water/grains and the volume of

grains V_{grains} is the ratio between the mass of grain poured and its density.

$$\phi_i = \frac{V_{grains}}{V_{bulk}} \tag{6.1}$$

A second method is proposed by Ceccato *et al.* [50]. They used the porosity to get the volume fraction. They filled the tank with water and then poured in a fixed mass of sand m_s until the column formed had the desired dimensions ($H_i \times L_i \times W_i$). The porosity n_{ms} and the volume fraction were computed.

$$n_{ms} = 1 - \frac{m_s}{\rho_s H_i L_i W_i} \tag{6.2}$$

$$\phi_i = 1 - n_{ms} \tag{6.3}$$

Both methods have been performed for our experiment even if our grains are not perfectly spherical and regular, unlike those used by Lee *et al.* [30]. On the one hand, we obtain a volume fraction of 0.4948. On the other hand, with a porosity of 0.505, we obtain a volume fraction of 0.495. These two results seem to be in agreement with each other and one might think that the volume fraction in our laboratory experiments is equal to 0.495. However, for a numerical simulation with such a volume fraction, the result obtained is not the one expected and is not close enough to the reality measured in our experiments. Indeed, as visible on Figure 6.2, the deposit of the simulation for an initial volume fraction $\phi = 0.495$ and an aspect ratio $A = 2$ is rather domed, not triangular enough. The slope is not large enough compared to the laboratory observation of Figure 6.1. Besides, the height ratio between initial H_i and final H_f conditions is equal to 0.49 for the simulation while we observed a ratio $H_f/H_i = 0.6407$ in our experiment (See Figure 6.1).

Several simulations can then be carried out to see if another column concentration gives a result closer to what is observed in the laboratory.

Figure 6.2: Simulation results (Initial and final situation) from the model and algorithm of Chapter 2 for aspect ratio A=2, initial volumetric fraction of 0.495 and parameters of sand used in laboratory.

Trial and error computation

Simulations are dimensionless. To compare more easily simulations and experimental data, simulation quantities can be converted into dimensional quantities. It enable us to superimpose on the same graph the collapse patterns obtained by experiments and by simulations. Imposing the width L_i of the simulated column, the correct lengths can be assigned to the simulation images during the pixel-to-centimetre conversion via `Matlab` procedure. The resulting graph is available in Figure 6.3. On this graph, all columns have the same initial height and length $H_i = 30[cm]$ and $L_i = 15[cm]$. The only difference between the different curves is the initial volume fraction. The final height H_f of the column with 0.495 as initial volume fraction (pink curve) is the furthest from the reference experiment (black curve). As already written in the section 3.2, a volume fraction higher than 0.58 is considered to be dense and is represented by the cyan curve on Figure 6.3.

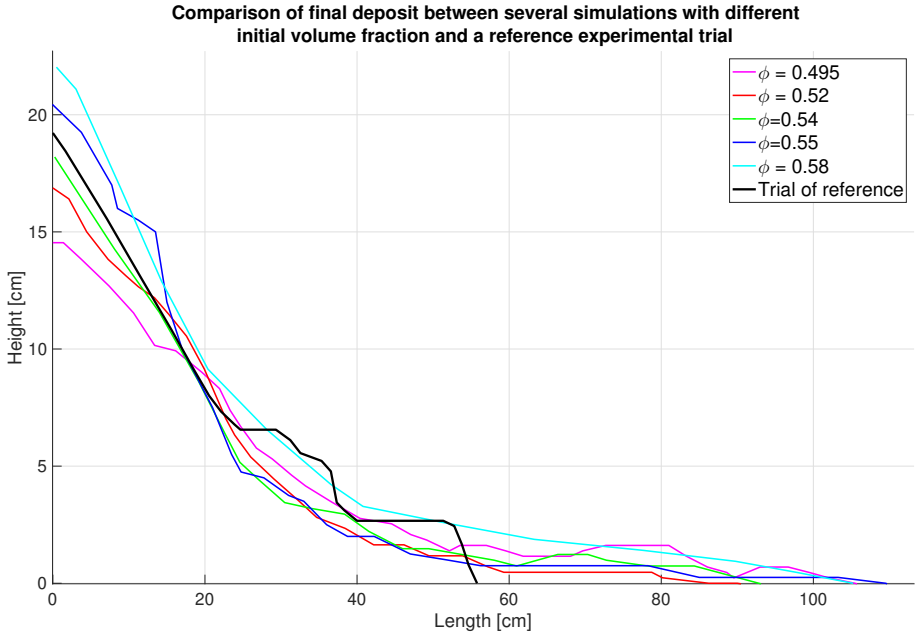

Figure 6.3: Finding the effective volume fraction for an experiment with an initial aspect ratio of 2

Since the run out distance of the experimental trial does not seem to match the simulations, the determination of our effective volume fraction will be made on basis of the ratio H_f/H_i. The principle is to seek by trial and error method which volume fraction will give a H_f similar to one obtained experimentally. Ratios H_f/H_i are available in the Table 6.4. Based on this table, for the analysis of the aspect ratio in simulations, the simulations will be performed with a volume fraction of 0.545. This volume fraction is considered to be the effective initial volume fraction obtained following the experimental procedure described in chapter 4. An encouraging fact is that by trial and error, Lee *et al.*[30] had found a volume fraction equal to 0.55 through their experiments on collapsing columns of glass beads in water. This value is relatively close to the one we obtained.

Volume fraction ϕ	Ratio H_f/H_i
Effective volume fraction	0.6407
0.495	0.4866
0.52	0.5625
0.54	0.6066
0.55	0.6833
0.58	0.7344

Figure 6.4: Ratio H_f/H_i for several volume fraction

6.2 Comparison between simulations and experimental data in terms of shape of deposit

After determining the effective volume fraction based on the experiment with an aspect ratio $A = 2$, we expected that the comparison between the experimental and the numerical data would coincide with a different aspect ratio. However, with an aspect ratio $A = 0.5$, we find that the H_f/H_i ratio does not match with the results previously obtained with $A = 2$. Since the volume fraction is not uniform within the column, and especially in the vertical direction, it is possible that the initial height itself has an influence on the effective volume fraction in the laboratory. It would be interesting to determine the relationship between the height of the column and its effective volume fraction. Nevertheless, the following comparison is made with simulations with initial volume fraction equal to 0.545 for all different initial aspect ratios.

With $A = 0.5$, a snapshot is taken at $t = 0.6[s]$ and is compared to the simulation obtained with the same initial conditions, the same sand and the same instant $t = 0.6[s]$ (See Figure 6.5). The shapes of the deposits may look the same but the difference becomes obvious in the Figure 6.6 when simulations are resized in centimeters (instead of being dimensionless). In the simulation, the deposit's height decreases more than during the laboratory experiment. The run out distance is also longer. In the simulation, however, we also find two small vortices like those observed in the laboratory and showed at Figure 5.1.

(a) Experimental

(b) Numerical with $\phi = 0.545$

Figure 6.5: Collapsing of the column with $A = 0.5$ at time $t = 0.6[s]$

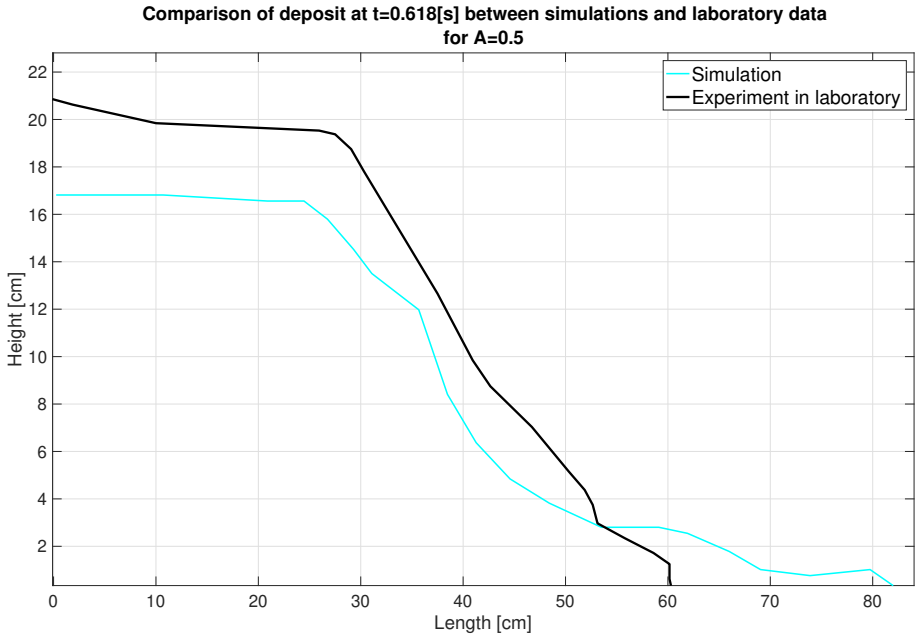

Figure 6.6: Comparison between experimental trial and simulation for an assumed effective volume fraction equal to 0.545

Final deposit of simulation and experimental trial can also be compared when $A = 1$. In laboratory, the collapsing duration of such a column is equal to $1.046[s]$. A very interesting fact is that in the simulation of such a column, it is also at this moment that the deposit does not seem to vary significantly. Moreover, while a triangular deposit is observed experimentally, the simulation predicts a trapezoidal deposit. A reader could observe that with $A = 1$ in the dense case (See Figure 5.25) where the final deposit is also trapezoidal. However, in the dense case with trapezoidal final deposit, the final

height H_f is equal to the initial height H_i while in the simulation with trapezoidal final deposit, the final height is clearly lower (See final deposit in Appendix C.9).
Again, the run-out distance is longer in simulation but it could be explained by the fact that the ratio H_f/H_i in the simulation is equal to 0.7466 when the one of the experimental trial is equal to 0.933 (See final deposit in Appendix C.9). It is possible here that the quantity of sand which is stayed at the top of the experimental column is, in the simulation, carried to the bottom of the channel.

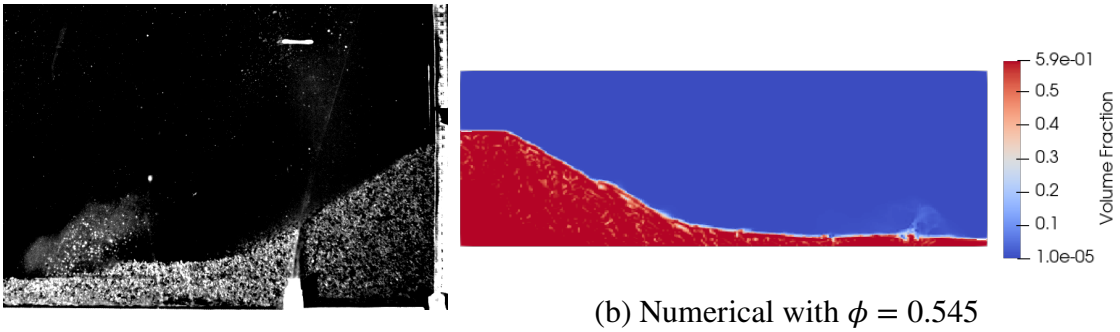

(a) Experimental

(b) Numerical with $\phi = 0.545$

Figure 6.7: Collapsing of the column with $A = 1$ at time $t = 1.046[s]$

Comparison of final deposit of experimental and numerical data with the column with an aspect ratio $A = 2$ is already shown on Figure 6.3. However, in the simulation of such a collapsing column with aspect ratio $A = 2$, the final deposit is obtained when $t = 0.92[s]$ while it lasts 1.391 seconds in the laboratory. On the one hand, the final instant in laboratory is not so easy to determine since grains are in suspension in the water and when the flow is considered to be finished is arbitrarily determined. On the other hand, the final deposit of a simulation is also quite arbitrarily decided because the deposit is considered to be final when, after several steps of time, the deposit does not seem to change anymore. Anyway, we can compare the experiments and the simulations for the time step $t = 0.92[s]$ (See Figure 6.8). As expected, we see that at $t = 0.92[s]$, the experimental collapse is not over: a non-negligible amount of sand is still suspended in the water and two vortices can clearly be seen. However, in the simulation, no vortex is observed anymore.

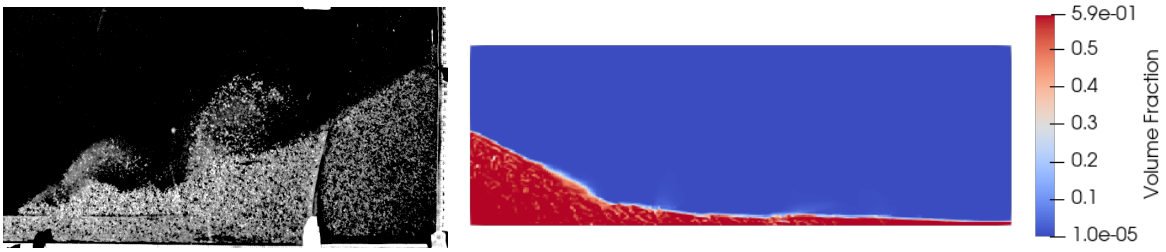

(a) Experimental

(b) Numerical with $\phi = 0.545$

Figure 6.8: Collapsing of the column with $A = 2$ at time $t = 0.92[s]$

It is important to remember that these comparisons are made for an estimated volume fraction value and that the differences may indicate that this estimated value is not necessarily the right choice. The model and the algorithm used to obtain the simulations have been validated and these remarks do not question the efficiency of the model. Nevertheless, in reality, the volume fraction is not uniform along the z-axis of the column. With a initially 30 cm high column, we observe similar H_f/H_i ratios. This is not the case with initially 15 and 20 cm high columns. It would therefore be necessary to determine the effective volume fraction for each aspect ratio of column by trial and error in order to compare experiments and numerical results more efficiently. Then, despite this difficulty in determining the volume fraction, considering these comparisons, we observe that the run out distance is always longer in the simulations than in the laboratory experiments. Moreover, it seems that for a sand of the size used in this master thesis, vortices are not very present in the simulations as developed in the following section 6.4.

6.3 Collapsing process and velocities simulations: comparisons with the experimental results

Results given by simulations are dimensionless. To compare those simulations with our experimental results, quantities are multiplied by t_{ref} and u_{ref} knowing Equations 6.3 and 6.3 in order to obtain dimensional quantities. Figures obtained with `Davis 8` show normal velocities whereas simulations are given in x-velocity and z-velocity separately. Moreover, not all t instants are exploitable via `Davis 8`. We are limited by the efficiency of the vectors' detection on the images. Thus we cannot compare exactly the same t instants between simulations and `Davis 8`'s results. The represented velocities are those of the solid phase (i.e. of the sand).

$$t = t_{adim} t_{ref} \tag{6.4}$$

$$t_{ref} = \frac{0.3}{\sqrt{2 \cdot 9.81 \cdot 0.3}} \tag{6.5}$$

$$u = u_{adim} u_{ref} \tag{6.6}$$

$$u_{ref} = \sqrt{2 \cdot 9.81 \cdot 0.3} \tag{6.7}$$

The main stages of the collapse of each column are visible in the simulations. The color legend is not the same for each figure, to allow us to observe the simulations image by image. The difference of the values on the legend is enlarged or reduced according to the needs.

Indeed, with $A = 0.5$, at Figure 6.9, we observe a mass of sand at $t = 0.22[s]$. We can see that the shape formed by these velocities is not the same in x as in z. That means that the sand going upstream in this mass can have a zero velocity in the z-direction. In the laboratory experiments, two smaller vortices were observed (See Figure 5.1) which is not the case in the simulations.

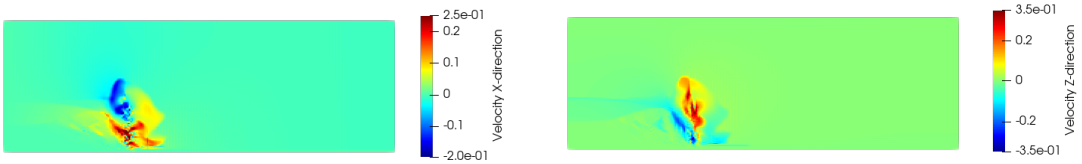

Figure 6.9: $A = 0.5$,$t = 0.22[s]$, left is x-velocity and right is z-velocity

With $A = 1$, a mass of sand that seems to detach from the column goes downstream and could be similar to the vortex observed with the naked eye in the experiments. Via `DaVis8`, at the beginning of the collapse, at $t = 0.074[s]$, we observed velocities up to $0.18[m/s]$ whereas in the simulations, at $t = 0.11[s]$, we observe normal velocities of the order of $1.21[m/s]$ (See Figure 6.10). `Davis 8` would thus detect velocities almost 7 times smaller than the simulations.

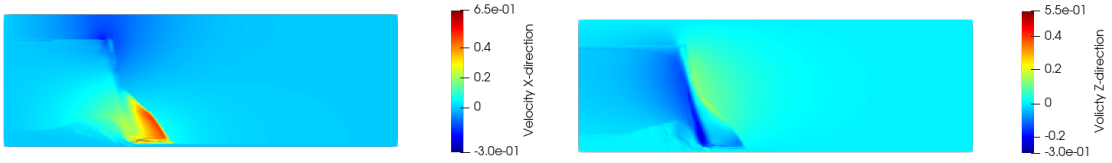

Figure 6.10: $A = 1$, $t = 0.11[s]$, left is x-velocity and right is z-velocity

At $t = 0.17[s]$, the simulations indicate maximum velocities around $0.97[m/s]$ in the x-direction and $0.72[m/s]$ in the z-direction. While `Davis 8` indicates for $t = 0.34[s]$ a maximum velocity of $0.4[m/s]$. Once again, the difference is noticeable when $t = 0.34[s]$, the observed velocities should be greater than those at $t = 0.17[s]$ since we are still in phase 1 where the grains acquire kinetic energy.

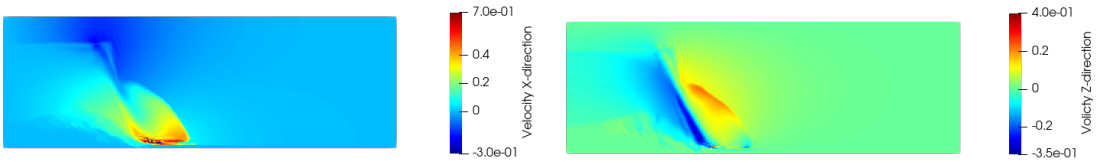

Figure 6.11: $A = 1$, $t = 0.17[s]$, left is x-velocity and right is z-velocity

At $t = 0.47[s]$, the simulations show a clear vortex on the front of the collapse. This suggests that it corresponds to the vortex observed in Figure 5.21. However, while `Davis 8` indicates that it advances with a maximum normal velocity of $0.35[m/s]$, the simulations predict x-velocities around $0.48[m/s]$ and z-velocities around $0.97[m/s]$.

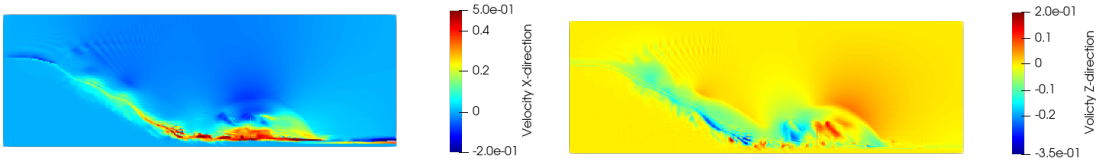

Figure 6.12: $A = 1$, $t = 0.47[s]$, left is x-velocity and right is z-velocity

Considering the column of aspect ratio $A = 2$, it is clearly observed that we get the same results in the laboratory, with `Davis 8` at $t = 0.05[s]$ at Figure 5.17 and in our simulations at Figure 6.13. Indeed, the column starts by collapsing on itself regardless of the tool used to analyse it. While only the corners of the column are moving in the x-direction, we can see that the entire column is moving downward in the z-direction. The whole column collapses on itself before a part of it collapses downstream. In the z-direction, the maximum velocities detected by `Davis 8` are $0.18[m/s]$ and the simulations are about $0.24[m/s]$ over the whole column.

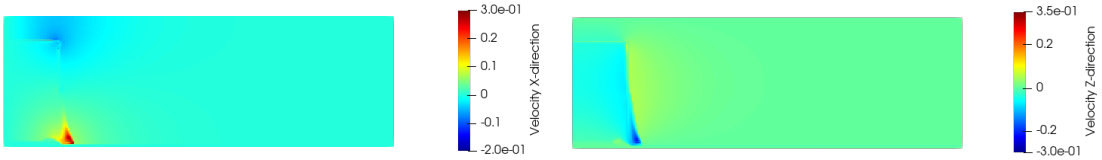

Figure 6.13: $A = 2$, $t = 0.09[s]$, left is x-velocity and right is z-velocity

Then, while the bottom of the column becomes dense and immobile, the rest continues to move downstream and recirculation is observed at Figure 6.14. The sand that reaches the bottom of the channel moves up and back and goes back on the mass of the column that is collapsing downstream. Finally, the sand continues to move forward and we can hardly see the two vortices observed in the laboratory (See Figure 6.15). It is harder in the simulations to distinguish the two vortices observed both in the laboratory and via `Davis 8`.

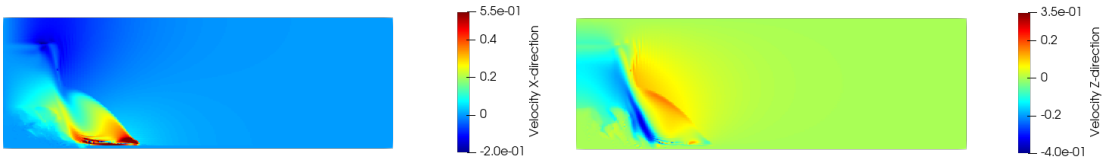

Figure 6.14: $A = 2, t = 0.17[s]$, left is x-velocity and right is z-velocity

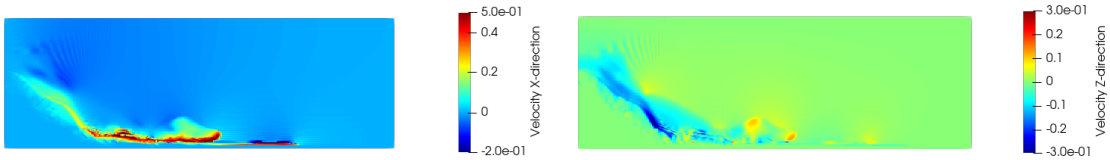

Figure 6.15: $A = 2, t = 0.47[s]$, left is x-velocity and right is z-velocity

6.4 Influence of the grain-size parameter

In the simulations, the influence of the size of the sand grains is obvious. For the same initial conditions but with a much smaller sand size, we observe on Figure 6.16 that the results are very different. In the laboratory, the sand is characterized with a median diameter equal to 1.72 mm, whereas in the simulations, all sand grains are considered to have the same diameter. It can already create a difference between the experimental and numerical results.

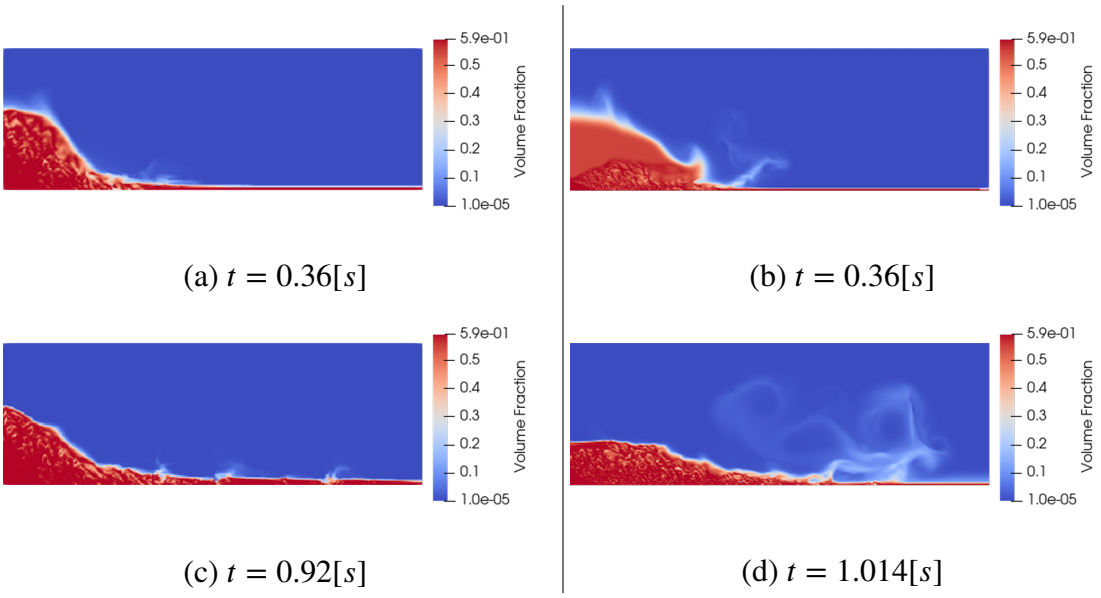

(a) $t = 0.36[s]$ (b) $t = 0.36[s]$

(c) $t = 0.92[s]$ (d) $t = 1.014[s]$

Figure 6.16: Initial aspect ratio $A = 2$ and Initial volume fraction $\phi = 0.55$ for both; (a) and (c): Sand used in laboratory of with a density of 2682 $[kg/m^3]$ and median diameter 1.72 [mm]. (b) and (d): Theoretical sand with a density of 2530 $[kg/m^3]$ and diameter 0.56 [mm]

Several vortices are observed in the laboratory when the aspect ratio $A = 2$. However, in the simulations, with the characteristics of the sand used in the laboratory, not enough vortices are observed. The model and the algorithm of the simulations are able to simulate the vortices as observable at Figure 6.16(b). Nevertheless, with a grain of $1.72[mm]$, we do not see vortices that are comparable to those observed experimentally. In addition, the shape of the final deposit changes from triangle for coarse sand to trapezoidal for very fine sand and the final height seems to be almost halved. Finally, small numerical instabilities are observed in the simulation with coarse sand (See 6.16(c)).

By comparing the simulations of the experimentally carried out trials in the section 5.2, we can observe the differences concerning the final deposit between the laboratory experiments and the simulations. Experimental comparison is made at Figure 5.24 and numerical comparison is made at Figure 6.17. In both cases, the aspect ratio is $A = 1$, the initial length of the column is $15[cm]$ and the effective initial volume fraction is considered to be equal to 0.545. In the laboratory, the run out distance is longer for the finer sand than for the coarse one and it is confirmed in the simulations. However, while in the laboratory the final height was the same as the initial height for both sands, it is observed that in simulations the two final heights are lower and are not equal to each other. Moreover, the trapezium of the final deposit is more visible in simulations than in experiments.

During the collapse of the columns into the channel, one vortex is observed with large grains whereas two are observed with small grains. In the simulations, this is more difficult to notice but it is still the case. We can note that the vortices seem to carry less grains in the simulations than in reality for grains of this size. For very fine sand like the sand in the Figure 6.16, the vortices are much more visible. We did not use this sand in the laboratory.

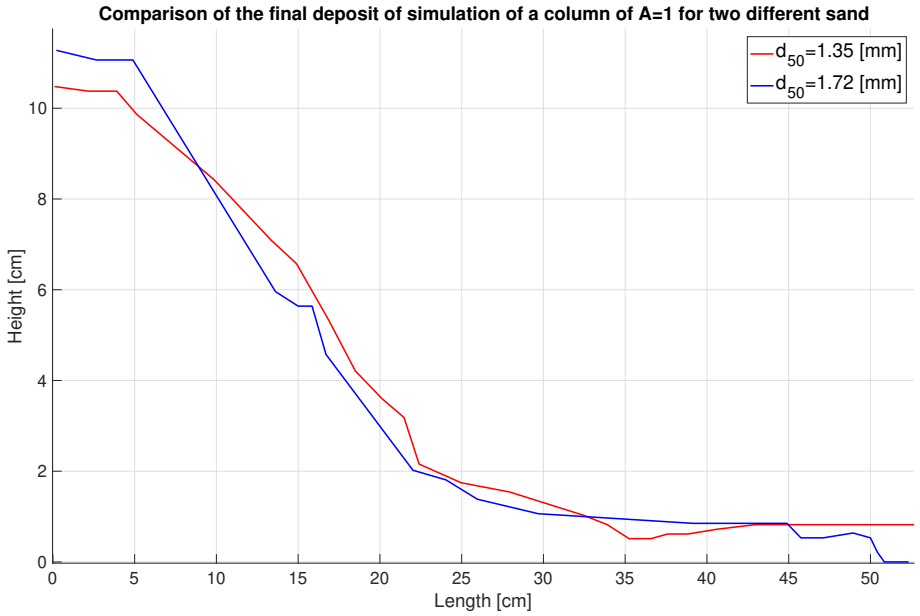

Figure 6.17: Comparison between a simulation with $A = 1$, $\phi = 0.545$ and a sand of diameter equal to 1.72 and an equivalent simulation with a sand of diameter 1.35

Conclusion

The research field of granular media still has a long way to go to meet the needs of today's world. Over time, things are progressing and I am glad that I was able, at my level, to contribute to this.
The introduction and the state of the art allowed us to become aware of the extent of the subject, the stakes and the needs resulting from the granular media.

A theoretical model and an algorithm to simulate column collapses were briefly described in the Chapter 2 and allowed us to compare experimental tests with numerical simulations.

Then, the Chapter 3 gave a summary of the main influencing parameters on granular column collapses and their particular values. This chapter will hopefully save a lot of research time for a novice student interested in the subject.

The Chapter 4 described the set-up and the experimental procedure performed in this master thesis. Particular attention has been paid to this set-up and to its improvement in terms of brightness, repeatability, accuracy of the analysed images but also to its limits. After several repairs on the channel and a search for luminosity facilitating the visibility, it was proved that this experiment was repeatable. In order to analyse the produced images, precautions were taken regarding the need to perform a calibration. With the used lens, no calibration was needed to observe interfaces. Finally, the influence of the free surface of the water was studied and shown to be negligible in the framework of this master thesis. Moreover, it is verified that the opening of the gate allowed us to obtain the initial conditions that can be considered as instantaneous.

In the Chapter 5, an analysis of the obtained images has been performed. It highlighted different collapsing features with different aspect ratios. Comparisons between the collapse of dense or loose columns and between two columns with similar initial conditions and different grain sizes were made.

To go further in the analysis of these images, two softwares were used. On the basis of the original images, `Matlab` was used to study and compare the involved interfaces,

the run out distances, the final tilt angles and the collapse times. Through `Davis 8`, we confirmed what was observed with the naked eye regarding the present vortices. It also gave an idea of the magnitude of the grain velocities.

It has been found that the size of the sand grains influences the mobility of the column, the collapsing duration and the number of observed vortices. The influence of the initial volume fraction has also been underlined. It causes a difference in the shape of the final deposit, which goes from triangular to trapezoidal. The idea of using `Davis 8` to analyse granular collapses seems to have a good potential. This master thesis indicates that this method can be chosen and improved to obtain more reliable results. It allows further analysis of the involved velocities in such collapses. To do so, it would be interesting to devote attention to the visibility of the grains in the water and the sharpness necessary for an optimal PIV analysis. However, this would be a challenging task

In the last Chapter, it was highlighted that it is not easy to determine through the trial and error method or experimentally what is the effective volume fraction of a column built in the laboratory. In practice, the problem would be the same: it is not easy to know the properties of the studied soil. It is also illustrated that a loose column will have a lower final height than a dense column in the same initial conditions in the simulations. Then, for a determined effective volume fraction, a comparison was made between the results obtained in simulations and those we got in the laboratory with four aspect ratios. Simulations are made dimensional thanks to `Matlab` to be compared with recordings. The influence of density and grain size in the simulations has been observed in parallel with their influence we experimentally observed. We saw that the simulations predicted a longer run out distance than what was obtained in the laboratory. We also found that for large grains such as those used in the laboratory, the simulations present vortices less easily than for very fine grains.

This dissertation topic could be expanded and deepened for years. An interesting approach would be to continue to focus on an optimal PIV analysis of these experiments, to find out what are the optimal conditions to properly observe sand mixed with water. In the future, it would be interesting to analyse these collapses in 3 dimensions through `Davis 8`. The concrete way to achieve this still need to be investigated. In a more practical and straightforward way, the analysis could be devoted to the study of the collapse behaviour of columns composed of other kinds and of grains with different shapes. This dissertation has provided videos of experimental trials of sand column collapses in water. The quality of the produced images is sufficient to allow researchers to make effective comparisons between these images and their own simulations.

Bibliography

[1] Davide Monsorno, Athanassios A. Dimas, and Miltiadis V. Papalexandris. Time-accurate calculation of two-phase granular flows exhibiting compaction, dilatancy and nonlinear rheology. *Journal of Computational Physics*, 372:799–822, November 2018.

[2] Olivier Pouliquen. Conférence Olivier POULIQUEN : "Les milieux granulaires : entre fluide et solide".

[3] Andreotti Bruno. *Les milieux granulaires : entre fluide et solide / Bruno Andreotti, Yoël Forterre et Olivier Pouliquen ; [préface [par] Étienne Guyon]*. Savoirs actuels Physique. EDP Sciences CNRS Édition, Les Ulis Paris, DL 2011.

[4] Le sable : enquête sur une disparition (Arte - 2013), 2021.

[5] Laurent Lacaze, Jeremy C. Phillips, and Rich R. Kerswell. Planar collapse of a granular column: Experiments and discrete element simulations. *Physics of Fluids*, 20(6):063302, June 2008.

[6] L. Rondon, O. Pouliquen, and P. Aussillous. Granular collapse in a fluid: Role of the initial volume fraction. *Physics of Fluids*, 23(7):073301, July 2011.

[7] Le tsunami de 1979 à l'aéroport de Nice.

[8] Bruno Savoye. Des avalanches sous la mer. Publisher: Pour la Science.

[9] Élisabeth Guazzelli and Olivier Pouliquen. Rheology of dense granular suspensions. *Journal of Fluid Mechanics*, 852:P1, October 2018.

[10] K Wieghardt. Experiments in Granular Flow. *Annual Review of Fluid Mechanics*, 7(1):89–114, January 1975.

[11] Ralph Alger Bagnold. Experiments on a gravity-free dispersion of large solid spheres in a Newtonian fluid under shear. *Proceedings of the Royal Society of London. Series A. Mathematical and Physical Sciences*, 225(1160):49–63, August 1954.

[12] R. T. Fowler and J. R. Glastonbury. The flow of granular solids through orifices. *Chemical Engineering Science*, 10(3):150–156, 1959.

[13] Maurice A. Carrigy. EXPERIMENTS ON THE ANGLES OF REPOSE OF GRANULAR MATERIALS1. *Sedimentology*, 14(3-4):147–158, January 1970.

[14] S. B. Savage and K. Hutter. The dynamics of avalanches of granular materials from initiation to runout. Part I: Analysis. *Acta Mechanica*, 86(1-4):201–223, March 1991.

[15] C S Campbell. Rapid Granular Flows. *Annual Review of Fluid Mechanics*, 22(1):57–90, January 1990.

[16] Jean Jacques Moreau. Modélisation et simulation de matériaux granulaires. In *35ème Congrès National d'Analyse Numérique*, La Grande Motte, France, June 2003. Le Département de Mathématiques de l'Université de Montpellier II et la SMAI.

[17] N. P. Kruyt and L. Rothenburg. Micromechanical Definition of the Strain Tensor for Granular Materials. *Journal of Applied Mechanics*, 63(3):706–711, September 1996.

[18] Margaux Boxho. *Estimateur derreur efficace a posteriori pour la résolution découlements granulaires immergés*. PhD thesis, 2019.

[19] D. Monsorno, C. Varsakelis, and M.V. Papalexandris. Poiseuille flow of dense non-colloidal suspensions: The role of intergranular and nonlocal stresses in particle migration. *Journal of Non-Newtonian Fluid Mechanics*, 247:229–238, September 2017.

[20] H.P. Zhu, Z.Y. Zhou, R.Y. Yang, and A.B. Yu. Discrete particle simulation of particulate systems: A review of major applications and findings. *Chemical Engineering Science*, 63(23):5728–5770, December 2008.

[21] Patrick Mutabaruka. Modélisation numérique des milieux granulaires immergés: initiation et propagation des avalanches dans un fluide. page 188.

[22] Jason E. Butler and Braden Snook. Microstructural Dynamics and Rheology of Suspensions of Rigid Fibers. *Annual Review of Fluid Mechanics*, 50(1):299–318, January 2018.

[23] Laurent Lacaze, Joris Bouteloup, Benjamin Fry, and Edouard Izard. Immersed granular collapse: from viscous to free-fall unsteady granular flows. *Journal of Fluid Mechanics*, 912:A15, 2021.

[24] Alexis Bougouin, Laurent Lacaze, and Thomas Bonometti. Collapse of a liquid-saturated granular column on a horizontal plane. *Physical Review Fluids*, 4(12):124306, December 2019.

[25] Yimin Jiang and Mario Liu. Granular solid hydrodynamics. *Granular Matter*, 11(3):139–156, May 2009.

[26] Mickaël Pailha and Olivier Pouliquen. A two-phase flow description of the initiation of underwater granular avalanches. *Journal of Fluid Mechanics*, 633:115–135, August 2009.

[27] Matthieu Constant, Frédéric Dubois, Jonathan Lambrechts, and Vincent Legat. Implementation of an unresolved stabilised FEMDEM model to solve immersed granular flows. *Computational Particle Mechanics*, 6(2):213–226, April 2019.

[28] GDR MiDi. On dense granular flows. *The European Physical Journal E*, 14(4):341–365, August 2004.

[29] Gert Lube, Herbert E. Huppert, R. Stephen J. Sparks, and Armin Freundt. Collapses of two-dimensional granular columns. *Physical Review E*, 72(4):041301, October 2005.

[30] Cheng-Hsien Lee, Zhenhua Huang, and Ming-Lan Yu. Collapse of submerged granular columns in loose packing: Experiment and two-phase flow simulation. *Physics of Fluids*, 30(12):123307, December 2018.

[31] Erica L. Thompson and Herbert E. Huppert. Granular column collapses: further experimental results. *Journal of Fluid Mechanics*, 575:177–186, March 2007. Publisher: Cambridge University Press.

[32] M. R. Baer and J. W. Nunziato. A two-phase mixture theory for the deflagration-to-detonation transition (ddt) in reactive granular materials. *International Journal of Multiphase Flow*, 12(6):861–889, November 1986.

[33] Jeffrey F. Morris and Fabienne Boulay. Curvilinear flows of noncolloidal suspensions: The role of normal stresses. *Journal of Rheology*, 43(5):1213–1237, September 1999.

[34] Sofiane Benyahia, Madhava Syamlal, and Thomas O'Brien. Extension of Hill-Koch-Ladd drag correlation over all ranges of Reynolds number and solids volume fraction. *Powder Technology*, 162:166–174, March 2006.

[35] D. Monsorno, C. Varsakelis, and M.V. Papalexandris. A two-phase thermomechanical theory for granular suspensions. *Journal of Fluid Mechanics*, pages 410–444, 2016.

[36] Miltiadis V. Papalexandris. A two-phase model for compressible granular flows based on the theory of irreversible processes. *Journal of Fluid Mechanics*, 517:103–112, October 2004.

[37] A. Dörr et al. A discrete model for the apparent viscosity of polydisperse suspensions including maximum packing fraction: :. *Journal of Rheology*.

[38] Miguel Cabrera and Nicolas Estrada. Granular column collapse: Analysis of grain-size effects. *Phys. Rev. E*, 99(1):012905, January 2019.

[39] JIAN CHEN. DISCRETE ELEMENT METHOD FOR 3DSIMULATIONS OF MECHANICALSYSTEMS OF NON-SPHERICALGRANULAR MATERIALS.

[40] Huabin Shi, Pengfei Si, Ping Dong, and Xiping Yu. A two-phase SPH model for massive sediment motion in free surface flows. *Advances in Water Resources*, 129:80–98, July 2019.

[41] Alexis Bougouin and Laurent Lacaze. Granular collapse in a fluid : Different flow regimes for an initially dense-packing. *Physical Review Fluids*, 3(6):064305, June 2018. Publisher: American Physical Society.

[42] Sylvain Courrech du Pont, Philippe Gondret, Bernard Perrin, and Marc Rabaud. Granular Avalanches in Fluids. *Physical review letters*, 90:044301, January 2003.

[43] Spinewine, Benoît. *Two-layer flow behaviour and the effects of granular dilatancy in dam-break induced sheet-flow*. PhD thesis.

[44] B Spinewine and Y Zech. Small-scale laboratory dam-break waves on movable beds Ondes de rupture de barrage expérimentales sur lit mobile. page 14.

[45] Ilaria Fent. DAM BREAK OVER MOBILE BED: EXPERIMENTAL AND NUMERICAL STUDY. page 321.

[46] LaVision GmbH. Fluid Mechanics FlowMaster.

[47] Correcting Lens Distortion In Adobe Lightroom.

[48] Robin Meurice, Sergio Martinez-Aranda, Masoumeh Ebrahimi, and Pilar Garcia-Navarro. Laser Prolometry to measure the bed evolution in a dam-break ow. *Submitted to the Journal of Hydraulic Research on 06 January 2021*, page 15.

[49] Guido Lauber and Willi H. Hager. Experiments to dambreak wave: Horizontal channel. *Journal of Hydraulic Research*, 36(3):291–307, May 1998.

[50] Francesca Ceccato, Alessandro Leonardi, Veronica Girardi, Paolo Simonini, and Marina Pirulli. Numerical and experimental investigation of saturated granular column collapse in air. *Soils and Foundations*, 60(3):683–696, June 2020.

[51] Multiphase Flow and Fluidization - 1st Edition.

[52] L. Staron and E. J. Hinch. Study of the collapse of granular columns using two-dimensional discrete-grain simulation. *J. Fluid Mech.*, 545(-1):1, December 2005.

Appendices

Appendix A

Laboratory manual

A.1 First experience of a trial day

- The computer available in the cellar is very very slow so the best is to take a computer on a cart with Fotron on it (be careful, one of the two computers does not receive the image via ethernet cable –> take the other one with blue ethernet plug). Be careful, the door does not open from the outside without a key –> don't forget to take the keys with you;
- Turn on the power via the electrical box;
- Check that the compressor is working properly and that the smaller compressor is gradually filling. To do this, you must have turned and pressed the button on the intermediate compressor to open the valve;
- Put the camera on the camera base and place the lens on the camera;
- Connect the camera to the mains and to the computer;
- Stick the tape measures on the wall of the channel to place the mark of what will be filmed;
- If the removable door is not in place, place it (See subsection A.5);
- Make the sand column If loose column: Put the water and then only the sand to avoid bubbles and to make it as loose as possible
  If dense column: Put the sand layer by layer and pack between each layer. Then pour the water through several sieves so as not to stir the column.;
- Turn on the camera;
- Pack the sand bed along the channel;

- Wait until the camera is ready (it has had time to warm up) and then open the Fotron software on the computer;
- Place the camera correctly at the desired location (tips: mark on the ground the exact location where the camera is placed OR measure the distance between it and the channel);
- Check that the pit under the channel is not filled (otherwise RIP flooding). If it is filled, put the pump in the pit, push the pump hose into the large blue hose and tighten the clamp. Check that the other end of the dark blue pipe is in the drain and then connect the pump;
- Fill the canal with water: insert the hose from the vacuum pump into the drilled pipe. Be prepared to put boards if necessary where the jet will come out too strong. Fill up to 30 cm (10 cm of sand and 30 cm of water);
- Fill 3 or 4 cans with water to be able to adjust the water level without moving the free surface again;
- Make the calibration (See subsection A.3);
- Place the black background;
- Place the spotlight correctly so as not to see a reflection on the camera;
- Check that the compressor is at 8 bar. If it is not, switch it on, otherwise the door may not go down and while waiting for the other movements, the water level will already be too low before the 8 bar is reached;
- While the free surface is stabilizing, adjust the water level above the column to a level slightly higher than the water level in the rest of the channel to give you time to get down to the computer before the water level in the column falls below the water level in the rest of the channel;
- Click on "Registration" (Enregistrements) to see "Ready" (Prêt) in green on the screen;
- When the water level is the same on both sides of the main door, press and hold the green button and the button with the down arrow until the main door of the channel goes down. The recording takes place;
- When the recording is finished, raise the main door with the button with the upward arrow to stop as much water loss to the pit as possible;
- On the computer, choose the path where you want to save the video, choose the MP4 or TIFF or BMP format and save.

A.2 Following experiments

When an experiment has just been done, there is water in the channel and sand. It would be interesting to find a solution to avoid emptying the water every time but still have a smooth and well packed bed.
To make the conditions as ideal as possible, it would be necessary (in the loose case) to stir all the sand of the column that remains so that the density is again loose. Then repeat the procedure A.1.

A.3 Calibration

- When the channel is filled with water, place the calibration plate in the water with the arrow to the right;
- On the computer, activate light ON (you can see very clearly) ;
- Indicate the path where to save the photo;
- Save the picture in TIF or BMP format;
- Deactivate the light mode to be able to make the video.

A.4 End of the experiment session

Before leaving, you have to:

- Empty the water from the canal with the pump;
- Empty the safety compressor ;
- Turn off the power to the electrical box;
- Bring back the computer upstairs (attention office closed after 16:30);
- Store the camera in a safe place;
- Turn off the light and slam the door on your way out.

A.5 Installation of the removable door

- Insert the vertical part of the door. Put it as straight as possible by tapping with the foot on both sides of it.
- Using a bellows borrowed from the laboratory, remove all the grains of sand from the bottom of the channel on the surface where we will put the horizontal part of the door;
- Place the horizontal part of the door and tighten the 4 nuts that allow to fix the brackets of the horizontal part on the vertical part;
- Place the available weights on the horizontal part so that the weight of the water does not make this door move;
- Place the tape measures as markers;
- Reinforce the door seal with modeling clay.

Appendix B

Time Line of granular media

This page is deliberately left blank so that the next page is full page

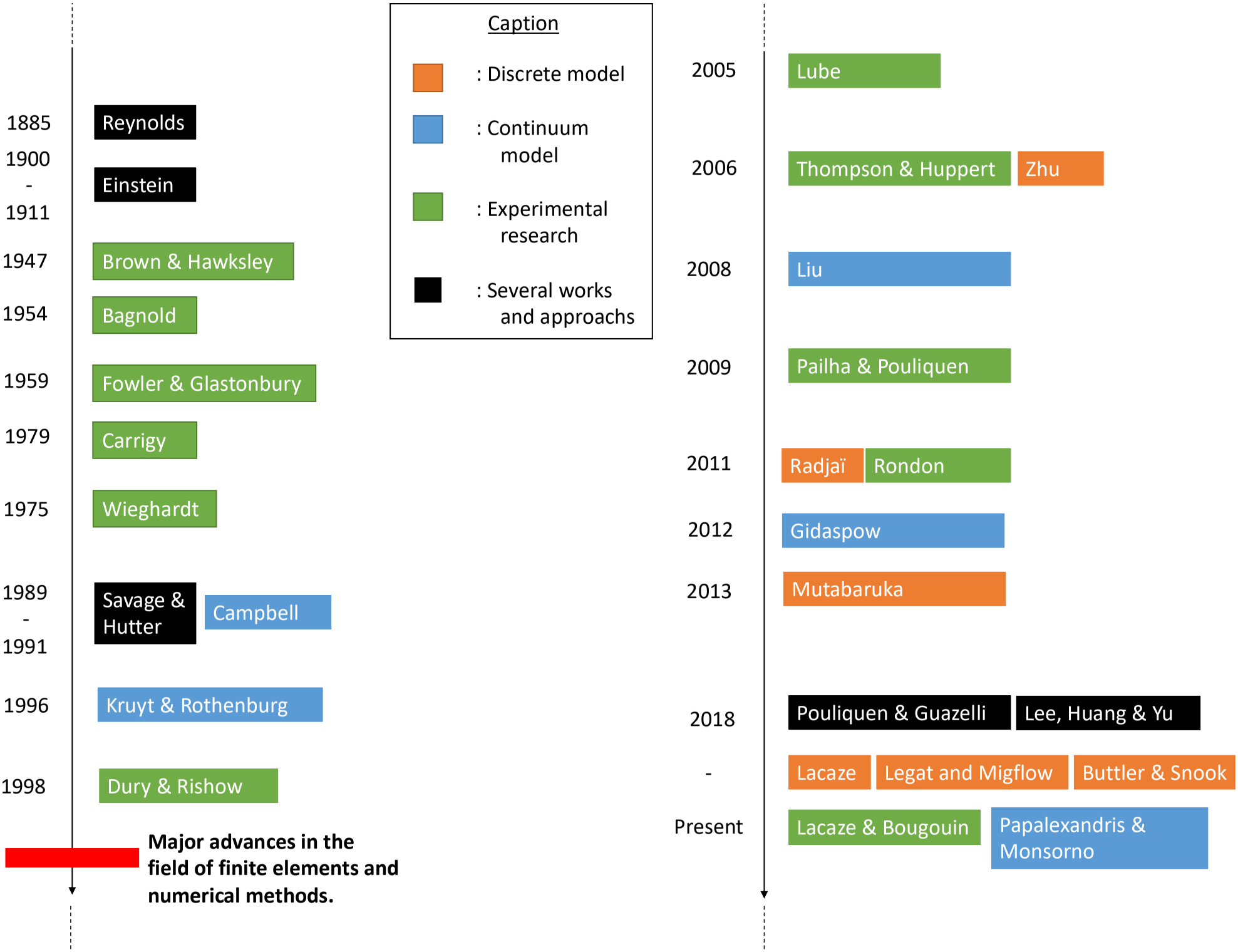
Caption
: Discrete model
: Continuum model
: Experimental research
: Several works and approachs
1885
Reynolds
1900 - 1911
Einstein
1947
Brown & Hawksley
1954
Bagnold
1959
Fowler & Glastonbury
1979
Carrigy
1975
Wieghardt
1989 - 1991
Savage & Hutter
Campbell
1996
Kruyt & Rothenburg
1998
Dury & Rishow
Major advances in the field of finite elements and numerical methods.
2005
Lube
2006
Thompson & Huppert
Zhu
2008
Liu
2009
Pailha & Pouliquen
2011
Radjaï
Rondon
2012
Gidaspow
2013
Mutabaruka
2018 - Present
Pouliquen & Guazelli
Lee, Huang & Yu
Lacaze
Legat and Migflow
Buttler & Snook
Lacaze & Bougouin
Papalexandris & Monsorno

Appendix C

Additional illustrations

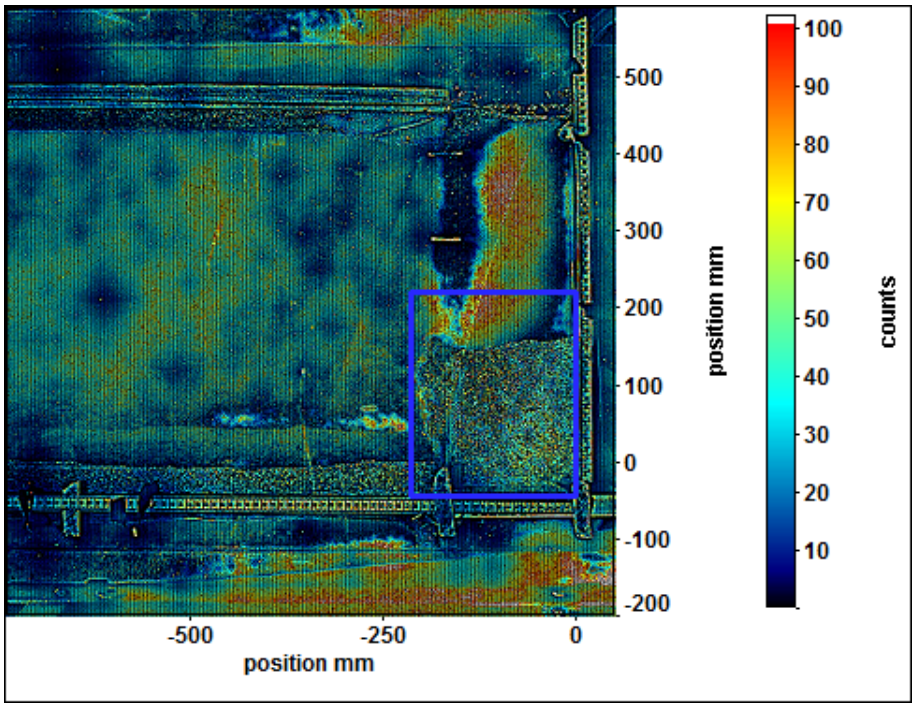

Figure C.1: Image preprocessing

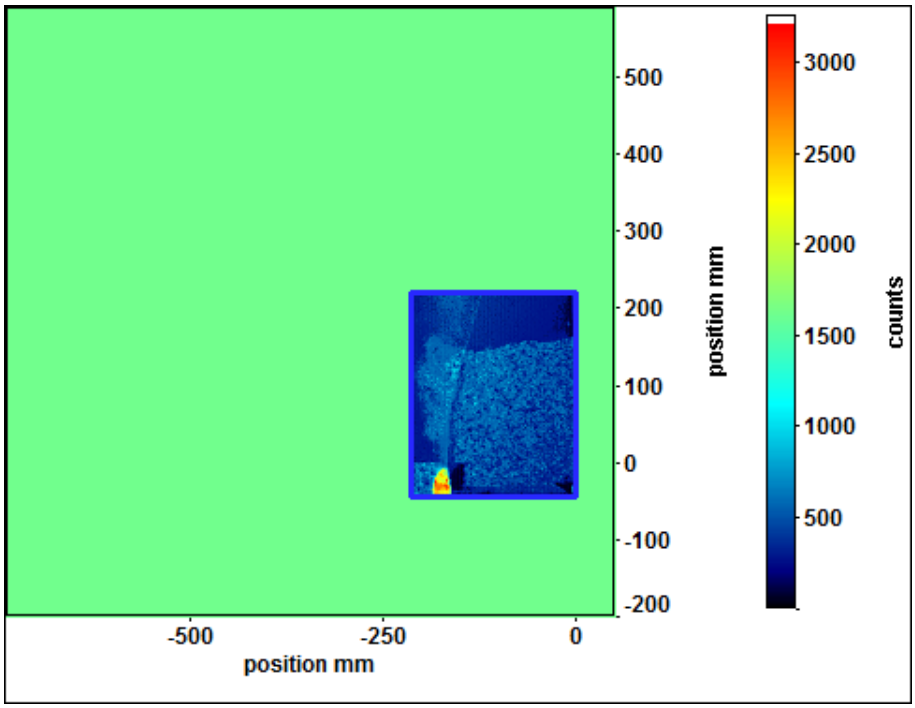

Figure C.2: Geometric mask that can be applied via `Davis 8`

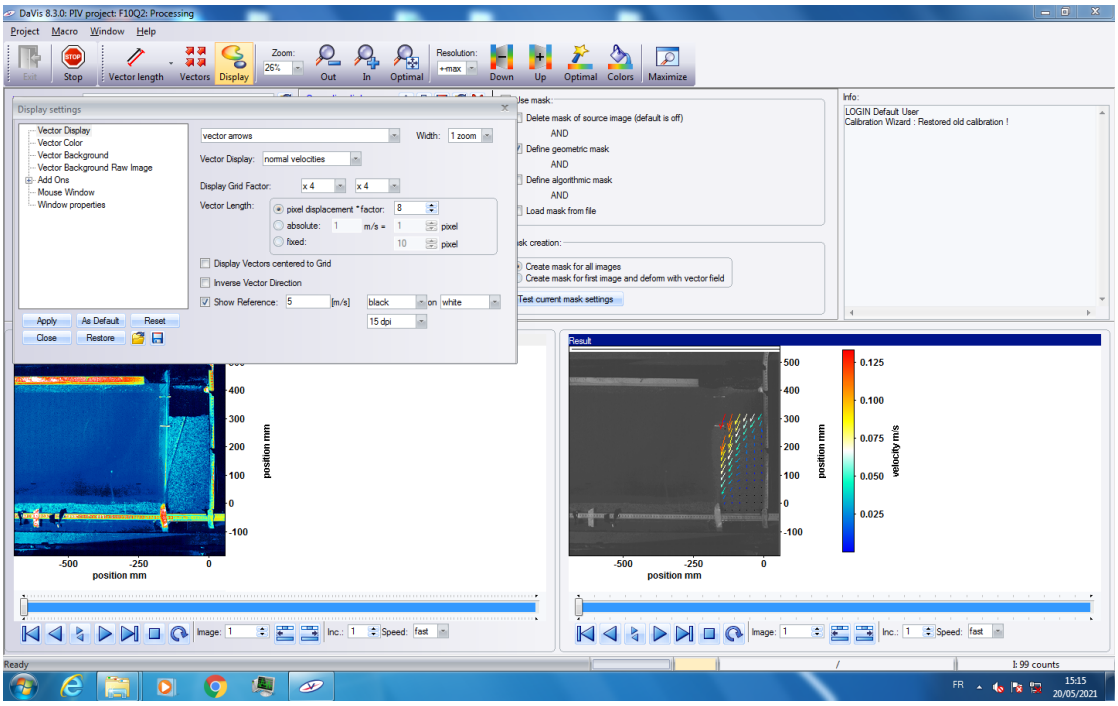

Figure C.3: Display tool of `LaVision`

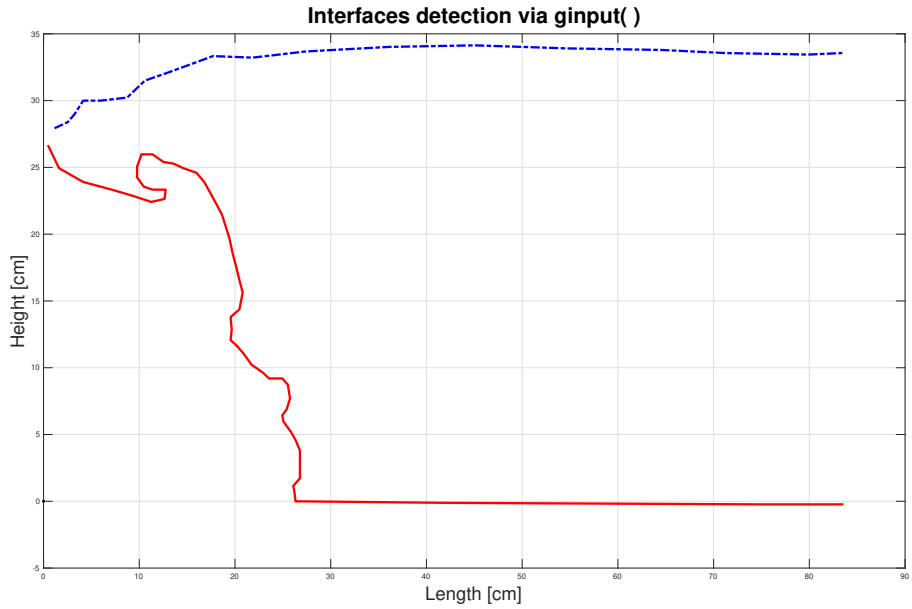

Figure C.4: Example of interfaces drawn via `Matlab` and the `ginput()` function

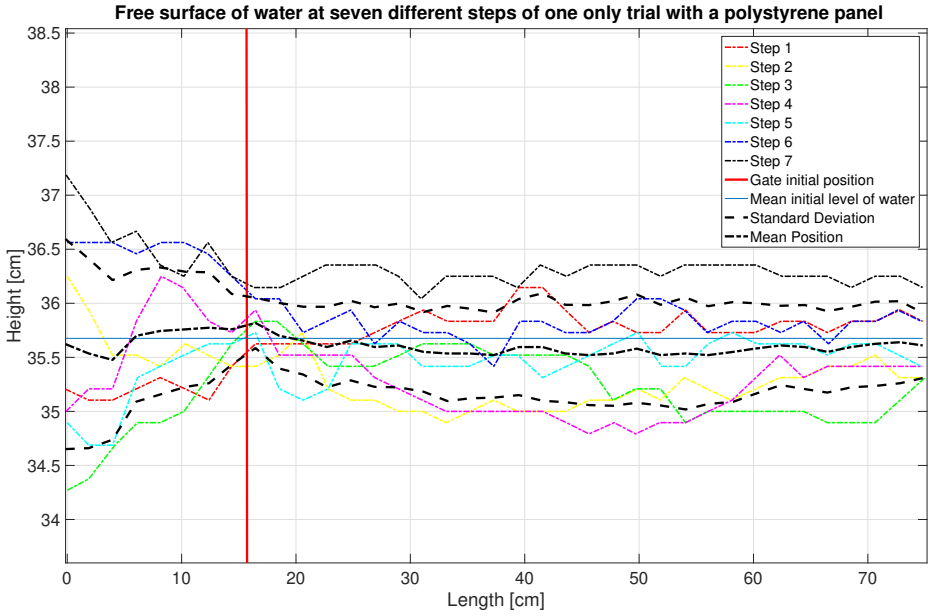

Figure C.5: Figure 4.17 but with lines to see the complete level of water

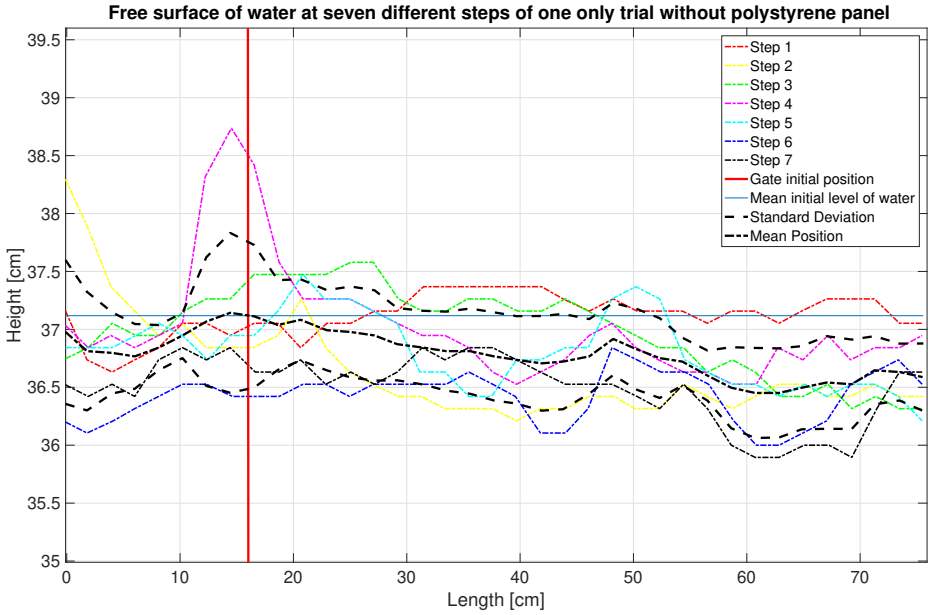

Figure C.6: Figure 4.16 but with lines to see the complete level of water

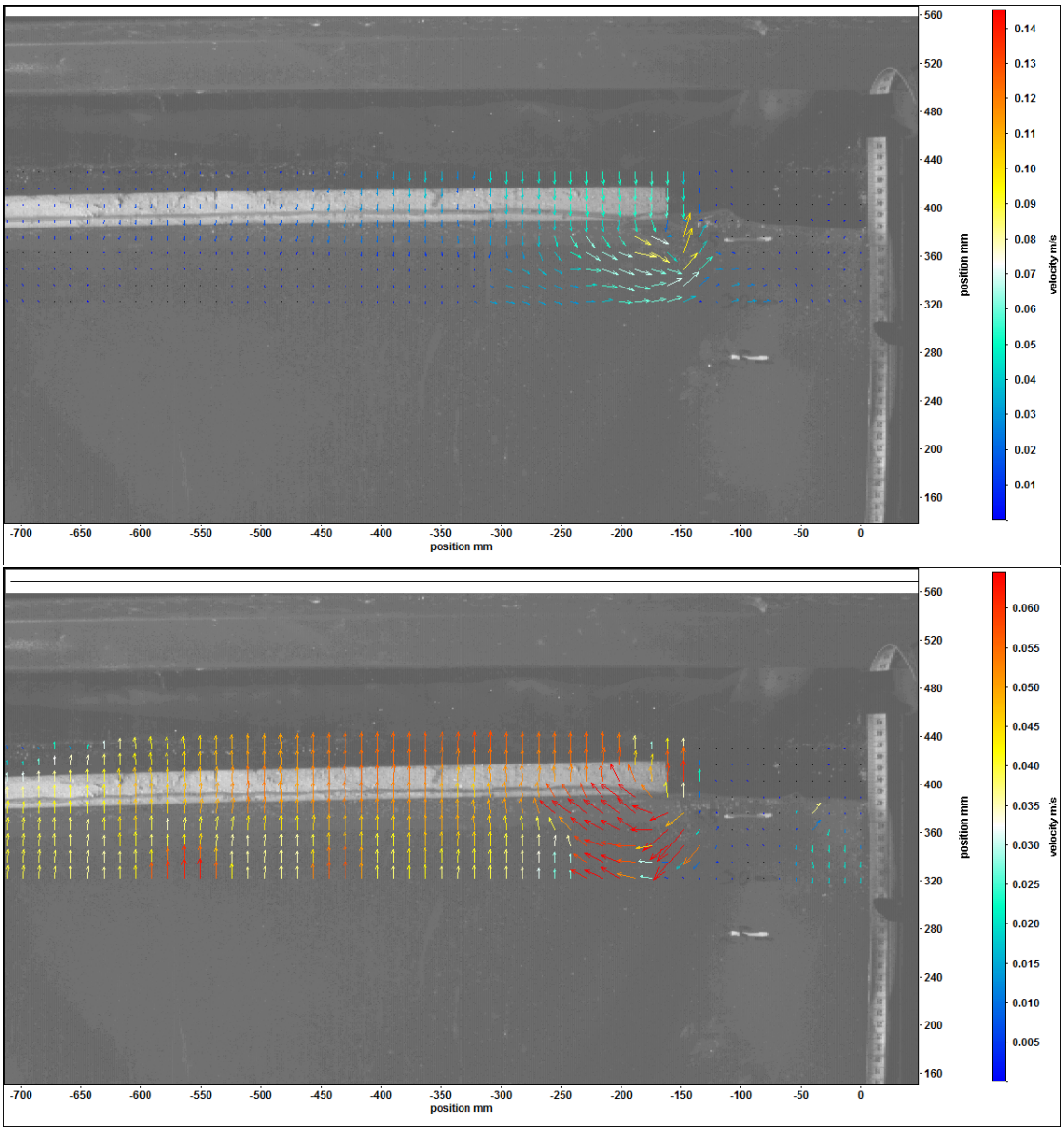

Figure C.7: Detected vectors at free surface int the case with a polystyrene panel

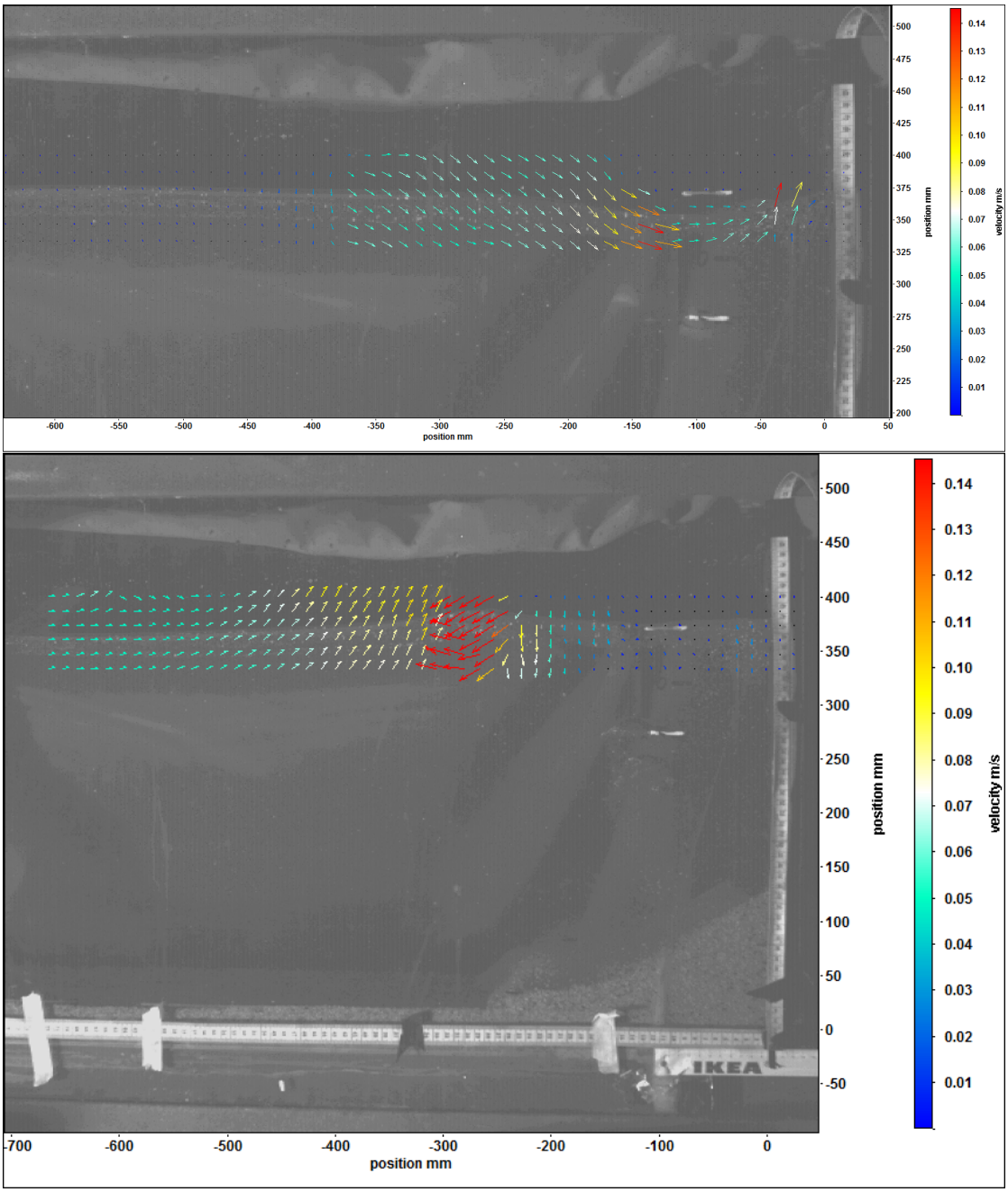

Figure C.8: Detected vectors at free surface int the case without any polystyrene panel

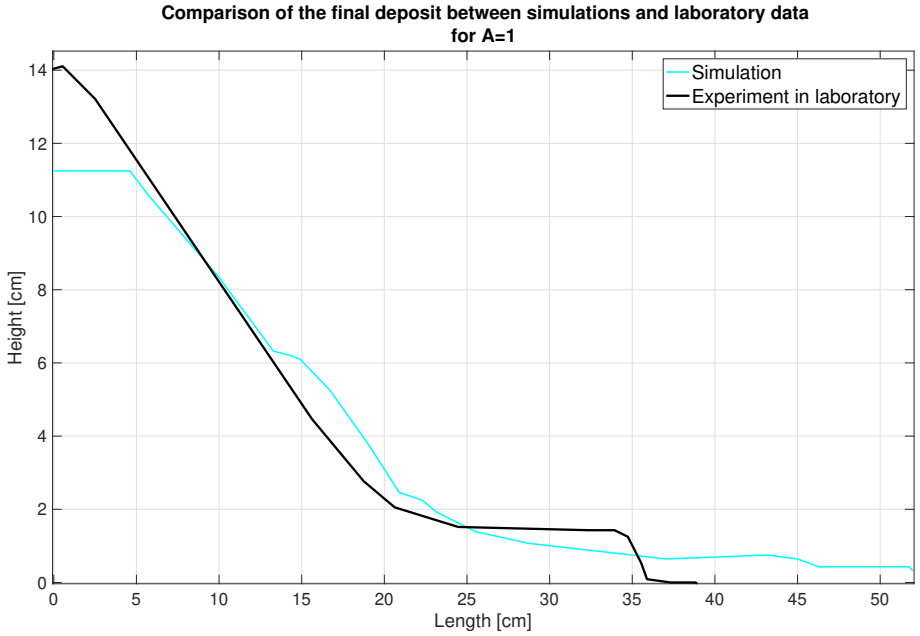

Figure C.9: Comparison between simulation and experimental data for $A = 1$ with initial height of 15[cm] and an effective volume fraction equal to 0.545

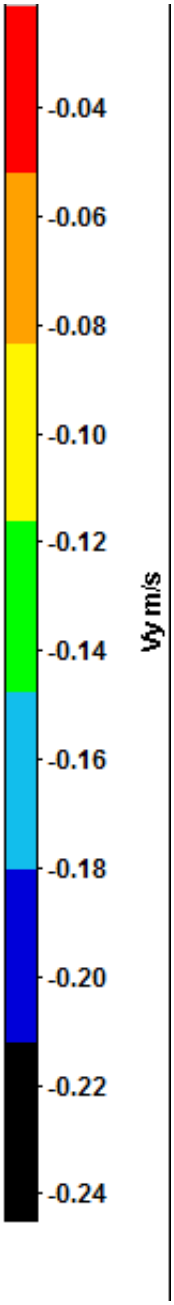

Figure C.10: Zoom of the color code of the vertical component of the velocity vectors

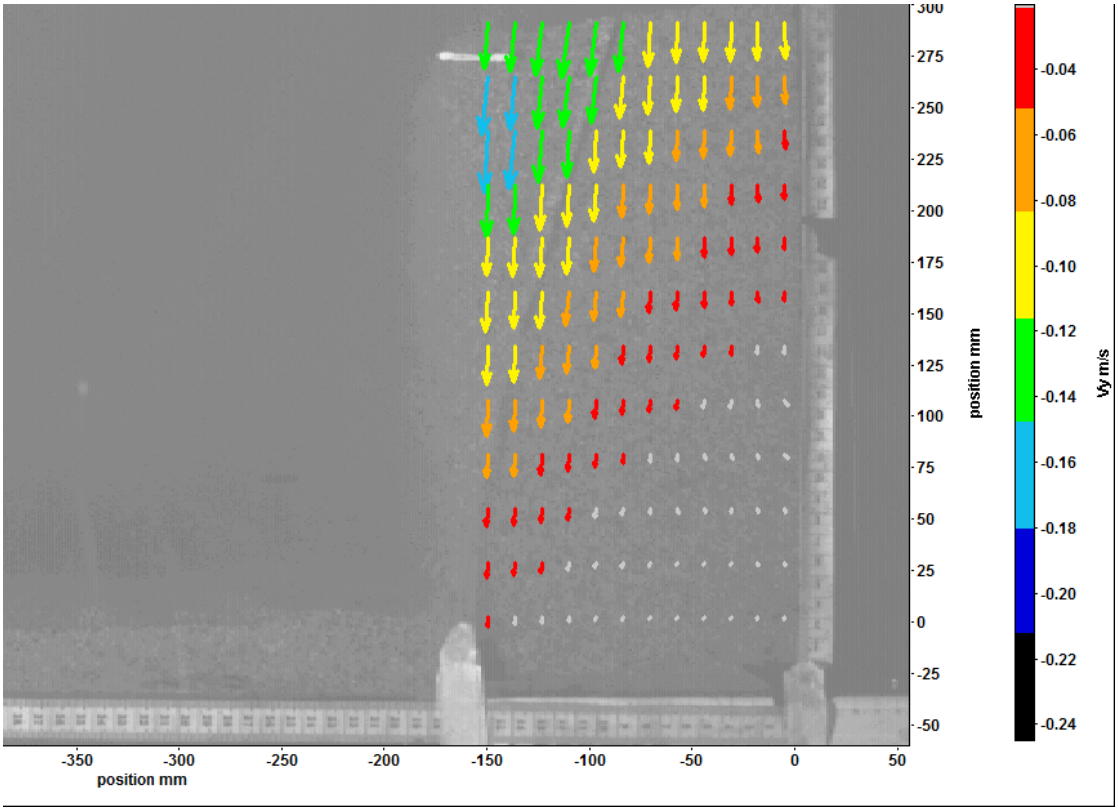

Figure C.11: $A = 2$,$t = 0.05[s]$, velocity vectors obtained via PIV

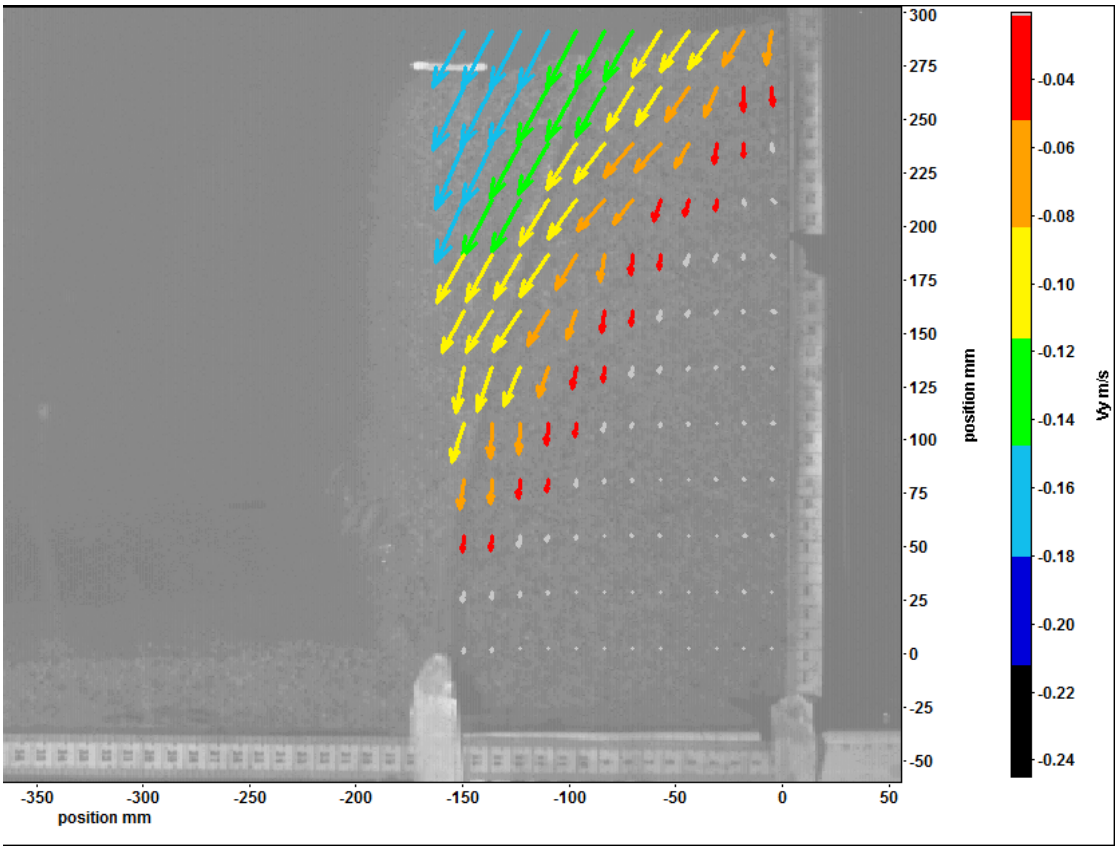

Figure C.12: $A = 2$,$t = 0.144[s]$, velocity vectors obtained via PIV

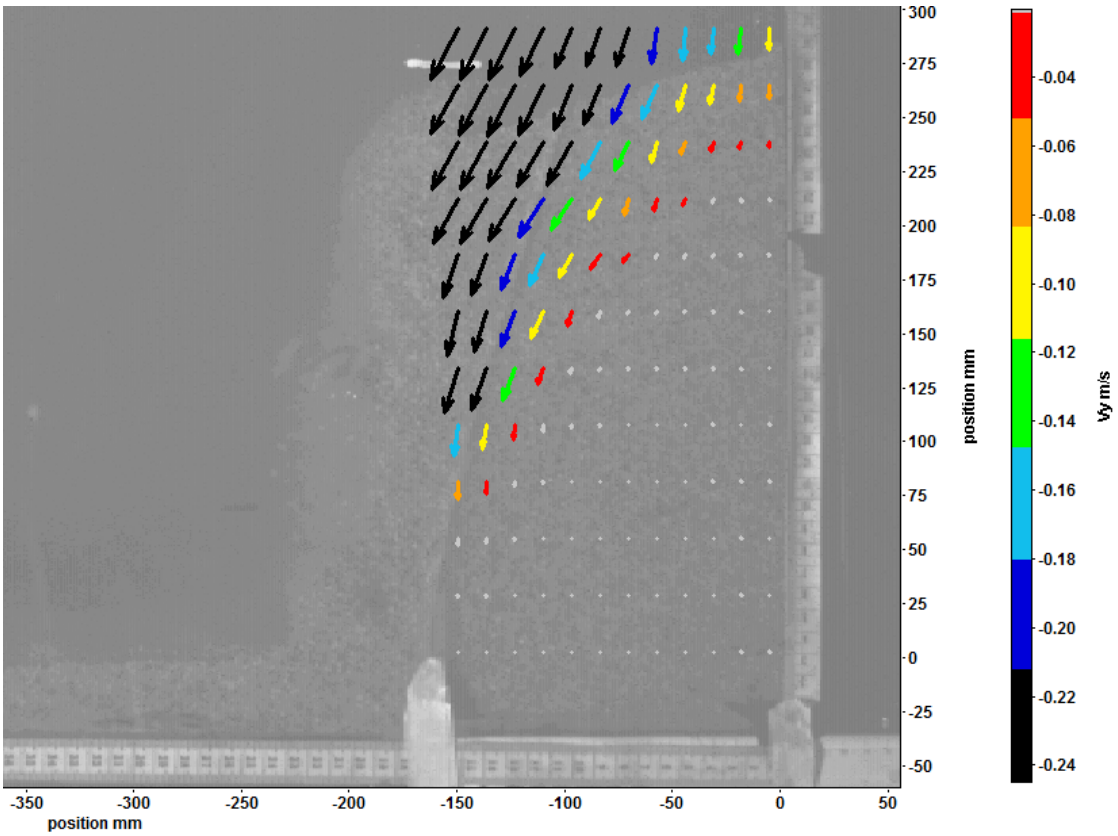

Figure C.13: $A = 2$,$t = 0.28[s]$, velocity vectors obtained via PIV

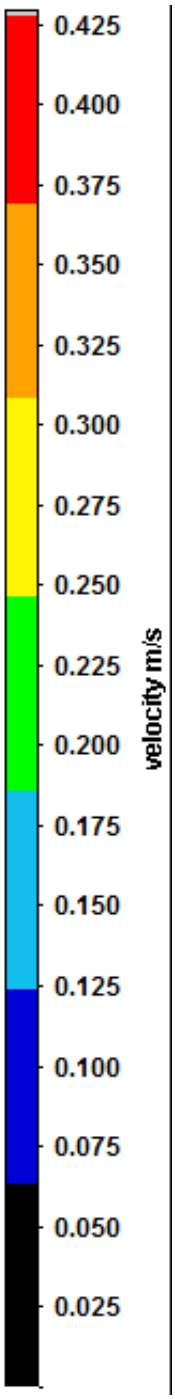

Figure C.14: Zoom of the color code of the velocity vectors

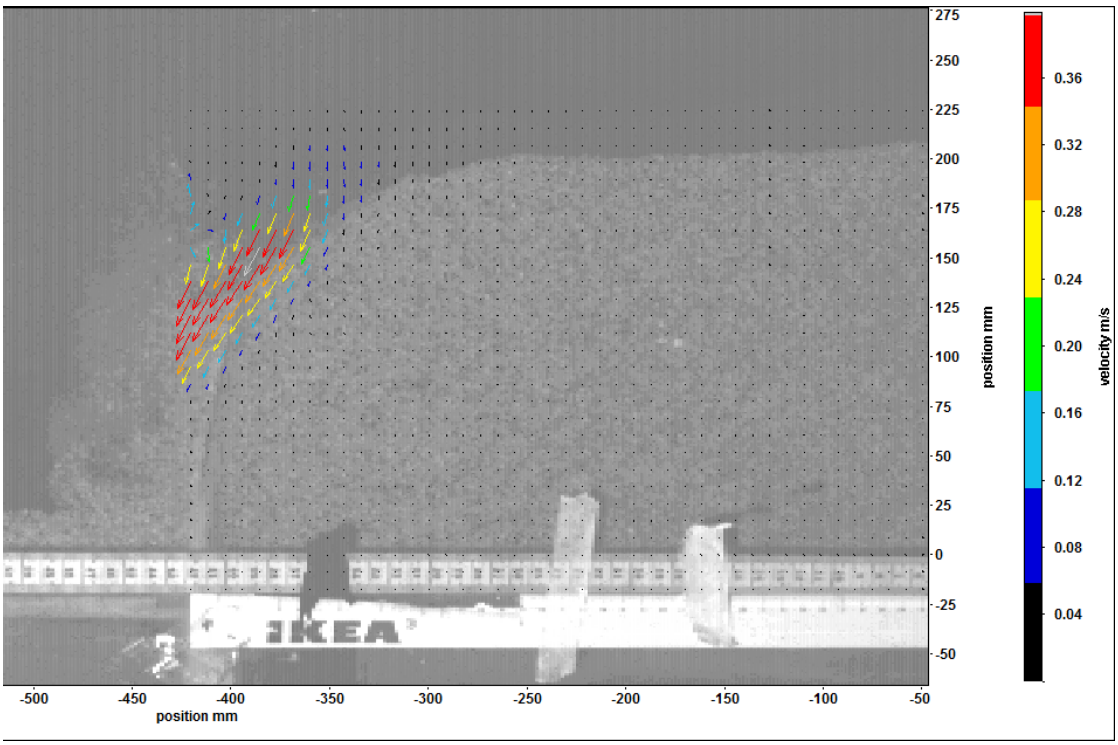

Figure C.15: Additional illustration of the fact that after collapsing on itself, the column changes its collapse direction and is oriented downstream

UNIVERSITÉ CATHOLIQUE DE LOUVAIN
École polytechnique de Louvain
Rue Archimède, 1 bte L6.11.01, 1348 Louvain-la-Neuve, Belgique | **www.uclouvain.be/epl**